2013-07-24

Studies of Molecular Encapsulation and Preparation of Novel Cage Molecules

Yanhua Qiu
University of Miami, qiu-yanhua@hotmail.com

UNIVERSITY OF MIAMI

STUDIES OF MOLECULAR ENCAPSULATION AND PREPARATION OF NOVEL CAGE MOLECULES

By

Yanhua Qiu

A DISSERTATION

Submitted to the Faculty
of the University of Miami
in partial fulfillment of the requirements for
the degree of Doctor of Philosophy

Coral Gables, Florida

August 2013

UNIVERSITY OF MIAMI

A dissertation submitted in partial fulfillment of
the requirements for the degree of
Doctor of Philosophy

STUDIES OF MOLECULAR ENCAPSULATION AND PREPARATION OF NOVEL CAGE MOLECULES

Yanhua Qiu

Approved:

_____	_____
Angel E. Kaifer, Ph.D.	M. Brian Blake, Ph.D.
Professor of Chemistry	Dean of the Graduate School
_____	_____
Burjor K. Captain, Ph.D.	James N. Wilson, Ph.D.
Professor of Chemistry	Professor of Chemistry

_____
Xiangyang Zhou, Ph.D.
Professor of Mechanical
and Aerospace Engineering

QIU, YANHUA (Ph.D., Chemistry)

Studies of Molecular Encapsulation and Preparation of Novel Cage Molecules (August 2013)

Abstract of a dissertation at the University of Miami.

Dissertation supervised by Professor Angel E. Kaifer
No. of pages in text. (122)

This dissertation deals with studies of molecular encapsulation and preparation of novel molecular cages. The author begins in Chapter 1 with a short discussion of molecular encapsulation and some of the molecular hosts such as cavitands, carcerands, hemicarcerands, hexamericresorcinarene capsules and molecular cages and then presents more introductory material on a deep cavity cavitand and cucurbit[7]uril since the author's research is majorly based on these two molecular hosts. The author is interested in the electrochemistry studies of redox-active guests and their electrochemical kinetic changes before and upon encapsulation in aqueous solution so as to mimick the behavior of redox proteins in biological systems or be potentially used for drug delivery. The author carries out a series of characterization experiments such as ^{1}H NMR, ESI-TOF MS, DOSY NMR, COSY NMR, UV-Vis and so on to prove the formation of host-guest complexes before running any

electrochemistry experiments. Some experiments fail to provide convincing evidence for redox-active guests encapsulated in the host molecules. Therefore the author does not include these systems in the dissertation. The author gives two encapsulation examples in Chapter 2 and Chapter 3 respectively with tetrathiafulvalene (TTF) and bulky adamantylferrocene derivatives in a dimeric capsule formed by two deep-cavity cavitands.

In Chapter 4, the author investigates binding of cucurbit[7]uril with a newly synthesized tris(viologen) derivative guest. Upon viologen moiety encapsulation inside cucurbit[7]uril, the surrounding guest protons that are close to the oxygen portal of cucurbit[7]uril will have strong interactions with the oxygens and show interesting complexation-induced chemical shifts in ^{1}H NMR experiments. The author also reports data on two control compounds to help explain the interesting phenomena.

In Chapter 5, the author attempts to synthesize a novel molecular cage glued by “click” reactions. With trial-and-error, the author ends up with insoluble polymers since the “click” reactions are super-efficient and undirected. The results show that the design of the starting materials will affect the formation of the cage molecules and intramolecular reactions must overcome

intermolecular cross-linking reactions after the first “click” made. Highly diluted experimental conditions and a suitable template are also important for the successful formation of cage molecules.

ACKNOWLEDGEMENT

This dissertation discusses research completed over the last four years during my studies at the University of Miami. This entire endeavor would not have been possible without the support and encouragement of my Ph.D. advisor Dr. Angel E. Kaifer. I am deeply grateful that I have such a kind, generous, talented and wise person as my advisor and was able to carry out my research work smoothly and productively over the past four years.

I want to thank Dr. Burjor K. Captain and Dr. James N. Wilson as my Ph.D. committee members, who provided me with meaningful suggestions and advice for my research. I also want to thank my lab members Song Yi, Feifei Xin and Wei Li whose help and support greatly aided my research experiments.

My dear husband, Weihua Mao, has been so supportive of my dreams in every possible way. I am so lucky to have him as my husband; he made it possible for me to fully dedicate myself to my desired career because of our stable, loving and trusting relationship.

My parents, Shengwang Qiu and Zhuheng Chen, as always, are my soul supporters. They have taught me to be an

aspiring person and always encouraged me to pursue my dreams.

And last, but never the least, Dr. Xiangyang Zhou, Dr. Tegan Eve, Dr. Francisco Raymo, thank you all for giving me helpful guidance during my Ph.D. study.

TABLE OF CONTENTS

LIST OF FIGURES

LIST OF SCHEMES

CHAPTER 1

AN INTRODUCTION TO MOLECULAR ENCAPSULATION

1.1 Molecular Encapsulation

In supramolecular chemistry,[1] molecular encapsulation is defined as the application of programmed molecules that assemble into larger molecular architectures via intermolecular noncovalent bonds while including smaller molecules inside the assembly.[2,3] An important class of supramolecular structures is the host–guest assemblies, where the host is a receptor that selectively binds (generally smaller) guest molecules.[4-6] Since only weak intermolecular interactions such as hydrogen bonds, hydrophobic effects and metal–ligand interactions are involved, the formation and dissociation of the host-guest complexes is reversible and controllable, which provide a possible way to explore the chemical reactivity of guests that are unstable or insoluble in bulk solution.

Cram demonstrated the first example of molecular encapsulation in 1991.[6,7] Up to now, the field of molecular encapsulation has seen a remarkable development. This chapter will begin with a brief introduction of the resorcinarene-based hosts (receptors), cucurbit[n]urils

(CBn) and molecular cages. Then the emphasis will shift to redox-active guests that can be encapsulated into the cavities of the host molecules.

1.2 Cavitands, Carcerands, Hemicarcerands and Hexameric Resorcinarene Capsules

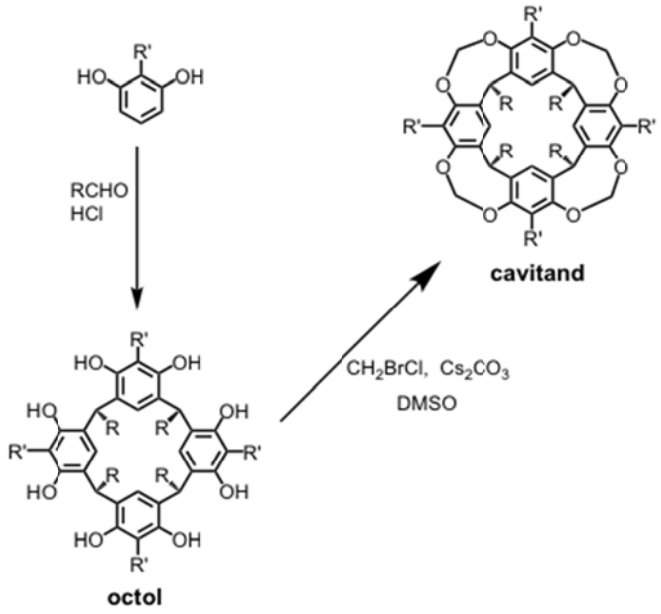

Scheme 1.1 *General synthesis of octols and cavitands from resorcinol.*

Cavitands are hosts formed in acidic condensation reactions between resorcinol derivatives and aldehydes (Scheme 1.1). The resulting cyclic octol compounds are usually tetrameric and contain four aromatic units that form a relatively shallow bowl in the preferred C_{4v} conformation. The structure of the octols can be elaborated

further for various purposes. Most commonly, the main objective of additional synthetic work is to fix the conformation of these compounds in C_{4v} symmetry with a well-defined, albeit small cavity.

Cram developed this chemistry during the 1980s and 1990s by preparing compounds consisting of two covalently connected cavitands facing each other.[6,7] When the two cavitands are forced to be close to one another, with very small openings between them, the resulting compounds were termed *carcerands*, as they could trap or encapsulate ("incarcerate") small guests (Figure 1.1). Once the host/guest complex (carceplex) was formed, the guest will be retained in the interior of the host, maintaining the structural integrity in the gaseous, liquid and solid state.

More interesting was the synthesis of larger compounds, in which the connectors between the two facing cavitands provide larger open spaces between them, which effectively become openings (portals) into the host's inner cavity. These host compounds were baptized as *hemicarcerands*, because the encapsulation of guest molecules was not complete, as opposed to what was observed with carcerands (Refer to Figure 1.1).

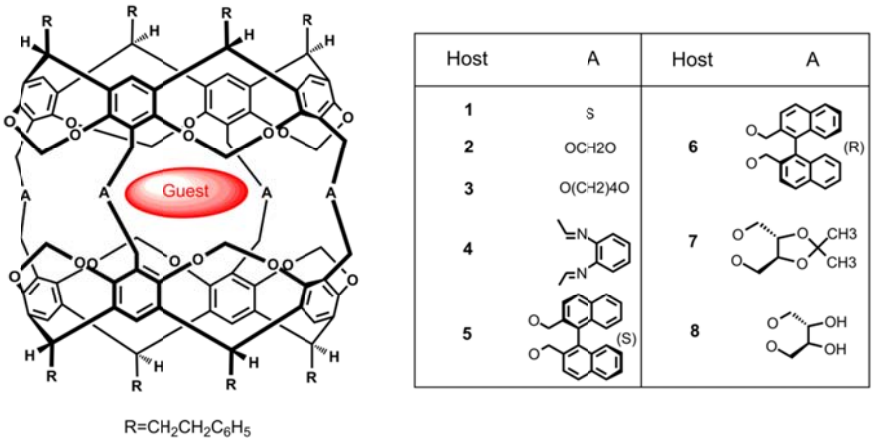

Figure 1.1 *Carcerand (host **1**) and hemicarcerands (host **2**–**8**).*[8]

If the sizes (cross-section) of the guests and the cavity portals are comparable, direct inclusion of the guest inside the host does not take place at room temperature. However, heating of the guest and the hemicarcerand in solution affords enough kinetic energy so that some collisions can overcome the barrier (constrictive binding energy)[9,10] and push the guest to enter the inner cavity of a hemicarcerand through a size-restricting portal host's skin, which leads to the formation of the inclusion complex or *hemicarceplex*. Upon cooling, the complex is stabilized by the intrinsic binding force, and the guest does not have enough energy to overcome the constrictive binding energy. Thus the inclusion guest becomes trapped inside the host and cannot escape through the tight portals

(Figure 1.2 top). Conceptually, the situation is similar to that found in rotaxanes, in which the macrocyclic wheel (bead) cannot dissociate from the axle component (thread) because the latter is terminated in bulky stopper groups that prevent the wheel component from sliding away (Figure 1.2 bottom).

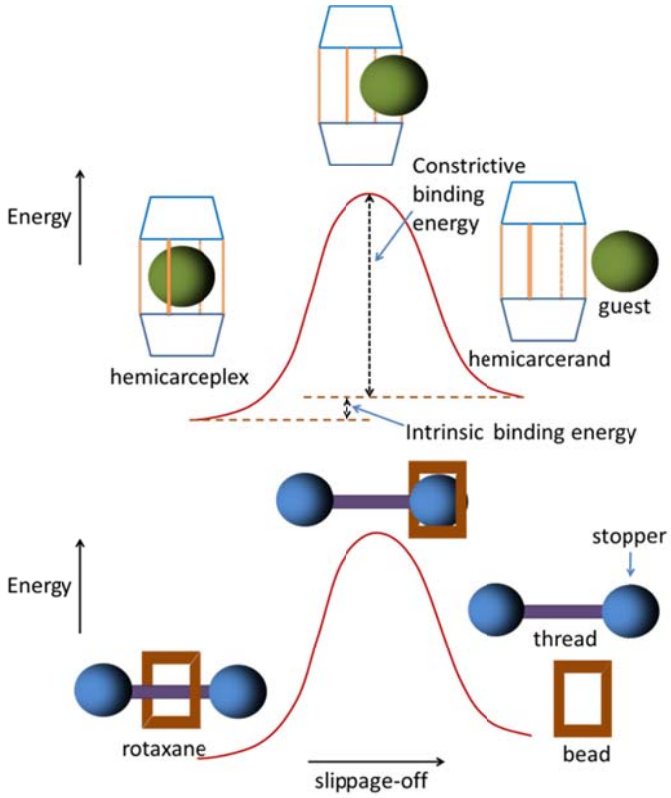

Figure 1.2 *Energy profiles of hemicarceplex dissociation (top) and rotaxane slipping-off (bottom).*[8]

The pioneering report[11] by MacGillivray and Atwood in 1997 opened up the possibility of using self-assembled hexameric capsules of resorcinarenes to encapsulate guests.

The resorcinarenes are tetrameric macrocyclic octols prepared by the condensation of resorcinol in the presence of an aldehyde (see "octol" structures in Scheme 1) and mineral acid as the catalyst. While the chemistry of the resorcinarenes has been well known since the 1970s, MacGillivray and Atwood found that the simple host **9** (see Figure 1.3) crystallizes forming a fascinating hexameric molecular capsule.[11] Each capsule adopts a snug cube conformation with the six resorcinarenes and eight water molecules held together by a network of sixty hydrogen bonds. The internal volume for each capsule is estimated at ca. 1375 $Å^3$. This report attracted attention from several groups and it was shown quickly that similar hexameric molecular capsules were formed by a number of resorcinarenes in the solution phase.[12-14] For instance, Rebek reported a complex with eight benzene molecules inside the self-assembled hexameric resorcinarene **10** capsule.[15] Due to its solubility in low polarity solvents, resorcinarene **10** has been utilized extensively as the monomer for hexameric capsule formation in $CHCl_3$ and CH_2Cl_2 solution.

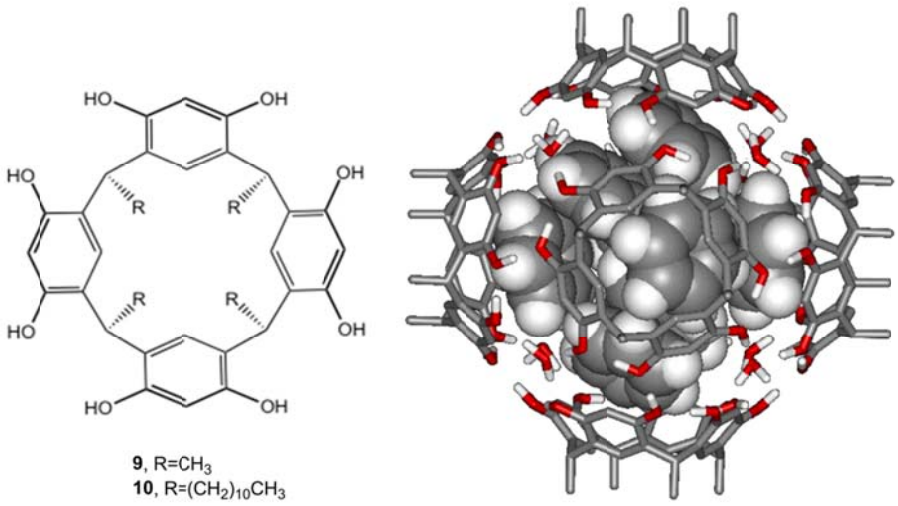

Figure 1.3 *Structures of the resorcinarenes **9** and **10** (left) and the complex of eight benzene molecules inside a hexameric resorcinarene capsule (right).*

1.3 A Dimeric Molecular Capsules Formed by Two Deep-Cavity Cavitands

The deep-cavity cavitand (octaacid cavitand) **11** (Figure 1.4a) developed in Gibb's group is a resorcinarene-based molecular host whose cavity is built up from twelve aromatic rings.[16,17] Four aromatic rings constituting the starting resorcinarene (first row) lie on top of the "feet" of the molecule. Another set of four aromatic rings deepens the hydrophobic cavity beyond the first row considerably (second row). The third row of rings rigidifies the binding pocket whilst providing the host with a wide hydrophobic rim located at the "mouth" of the molecule. The water-solubility of the deep-cavity cavitand is enhanced by the

external coat of eight carboxylic acids, four of them located at the rim, while the rest are at the feet ends.

Cavitand **11** has limited solubility (tens of micromolar) in neutral aqueous solution, presumably because not all the carboxylic acids are deprotonated at pH 7. Increasing the pH to values where the eight external carboxylic acid groups are ionized, affords this host a substantial negative charge (-8) and allows its dissolution up to millimolar concentrations. At concentrations of 10 millimolar or above, **11** will not exist as monomeric but as a disordered aggregate.

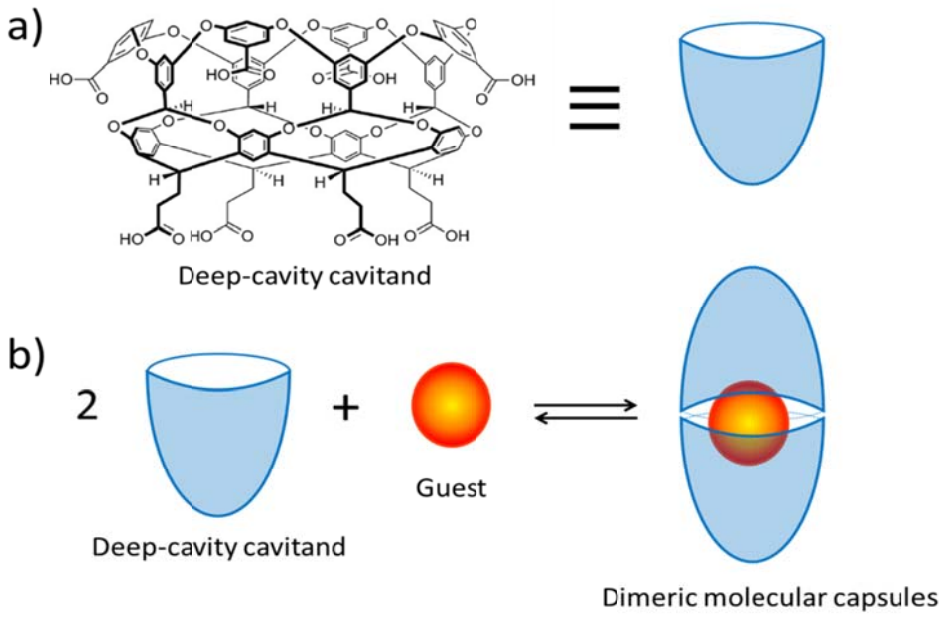

Figure 1.4 *a) Gibb's deep-cavity cavitand; b) Self-assembly of two cavitands with a suitable guest.*

It is now well known that in the presence of suitable hydrophobic guests, two molecules of cavitand **11** will come together, assisted by hydrophobic effects, to yield a well-defined dimeric molecular capsule (Figure 1.4b).[16] To probe the shape and size of the cavity of the capsule, Gibb's group examined a range of steroids and their encapsulation by capsule $\mathbf{11}_2$.[16,17] It was found that the strength of binding, allied to the size of the internal volume of the capsule, make possible for several molecules to be trapped within the capsule. Ramamurthy's group examined the interior of the cavity and how the capsulation influenced photoreaction of encapsulated guests via fluorescence spectrometry.[18-22] Recently they reported that capsule $\mathbf{11}_2$, acts as a molecular host that can effectively facilitate photo-induced electron transfer between an incarcerated donor and a free acceptor in aqueous solution. The donor, trapped by the $\mathbf{11}_2$ capsule and isolated from the bulk solution, is excited to produce an electron that is transferred through the molecular wall of the capsule directly into the electrostatically exterior-attached acceptor without any solvent relaxation effects, reducing the electron transfer rate from 631 picoseconds in free solution to 20 picoseconds as molecular assembly (Figure 1.5).[23] Our own group has been interested in the

encapsulation of redox-active guests[24-27] such as ferrocene in capsule **11**$_2$ and more details will be given below.

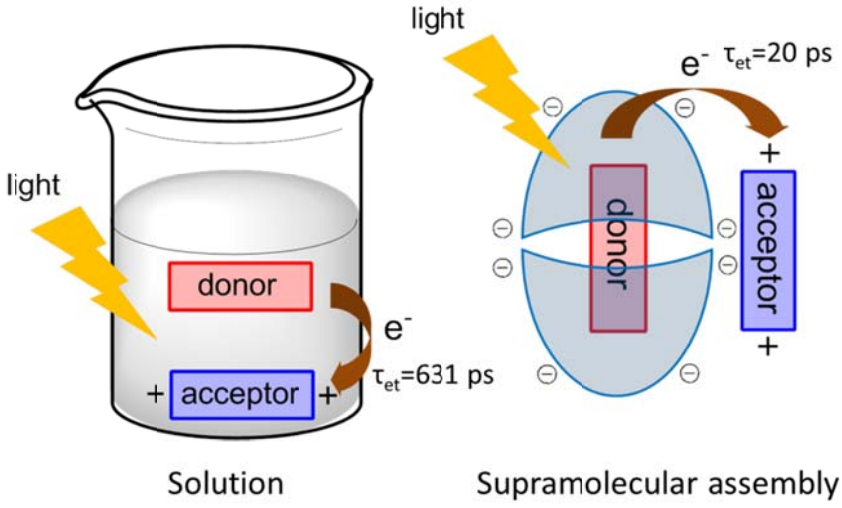

Figure 1.5 *Photo-induced electron transfer between donor and acceptor in free solution (left) and in supramolecular assembly (right).*[23]

1.4 Cucurbiturils

The cucurbit[*n*]urils (CBn) are a family of receptors prepared by the condensation of glycoluril and formaldehyde in acidic medium.[28,29] The growing research interest on CBn receptors, evident during the last decade, can clearly be traced to the development of methods for the isolation of CBn receptors with *n*>6, such as CB7 and CB8 (Figure 1.6). These hosts have a barrel-shaped hydrophobic cavity, which can be accessed through two identical portals and form high affinity complexes with positively charged or cationic

hydrophobic compounds, attributed to the carbonyl groups that line each end of the cavity and interact with cations in a similar fashion to crown ethers. Hydrophobic forces also play an important role in driving the formation of host-guest complexes. In optimal cases, these complexes reach extremely high binding affinities (K ~ 10^{15} M^{-1}) similar to those observed with the avidin-biotin host-guest pair.[30]

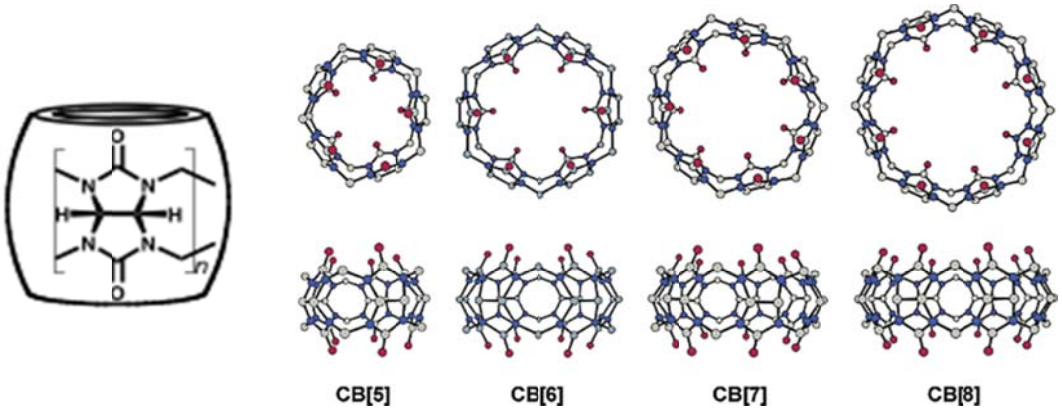

Figure 1.6 *The structures (left) and X-ray crystal structures (right) of cucurbit[n]uril hosts. Color codes: carbon, gray; nitrogen, blue; oxygen, red.*[31]

The varying cavity and portal sizes of CBn lead to remarkable molecular recognition properties.[28] CB5 as the smallest homologue can only encapsulate small molecules such as N_2 in the cavity and binds cations such as NH^{4+} and Pb^{2+} at the portals. CB6 can form very stable complexes with larger guest molecules such as protonated diaminoalkanes

($^{+}NH_3(CH_2)_nNH_3^{+}$, n=4-7, K>10^5 M^{-1}) and neutral molecules such as tetrahydrofuran and benzene in aqueous solution. CB7 can form 1:1 complexes with protonated adamantylamine, methyl viologen dication (N,N'-dimethyl-4,4' bipyridinium, MV^{2+}), ferrocene, carborane and many other guests in aqueous solution. However, CB8 can store two different guest molecules such as MV^{2+} and 2,6-dihydroxynathphalene (HN) in the even larger cavity.

1.5 Molecular Cages

The self-assembly of coordination complexes with various sizes and shapes, such as tetrahedral, octahedral, cubic, dodecahedral and so on, has been developed very fast during the past few years.[32] These cage-like architectures are built from metal connecting points and rigidly preorganized organic ligands. For example, Raymond and co-workers assembled a chiral tetrahedral $[M_4L_6]^{12-}$ coordination cage with metal ions such as Ga^{3+} situated at the corners of the tetrahedron and six naphthalene-based bis-bidentate catechol amide ligands on the edges of the tetrahedron by the presence of an appropriate guest template (Figure 1.7a).[33] Fujita and co-workers developed an octahedral $[M_6L_4]^{12+}$ coordination cage consisted of six *cis*-protected

square planar $[Pd(en)]^{2+}$ complexes and four panel-like ligands (triangular tridentate 2,4,6-tris(4-pyridyl)-1,3,5-triazine)(Figure 1.7b).[34] These coordination cages are soluble in water and contain hydrophobic cavities. Neutral guest molecules such as ferrocene can be encapsulated driven by hydrophobic effects in aqueous solution. A variety of anionic guests strongly attracted by the positively charged vertexes can also form stable host-guest complexes.

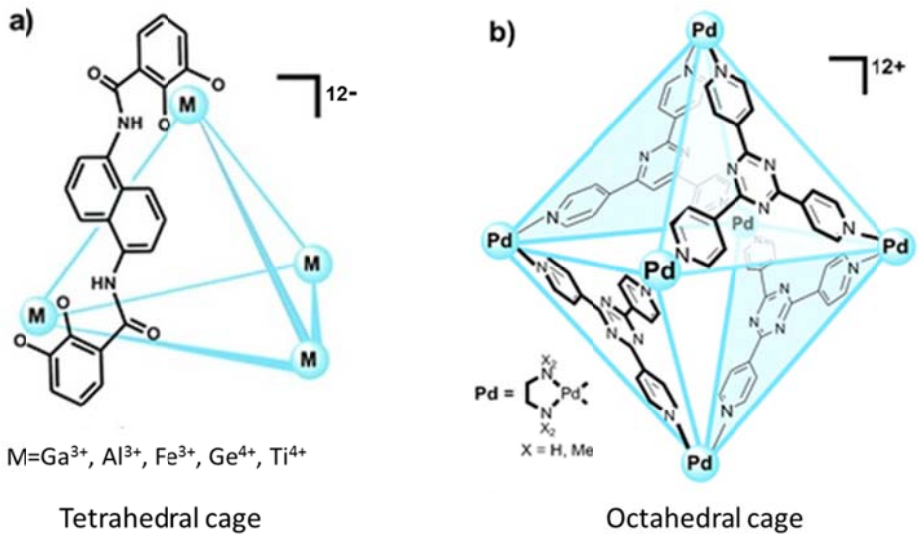

Figure 1.7 *a) Tetrahedral M_4L_6 coordination cage; b) Octahedral M_6L_4 coordination cage.*

1.6 Electrochemistry Study

Strong interest has been put in the development of simple synthetic models that mimick the behavior of redox

proteins. These biological macromolecules show interesting properties regarding their electron transfer (ET) reactions. Usually, the redox centers are partially buried in the polypeptide framework and the redox centers are more or less available for ET reactions depending on the spatial relationship between the redox center and the reacting partner. Since the rates of ET reactions decay exponentially with the distance between the reacting centers, it seems clear that Nature uses this strategy to control the ET reactions in which redox proteins may engage. From an electrochemical point of view, this fact translates into either fast or slow electrochemical kinetics for a redox protein depending on the chemical nature of the electrode and the preferred orientation that the protein may adopt near the electrode surface. Thus, orientations in which the redox active group is positioned close to the electrode surface give rise to relatively fast electrochemical kinetics, that is, fast heterogeneous ET rates, while orientations in which the redox group is located relatively far away from the electrode surface result in slower or more sluggish electrochemical kinetics. If the interactions between the electrode surface and the protein surface do not induce a specific interfacial orientation of the protein, then, the prevailing kinetics

will result from the integration of the rates for all possible orientations. Although a good number of redox proteins could be cited as examples, perhaps the most heavily investigated case is that of cytochrome *c*, which contains an iron heme redox center partially buried in a region of the protein surface decorated with a number of positively charged lysines. Among other schemes, modification of the electrode surface with a carboxylate-terminated monolayer leads to relatively fast ET, as the lysine-carboxylate interactions arrange the iron heme center on the protein side facing towards the electrode surface.[36]

The quest to develop and investigate synthetic structures with similar ET properties requires, as a first step, the placing of the redox center at some distance from the electrode surface. In supramolecular systems, non-covalent methods are employed to accomplish this goal. Our group has always preferred to work in aqueous media and the experimental work with hemicarcerands had to be done in solvents of considerable low polarity, such as dichloromethane and tetrachloroethane. Therefore, we developed our interest in CB7 host and water-soluble

cavitand-type hosts which has considerable solubility in aqueous solution.

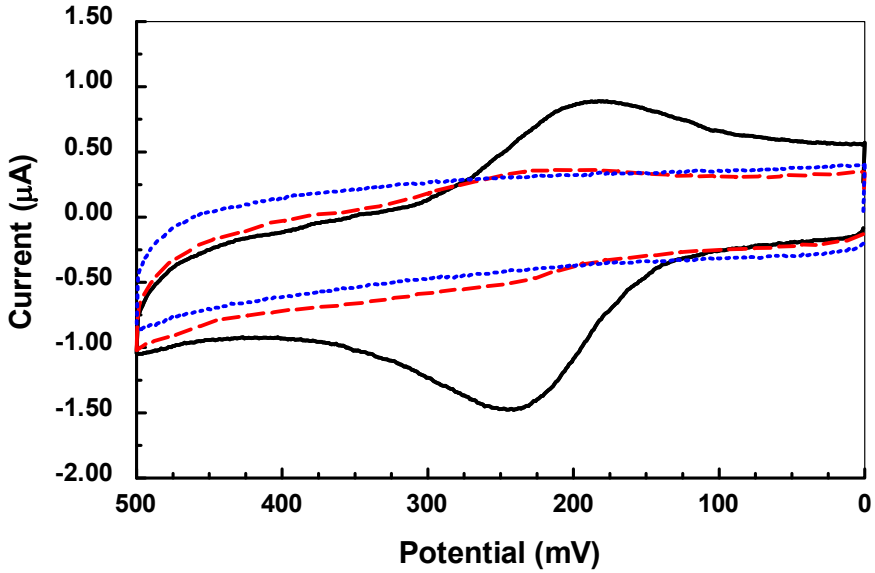

Figure 1.8 *Cyclic voltammetric response of 0.5 mM ferrocene in 10 mM borate buffer (pH 8.9) also containing 50 mM NaCl in the absence of* ***11*** *(solid line), and in the presence of 1.0 equiv (discontinous line) and 2.0 equiv (dotted line) of host* ***11****.*

Kaifer's group had previously studied the encapsulation of ferrocene (Fc) in capsules formed by two deep cavity cavitands using electrochemistry.[24] The ferrocene voltammetric response of Fc@**11**$_2$ was found to be completely flat in the potential range where its oxidation is observed (Figure 1.8). In other words, no current wave for one-electron oxidation of Fc was observed either by cyclic voltammetry or square wave voltammetry. However, the

expected current wave emerged as soon as the concentration of Fc exceeded the value that can be encapsulated, that is, [Fc] > [**11**]/2. This suggests that there is no passivation of the electrode resulting from any accumulation or precipitation of host on its surface. In fact, our data clearly support the voltammetrically silent character of Fc@**11**$_2$ under the conditions of our experiments.

Kaifer's group has also found that the negative charges around the **11**$_2$ dimeric capsule can also play very important roles. For instance, hydrophobic cations, such as viologens, bind strongly to the outer surface of the capsule,[24] due to the presence of four negative charges clustered at each polar end of the assembly and another eight negative charges gathered around the capsule's equator. Kaifer's group took advantage of these anionic surface charges to design a supramolecular system in which the oxidation of the encapsulated ferrocene becomes possible. Basically, Kaifer's group utilized the cationic ferrocene derivative (ferrocenylmethyl)trimethylammonium to mediate the electrochemical oxidation of ferrocene inside the **11**$_2$ capsule (see Scheme 1.2).[25] The supramolecular system consists of two molecules of host **11**, forming a dimeric capsule, which includes ferrocene, and has a

cationic ferrocene derivative strongly bound to its external, negatively charged surface.

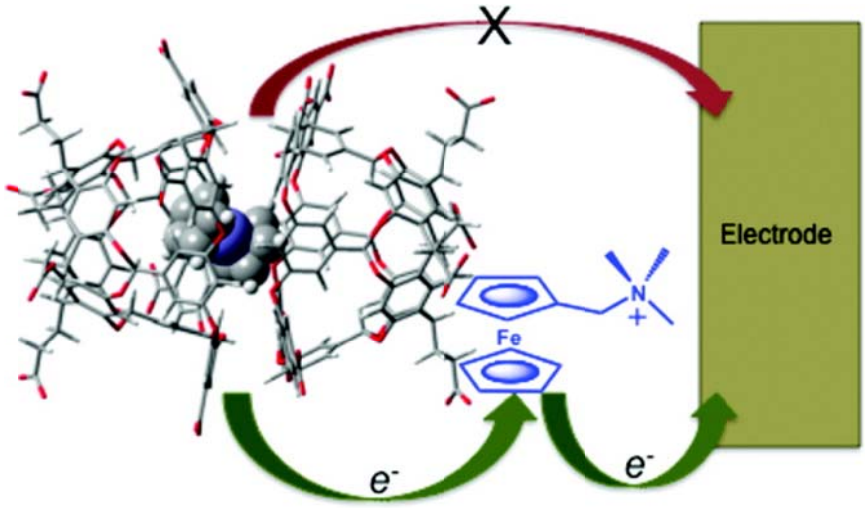

Scheme 1.2 *Oxidation of the Fc@**11**$_2$ supramolecular assembly mediated by the externally bound ferrocenylmethyltrimethylammonium cation.*[25]

In cyclic voltammetric experiments, the included ferrocene guest does not undergo direct oxidation, as discussed before. However, as the electrode potential becomes gradually more positive, the outside ferrocene eventually undergoes oxidation. At this stage, the outside oxidized ferrocenyl residue undergoes intramolecular electron transfer with the included ferrocene, extracting one electron from the inside of the capsule and leaving the external ferrocenyl group ready to undergo oxidation again. Overall, the cyclic voltammetric experiments show a two-electrode oxidation per supramolecular assembly (Figure 1.9)

and the oxidation of the central, included ferrocene nucleus leads to the breakup of the assembly, due to the fact that oxidized ferrocene is less hydrophobic than ferrocene itself. These experimental results are extremely interesting because they contain strong similarities to features found in the electrochemistry of redox proteins assisted by electron mediators.

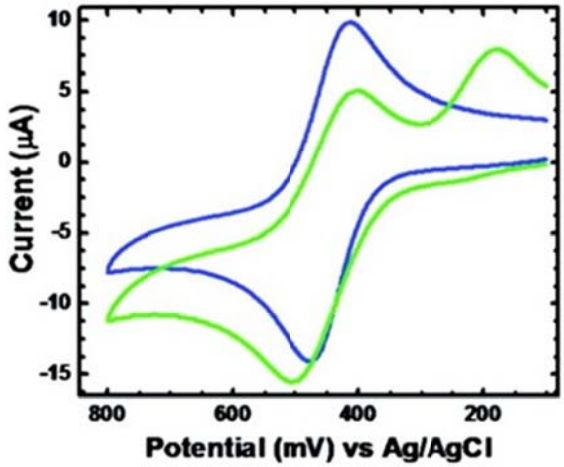

Figure 1.9 *CV responses on glassy carbon (0.071 cm^2) of 50 mM NaCl aqueous solutions buffered at pH 9 with 10 mM sodium borate. 1.0 mM cationic ferrocene derivative in the absence (blue) and in the presence (green) of 1.0 equiv of Fc@**11**$_2$.*[25]

Kaifer's group has investigated in detail the electrochemistry of 4,4'-bipyridinium (viologen) dications[37,38] and ferrocene derivatives[39] in the presence of the CB7 host. Both classes of redox active guests form stable CB7 inclusion complexes, although the binding

affinities with viologen guests are lower (K~10^5-10^6 M^{-1}) than those measured with ferrocene derivatives (K~10^8-10^{15} M^{-1}). In spite of these differences in the K values, both guests give rise quantitatively to CB7 inclusion complexes upon addition of 1.0 equiv of the host at the concentration levels (usually mM) employed in voltammetric experiments. In the absence of CB7, both guests exhibit very fast electrochemical kinetics and the observed voltammetric currents are controlled by diffusional effects. In electrochemical terms, their behavior is fully reversible. The viologen inclusion complexes also show reversible voltammetric behavior, indicating that viologen inclusion by CB7 does not have a significant effect on the electrochemical kinetics.[37,38] In pronounced contrast, CB7 inclusion complexes of ferrocene derivatives show a considerable decrease in electrochemical kinetics into the so-called "quasi-reversible" regime, where the standard rate constants for heterogenous electron transfer (k^o) can be readily measured.

The attenuation of electrochemical kinetics observed with the CB7 inclusion complexes of ferrocene derivatives reflects a hindrance to electron transfer that is probably related to the increased average distance between the redox

center and the electrode surface. This distance increase is a natural result of the encapsulation of the redox center inside the CB7 cavity. However, we should ask why the same phenomenon is not observed with viologens. Kaifer's group rationalizes these observations using the fact that viologens protrude from the CB7 cavity in the inclusion complex, while the ferrocene center is much better included in the cavity. In fact, Figure 1.10 displays the two inclusion complexes, in which the relevant frontier orbitals for the guests are clearly shown. As it is clear in the figure, the HOMO of the ferrocene derivative, the key orbital for the oxidation of this guest, is fully contained inside the host cavity. In stark contrast, the LUMO of methylviologen, the most relevant orbital for guest reduction, has regions that escape out of the cavity through both portals. We view these regions as "leaky" areas in which the electron transfer is not curtailed by the surrounding host, thus facilitating electron transfer to the viologen inclusion complex.

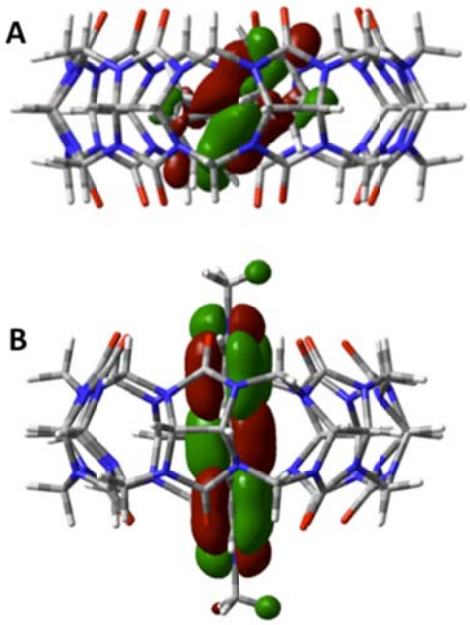

Figure 1.10 *Energy minimized structures (PM3) of the CB7 inclusion complexes of (A) ferrocene, showing the HOMO of the guest, and (B) methylviologen, showing the LUMO of the guest.*

Overall, inclusion of the guests inside CBn hosts may lead to a considerable decrease in electrochemical kinetics, as long as the frontier orbital primarily involved in the electron transfer process is well contained inside the host cavity.

1.7 Conclusion and Outlook

The inclusion of small guest molecules within suitable host molecules has attracted considerable interest since the resulting constrained systems can exhibit novel

properties upon incarcerated. In the last decade, a number of molecular hosts based on various building blocks and non-covalent interactions have been developed. These well-defined architectures act like various containers, selectively confining guests in the protective inner phase and isolating them from bulky phase molecules. This chapter provides a brief introduction to the resorcinarene-based hosts, cucurbit[n]urils (CBn) and molecular cages. Water soluble hosts with large enough cavity, such as the deep-cavity cavitand (host **11**) and cucurbit[7]uril are of more interest for us because of their strong binding ability with redox active centers. Kaifer's group has shown that encapsulation of redox active compounds may have a pronounced effect on their kinetics of heterogeneous electron transfer. It is anticipated that this field of research will further grow with the development of largercavity hosts with better aqueous solubility.

CHAPTER 2

ENCAPSULATION OF TETRATHIAFULVALENE INSIDE A DIMERIC MOLECULAR CAPSULE FORMED BY TWO DEEP-CAVITY CAVITANDS

2.1 General discussion

Tetrathiafulvalene (TTF) and its derivatives constitute an important class of compounds for the design and preparation of highly conducting organic solids.[41-43] TTF derivatives undergo two consecutive one-electron oxidations at very accessible potentials. This ease of oxidation has also led to their extensive utilization in switchable molecules.[44] Typically, TTF is oxidized to its cation radical (TTF^{+}) or dication (TTF^{2+}) forms so that the development of positive charge on the TTF residue triggers the electrostatic repulsion with other positively charged components, leading to a measurable effect.

Gibb's octaacid[16] (compound **11** in Figure 1.4) is a deep-cavity cavitand with a well-defined "bowl" shape. Eight carboxylic acid groups on the outer surface of this cavitand increase its solubility to millimolar levels in basic aqueous solution. Under these conditions, octaacid cavitand **11** forms head-to-head dimeric molecular capsules in the presence of hydrophobic guests.[16,45] We have already

mentioned that ferrocene is included inside $\mathbf{11}_2$ molecular capsules in basic aqueous solution (Figure 1.7).[24] An intriguing result of this encapsulation is the loss of voltammetric response for the one-electron oxidation of ferrocene. Because of our long-standing interest on the electrochemical behavior or encapsulated redox centers,[46] we decided to extend our investigation to TTF as an interesting candidate for encapsulation by dimeric capsules of **11**.

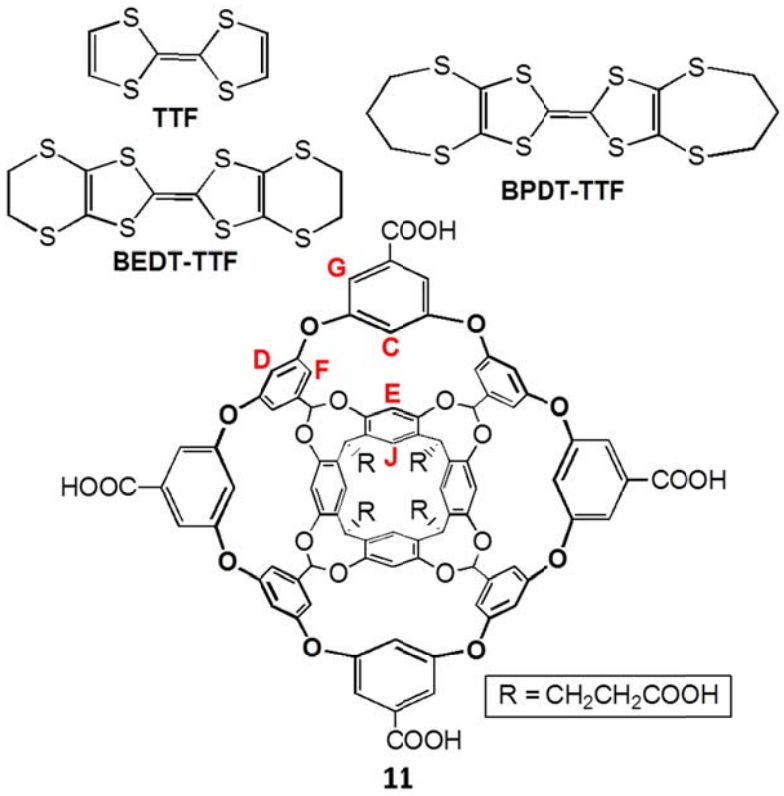

Figure 2.1 *Structures of the guests (TTF derivatives) and the host (octaacid cavitand **11**) used in this work.*

2.2 Experimental Results and Discussion

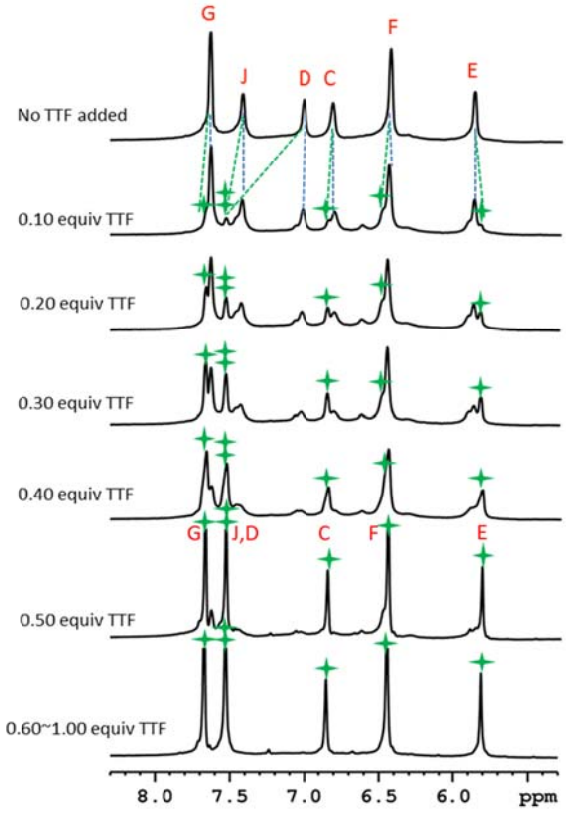

Figure 2.2 *Aromatic sections of the ^{1}H NMR spectra (500 MHz 10 mM borate buffer pH 8.9 in D_2O) of host* ***11*** *(1 mM) in the presence of increasing concentrations of TTF. Proton resonances labeled with a "cross" correspond to complexed* ***11****.*

We started our investigation by examining ^{1}H NMR spectroscopic data of **11** in the presence of variable amounts of TTF. The experimental data are shown in Figure 2.2. As TTF is added, a new set of peaks for the host protons appears and grows at the expense of the original peaks. In particular, the "D" protons, (see Figure 2.1 for

proton labels) undergo a pronounced downfield shift in the presence of TTF, but all aromatic protons are affected. Once the TTF concentration reaches the 0.5 equiv. mark, further additions of TTF no longer have any significant effect on the spectra. This finding is consistent with the anticipated stoichiometry for the inclusion of TTF inside a dimeric molecular capsule (an assembly that we will denote as TTF@**11**$_2$).

TTF is a very hydrophobic compound, and its aqueous solubility is well below the millimolar concentrations used in the ^{1}H NMR experiments.[47] The fact that we can dissolve TTF at a concentration of 1 mM in an aqueous solution containing 2 mM of **11** is by itself a strong indication that there is an efficient binding interaction between the two compounds. In the NMR experiments of Figure 2.2, additions of up to 0.5 equiv. of TTF result in perfectly transparent solutions. However, once the total amount of added TTF exceeds 0.5 equiv., the solutions become turbid, because the amount of host is not enough to bind and solubilize all the TTF added. Figure 2.3 shows two pictures taken to illustrate the completely different appearance of solutions with fully dissolved TTF (in the presence of **11**) and undissolved TTF guest (in the absence of **11**).

Figure 2.3 *Both solutions contain 1.0 mM TTF + 20 mM borate buffer in water. Left vial: 2.0 mM* ***11*** *added to solubilize TTF. Right vial: no* ***11*** *added.*

All these observations strongly suggested the encapsulation of TTF inside $\mathbf{11}_2$ assemblies. To confirm this point, we carried out diffusion coefficient measurements using pulse gradient spin echo (PGSE) NMR techniques.[48] The diffusion coefficient (D_0) was obtained from the slope of the linear plot $\ln(I/I_0)$ vs. G^2 in Figure 2.4, according to the equation: $\ln(I/I_0)=-[\gamma^2\delta^2G^2(\Delta-\delta/3)]D_0$, where γ: gyromagnetic ratio; δ: duration of the pulse; G: pulsed gradient strength; Δ: time separation between the pulsed-gradients; and D_0 was measured as $(1.95 \pm 0.05) \times 10^{-6}$ cm^2/s for free cavitand **11** (black line) and $(1.45 \pm 0.05) \times 10^{-6}$ cm^2/s for cavitand **11** in the presence of 0.5 equiv. of TTF

(red line). Further additions of TTF did not change the D_0 value (blue line) but led to turbid solutions as discussed before.

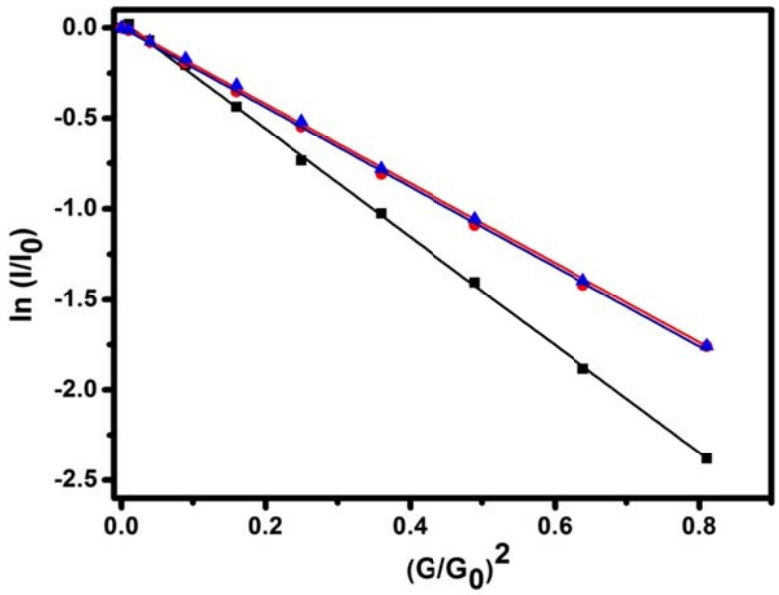

Figure 2.4 *Linear plot of $\ln(I/I_0)$ vs. $(G/G_0)^2$. Black: 1 mM **11** + 10 mM Buffer, red: 1 mM **11** + 10 mM Buffer + 0.5 mM TTF, Blue: 1 mM **11**+10 mM buffer + 1.0 mM TTF. The diffusion coefficient was obtained from the slope of this linear plot according to the equation: $\ln(I/I_0)=-[\gamma^2\delta^2G^2(\Delta-\delta/3)]D_0$.*

As mentioned above, TTF and its derivatives undergo two consecutive one-electron oxidations to first generate a cation radical (TTF^+) and eventually a dication (TTF^{2+}) at more positive potentials. In organic solvents, where TTF is sufficiently soluble, the electrochemical behavior shows the expected two sets of waves corresponding to the two reversible processes[44] ($TTF \leftrightarrow TTF^+ + e^-$ and $TTF^+ \leftrightarrow TTF^{2+} + e^-$).

In aqueous solution, the first oxidation is poorly developed because of the low solubility of TTF, but the second oxidation gives rise to a larger wave as the charged, oxidized TTF forms are considerably more soluble.[50] Therefore, we set out to record the electrochemical behavior of TTF trapped inside **11**$_2$ using cyclic voltammetry (CV). The experimental results are shown in Figure 2.5. The black trace depicts the voltammetric behavior in the absence of host **11**, showing the poorly developed anodic wave for the TTF → $TTF^+ + e^-$ oxidation process centered at +0.18 V vs. Ag/AgCl. The second anodic wave (at +0.48 V) exhibits a higher current level, but no peaks are observed on the reverse scan, suggesting the fast disappearance of the dication. In the presence of 2.0 equiv. of host **11** (red trace), the small anodic current for the first oxidation process disappears, in spite of the fact that the effective concentration of TTF in this solution is 0.5 mM (with the TTF molecules encapsulated inside **11**$_2$). We have reported very similar results for encapsulated ferrocene (Fc), that is, the Fc@**11**$_2$ assembly was found to be voltammetrically silent in the potential region corresponding to Fc oxidation. As the CV potential scan with TTF@**11**$_2$ extends to more positive values, a well-defined wave was recorded in the potential region corresponding to the second oxidation

process (at +0.56 V) and a small peak was observed on the reverse scan at potentials associated with the $TTF^{+} + e^{-} \rightarrow$ TTF reduction process.

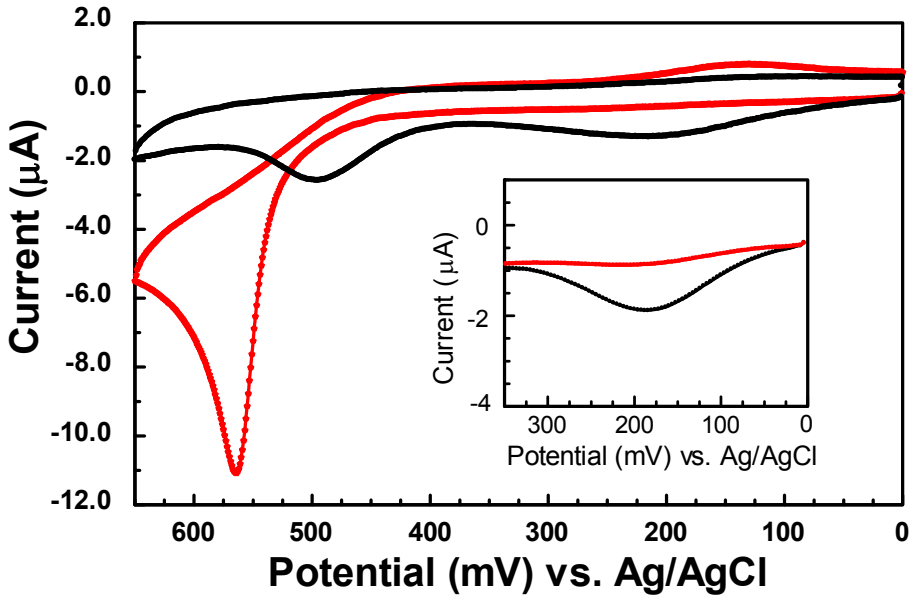

Figure 2.5 *CV responses on glassy carbon (0.07 cm^2) of a saturated TTF aqueous solution (black trace) also containing 50 mM NaCl and 10 mM borate buffer pH 8.9 and a 0.5 mM TTF + 1.0 mM* ***11*** *solution (red trace) in the same aqueous medium. Scan rate: 0.1 V s^{-1}. The insert shows the SWV responses of the same two solutions in the potential range associated with the first TTF oxidation.*

In order to confirm that the first one-electron oxidation of TTF is shut off upon encapsulation, we carried out voltammetric experiments using square wave voltammetry (SWV), a technique that has inherently better sensitivity than CV. In the absence of host **11**, we observed a small peak for the oxidation of the low concentration of TTF that

results from its limited aqueous solubility (see insert in Figure 2.5). However, in the presence of 2 equiv. of **11**, a 0.5 mM concentration of the TTF@**11**$_2$ assembly is present in the solution, but the SWV trace fails to reveal any significant faradaic current levels. Clearly, this result constitutes strong evidence for the hindered voltammetric response of encapsulated TTF.

The observed hindrance for the electron-transfer process from the guest (in TTF@**11**$_2$) to the electrode is probably due to very slow electrochemical kinetics, resulting from the increased distance between encapsulated TTF (compared to free TTF) and the electrode surface. We have used similar arguments to explain the lack of voltammetric response observed with the Fc@**11**$_2$ assembly.[24] However, oxidation of encapsulated Fc in the latter assembly can be accomplished using a cationic mediator,[25] which attaches itself quite strongly to the negatively charged surface of the **11**$_2$ capsule. In that case, oxidation of the guest leads to dissociation of the molecular assembly because the oxidized Fc^+ species is less hydrophobic than the neutral guest and does not serve as an effective molecular "glue" to keep the assembly together. In the case investigated here, slow oxidation of TTF@**11**$_2$

seems to take place, eventually leading to the observation of the TTF^{+} oxidation wave. However, the fact that the peak potential for this anodic wave is more positive than that observed for the same oxidation in the absence of host **11** is consistent with the release of TTF^{+} from the capsule. Furthermore, although the dicationic species (TTF^{2+}) decomposes rapidly under the basic pH conditions of our experiments, the reduction of a small amount of free TTF^{+} is observed in the reverse scan. All these observations clearly indicate that the slow electrochemical oxidation of TTF@$\mathbf{11}_2$ leads to the disassembly of the molecular capsule and the release of the less hydrophobic oxidized guest.

The oxidation of encapsulated TTF is quite slow but still allows the eventual observation of a more developed wave for the oxidation of TTF^{+}. This wave may also include faradaic components resulting from the kinetically hindered oxidation of TTF. The relatively loose fitting of TTF inside the $\mathbf{11}_2$ capsule may weaken the overall stability of the supramolecular assembly. The hypothesis that TTF fits loosely inside the inner space of the capsule (see Figure 2.6) is consistent with the lack of observation of an NMR resonance for the TTF protons in the assembly TTF@$\mathbf{11}_2$. This signal is likely to be broadened by the exchange of the

trapped guest among several possible locations inside the capsule. In contrast to this the bulkier ferrocene shows a relatively sharp resonance for its protons in the Fc@**11**$_2$ assembly.

Because of their importance in the research area of conducting organic solids, we also carried out experiments with two bulkier and more hydrophobic TTF derivatives, bis(ethylenedithio)tetrathiafulvalene (BEDT-TTF) and bis(propylenedithio)tetrathiafulvalene (BPDT-TTF) see structures in Figure 2.1). However, all our attempts to solubilize these TTF derivatives in aqueous solutions containing host **11** failed, preventing further experimentation with these guests. Two reasons can be put forward to rationalize the failure of these guests to drive the formation of **11**$_2$ capsules around them. First, these TTF derivatives are considerably more hydrophobic than TTF itself, which limits their aqueous solubility to even lower values and, thus, thwarts their binding interactions with host **11**. Second, both guests have larger molecular volumes than TTF, which restricts their inclusion in the cavity of the **11**$_2$ dimeric capsules. We have done some preliminary molecular modeling computations on these molecular assemblies and the results suggest that each of these

guests is bulky enough to prevent the hydrophobic head-to-head closing of the dimeric molecular capsules around them (see Figure 2.6).

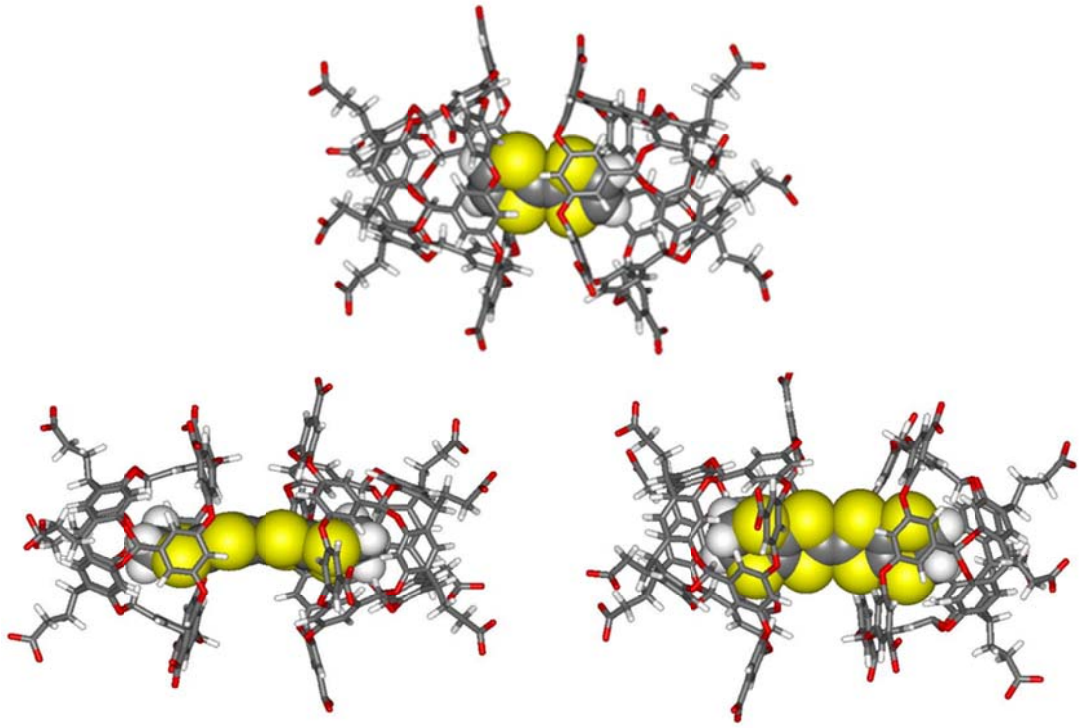

Figure 2.6 *Energy-minimized (PM3) TTF@**11**$_2$ (top) and BEDT-TTF@**11**$_2$ (bottom) supramolecular assemblies.*

2.3 Summary

In conclusion, we have demonstrated here that TTF is encapsulated inside a molecular capsule formed by the head-to-head assembly of two molecules of deep-cavity cavitand **11** in basic aqueous solution. The voltammetric response of TTF@**11**$_2$ is strongly hindered, although slow oxidation of

encapsulated TTF leads to the disruption of the molecular assembly. These results constitute an excellent example of two complementary phenomena. First, supramolecular structures can exert strong effects on the kinetics of heterogeneous electron transfer reactions. Second, electron-transfer reactions can be used to effectively destroy or disrupt supramolecular assemblies.

2.4 Experimental Section

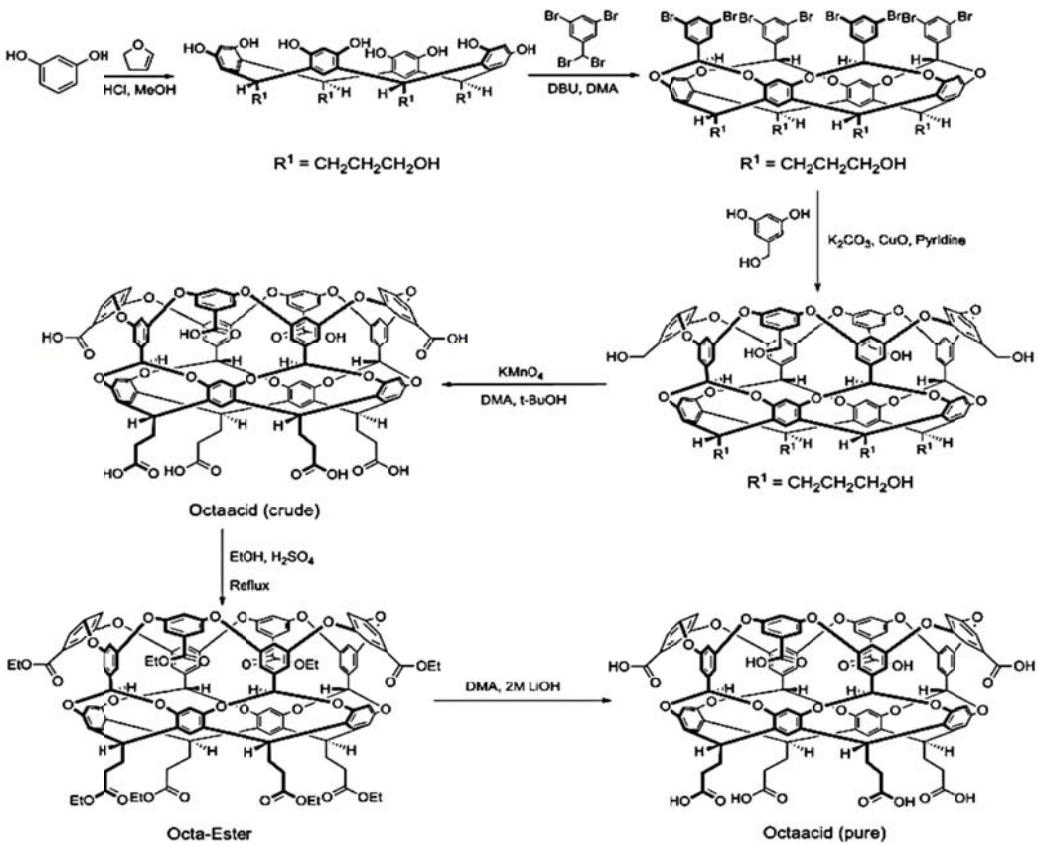

Scheme 2.1 *Synthesis route for cavitand host* ***11.***

Materials: The cavitand host (compound **11**) was prepared as reported by Gibb and co-workers (Scheme 2.1).[16,51] All other chemicals were of the highest purity available and purchased from commercial suppliers.

Electrochemistry: The voltammetric experiments were recorded using a single-compartment cell fitted with a glassy carbon working electrode (0.071 cm^2), a platinum auxiliary electrode, and a Ag/AgCl reference electrode. The working electrode was polished immediately before the experiments using a water/alumina (0.05 µm) slurry on a felt surface. The solution was thoroughly deoxygenated by purging with high purity nitrogen gas and maintained under a nitrogen atmosphere during the experiments.

***Computational Studies*:** Energy minimization of supramolecular structures was carried out using the PM3 semi-empirical method as implemented in the Gaussian software package (03 version).

CHAPTER 3

TRAPPING OF BULKY GUESTS INSIDE A DIMERIC MOLECULAR CAPSULE FORMED BY TWO DEEP-CAVITY CAVITANDS

3.1 General Discussion

In chapter 2, we presented our work on the study of encapsulating tetrathiafulvalene (TTF) inside the molecular capsule $\mathbf{11}_2$. In this chapter, we continue our research work by trapping bulky ferrocene-adamantane guests inside $\mathbf{11}_2$ dimeric capsules.

Adamantane (Ad) and ferrocene are two hydrophobic groups with pronounced differences from a chemical standpoint, but similar sizes. Both adamantane and ferrocene individually serve as hydrophobic guests to drive the formation of $\mathbf{11}_2$ capsules. Ramamurthy and co-workers have reported the entrapment of two adamantane molecules inside $\mathbf{11}_2$ assemblies under certain experimental conditions.[45,52] Given the availability in our group of compounds containing both units (see compounds **12-14** in Figure 3.1) we decided to investigate the possible encapsulation of these compounds inside $\mathbf{11}_2$ dimeric capsules.

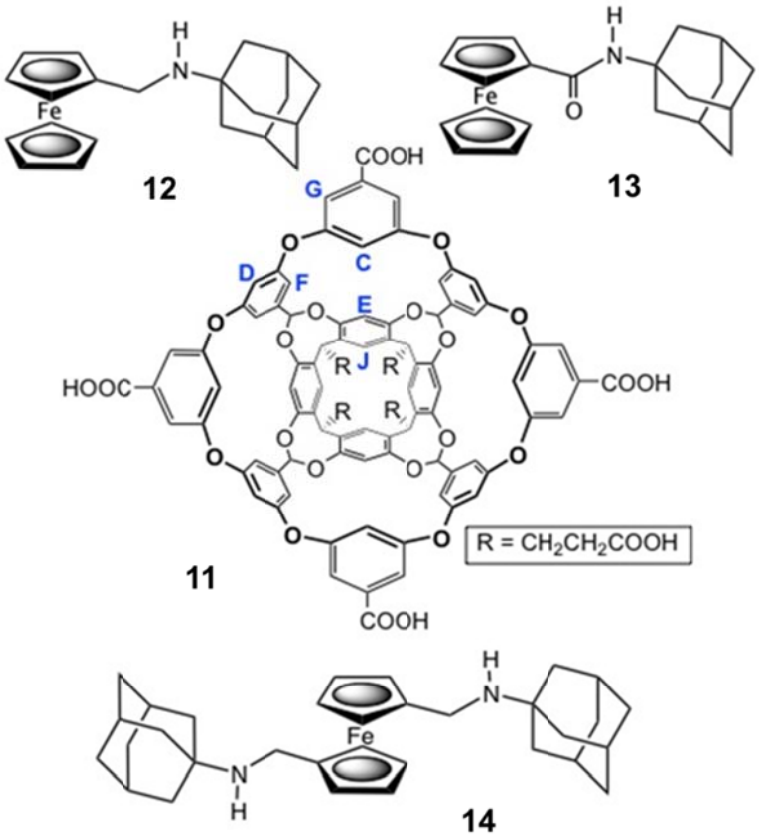

Figure 3.1 *Structures of the octaacid cavitand **11** and the guests (**12-14**) used in this work.*

3.2 Experimental Results and Discussion

In analogy with ferrocene, adamantane acts as an ideal hydrophobic guest leading to its encapsulation inside dimeric capsules of cavitand **11**. However, according to Ramamurthy and co-workers,[45,52] adamantane can also form 2:2 complexes with **11**, that is, when excess guest is present, two adamantane molecules are included inside the $\mathbf{11}_2$ assembly. In our investigation of ferrocene inclusion by $\mathbf{11}_2$

capsules we never found clear evidence for a similar 2:2 complex, in which two ferrocenes would share the inner space of the molecular capsule. Therefore, before starting any work with guests **12-14**, we attempted the simultaneous encapsulation of ferrocene and adamantane inside **11**$_2$. Unfortunately, our efforts were in vain and we could not collect any evidence for such supramolecular species. When an aqueous solution containing **11** was exposed to an equimolar mixture of ferrocene and adamantane, the resulting NMR spectrum (Figure 3.2) shows signals corresponding to both encapsulated guests. However, the signals for the host protons do not show any evidence for the reduced symmetry of the **11**$_2$ capsule that would be expected if two different bulky guests were included. Further analysis of this NMR spectrum using 2D NOESY techniques (Figure 3.3) reveals the spatial proximity of the encapsulated guest protons to some of the host protons, but no cross peaks between ferrocene and adamantane protons. All these data suggest the formation of Ad@**11**$_2$ and Fc@**11**$_2$, but no evidence for capsules containing both guests. Similarly, if we add excess adamantane to a solution already containing the Fc@**11**$_2$ complex, the final result is a solution containing the two 1:2 inclusion complexes. Under our experimental conditions, we could not obtain evidence

for the formation of any of the possible species containing more than one guest, that is, $(Ad)_2@\mathbf{11}_2$, $(Fc)_2@\mathbf{11}_2$, or (Ad-Fc)$@\mathbf{11}_2$. We must note that these experiments are complicated by the poor solubility of both guests in aqueous solution, a factor that also hinders the accurate quantitative determination of the adamantane/ferrocene selectivity exhibited by the $\mathbf{11}_2$ assembly. In general terms, these negative experimental results highlight the inherent entropic decrease associated with the assembly of four individual molecules (two guests and two hosts) to form a 2:2 supramolecular complex.

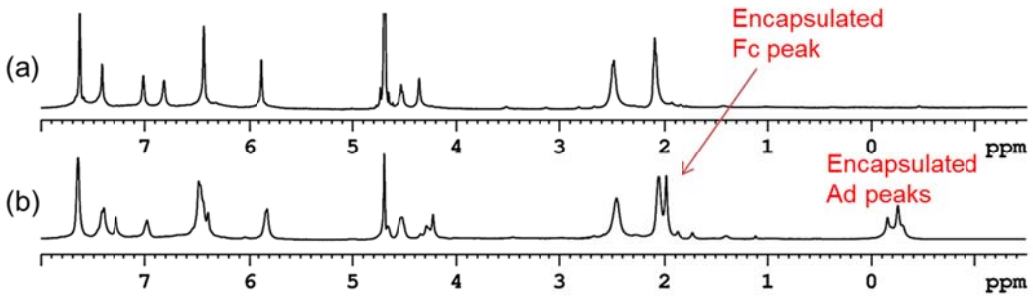

Figure 3.2 *^{1}H NMR spectra (500 MHz, 10 mM borate buffer pH 8.9 in D_2O) of host **11** (1.0 mM) (a) in the absence and (b) in the presence of Fc (0.5 mM) + Ad (0.5 mM).*

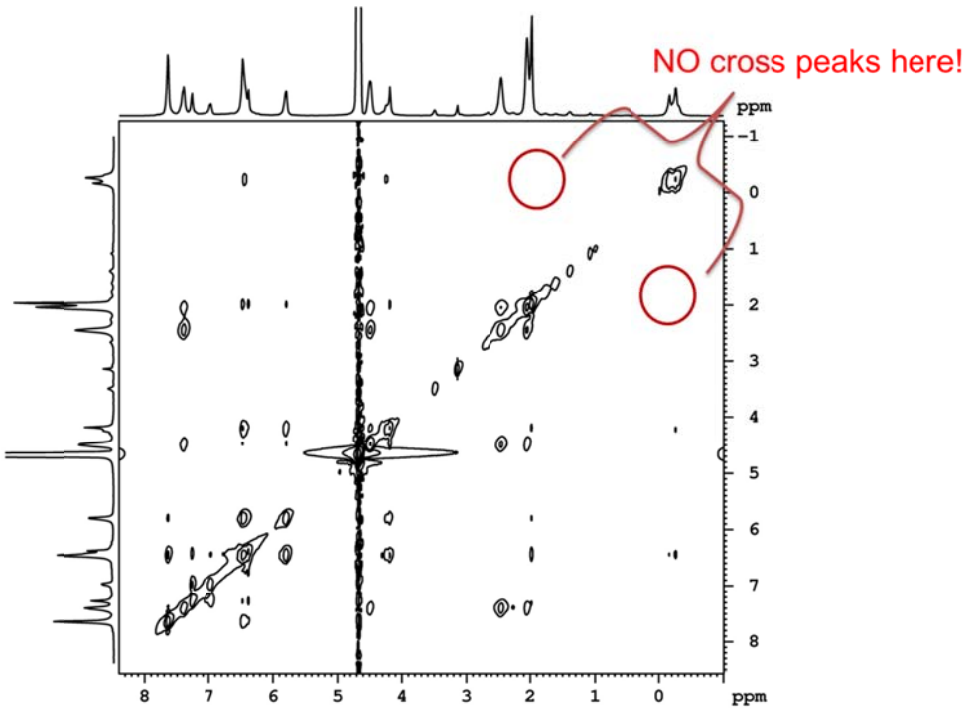

Figure 3.3 *NOESY NMR spectrum (500 MHz, 10 mM borate buffer pH 8.9 in D_2O) of host* ***11*** *(1.0 mM) in the presence of Fc (0.5 mM) + Ad (0.5 mM).*

Guests **12** and **13** have similar structures. Both contain ferrocenyl and adamantyl residues and their differences relate to the functional groups connecting them. Guest **12** is an amine, in which the central nitrogen is connected to ferrocenylmethyl and adamantyl groups, while guest **13** is a ferrocenecarboxylamide in which the adamantyl group is connected to the amide's nitrogen. Guest **12** can be protonated under acidic conditions. Following well-established methodology with cavitand **11**, we carried out all our experiments in mildly basic aqueous solution (pH =

8.9). Based on voltammetric titration data (Figure 3.4) the pKa of this compound was measured to be around 8.6, so guest **12** exists in our solutions as a mixture of protonated (**12**H^+) and unprotonated (**12**) species. However, given the hydrophobic character of the inner cavity of $\mathbf{11}_2$, it is reasonable to assume that only the basic species **12** is encapsulated inside the $\mathbf{11}_2$ capsular assembly. Similar arguments would apply to the bisamine guest **14**.

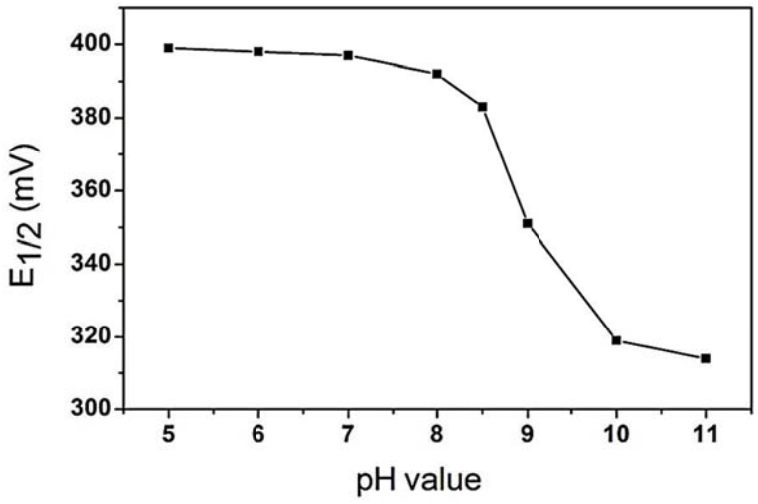

Figure 3.4 *Variation of the half-wave potential for the oxidation of guest **12** with the pH of the solution. Potentials measured by cyclic voltammetry on glassy carbon (0.07 cm^2) immersed in a 0.5 mM guest **12** solution also containing 50 mM NaCl. Scan rate: 0.1 V s^{-1}.*

Guest **12** appears to be readily included inside $\mathbf{11}_2$ as suggested by NMR spectroscopic data. Figure 2.5 shows the NMR spectrum of guest **12** in the absence and in the presence

of 2.0 equiv of cavitand **11**. Clearly, in the presence of **11**, both the ferrocenyl and adamantyl protons are strongly shifted upfield, as expected due to their encapsulation inside the aromatic walls of cavitand **11**. In addition to this, the signals corresponding to the cavitand protons are split into two sets (with the exception of the L and M protons, which are in the cavitand "feet", too far removed from the supramolecular action). This signal splitting of the host protons is in excellent agreement with the breakup of the equatorial symmetry of the $\mathbf{11}_2$ capsule, due to the inclusion of an asymmetric guest with two different ends (ferrocene and adamantane), which should lead to different chemical shifts for equivalent protons on the two cavitands forming the molecular capsule.

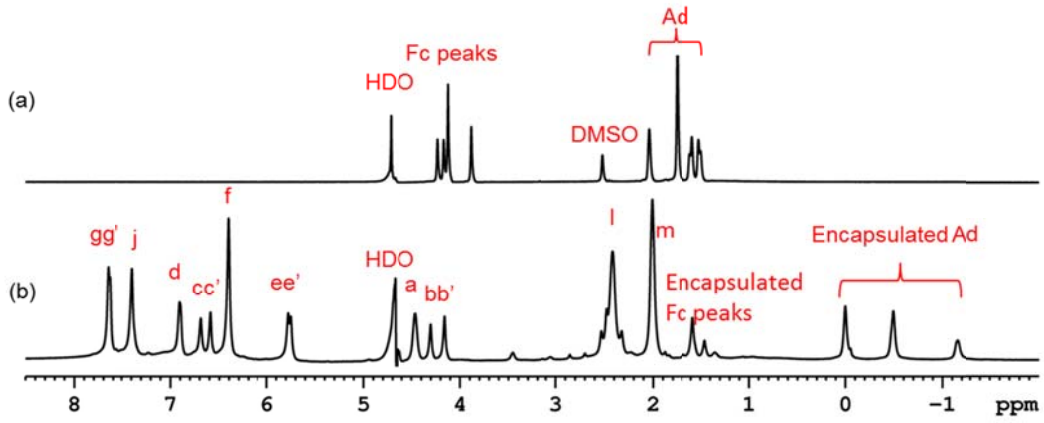

Figure 3.5 *^{1}H NMR spectra (500 MHz, 10 mM borate buffer pH 8.9 in D_2O) of guest **12** (0.5 mM) (a) in the absence and (b) in the presence of 2.0 equiv **11**.*

Figure 3.6 shows partial ^{1}H NMR spectra of cavitand **11** in the presence of increasing amounts of guest **12**. Addition of the guest to the solution containing cavitand **11** leads to the evolution of a new set of split peaks for the host protons. When guest **12** reaches about 0.5 equiv, only the proton signals corresponding to the **12@11**$_2$ assembly are visible, and further addition of guest **12** does not result in any change for the proton signals of **11**.

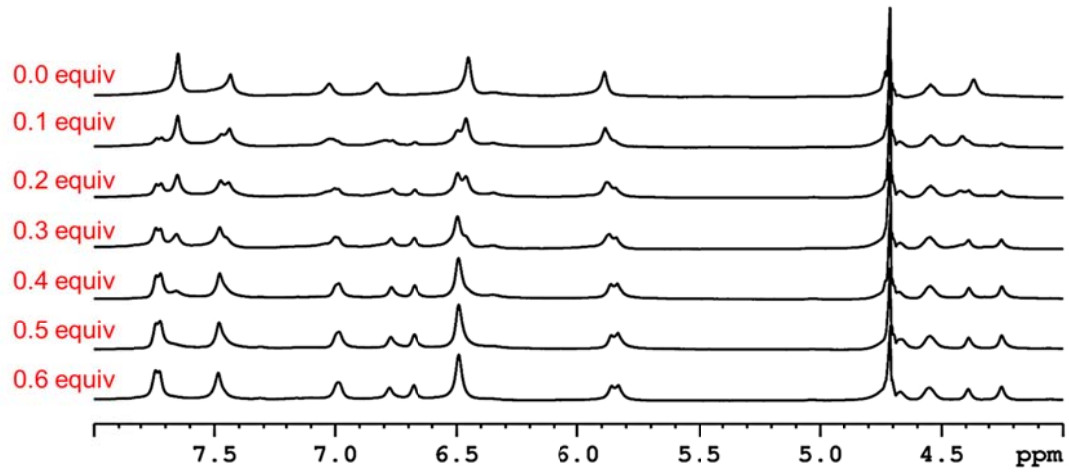

Figure 3.6 *Aromatic sections of the ^{1}H NMR spectra (500 MHz, 10 mM borate buffer pH 8.9 in D_2O) of host **11** (1 mM) in the presence of increasing concentrations of guest **12**.*

Two-dimensional DOSY NMR experiments are useful to determine diffusion coefficients (D_0) of molecules in the solution phase.[48] The corresponding 2D spectra show that all guest signals have identical D_0 values to those

corresponding to the host signals except peaks that are close to the water peak, an artifact that results from the irradiation of the water peak for suppression purposes. The measured diffusion coefficient of 1.45×10^{-6} cm^2/s is consistent with other D_0 values previously reported for guest@**11**$_2$ species,[27] further confirming the formation of the **12**@**11**$_2$ complex in aqueous solution.

Given our interest in the electrochemical behavior of encapsulated redox centers, we carried out cyclic voltammetric experiments with solutions containing variable concentrations of cavitand **11** and guest **12**, which contains a redox-active ferrocenyl residue in its structure. Our voltammetric data (Figure 3.7) clearly show that the current levels corresponding to the reversible one-electron oxidation of the ferrocenyl residue are gradually attenuated in the potential window from 0 mV to 600 mV, as the host/guest molar ratio increases. When 2.0 equiv of cavitand **11** are added to the solution, the cyclic voltammograms recorded for guest **12** are basically flat and no measurable faradaic currents associated with the oxidation of the ferrocenyl unit were detected in the potential range where its electrochemical oxidation is clearly observed in the absence of **11**. These experimental

results are very similar to those recorded with Fc@**11**$_2$ and suggest that the encapsulation of guest **12** leads to a considerable attenuation of the electrochemical kinetics for the oxidation of the ferrocenyl residue.[24,25]

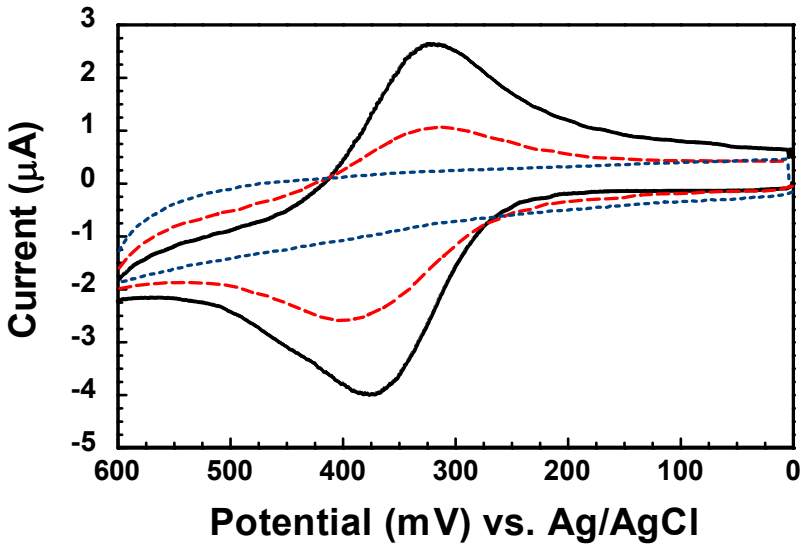

Figure 3.7 *Cyclic voltammetric responses on glassy carbon (0.07 cm^2) of 0.5 mM guest **12** in 10 mM borate buffer (pH 8.9) also containing 50 mM NaCl in the absence (solid line), in the presence of 1.0 equiv (discontinuous line) and 2.0 equiv (dotted line) of host **11**. Scan rate: 0.1 V s^{-1}.*

Guest **13** is basically insoluble in water due to its considerable hydrophobic character. When adding solid **13** to a solution containing cavitand **11**, we did not observe any dissolution of the guest immediately after its addition. However, after heating at 60 ^{0}C and 2 hours of sonication, guest **13** was gradually dissolved into the cavitand-containing solution. The appearance of signals

corresponding to the included guest and the splitting of host peaks in the ^{1}H NMR spectra clearly demonstrated the formation of the **13@11**$_2$ complex (see Figure 3.8). Due to the extremely low solubility of guest **13** in aqueous solution, no faradaic currents could be recorded when running cyclic voltammetry with the free (undissolved) guest. But in analogy to the **12@11**$_2$ complex, **13@11**$_2$ showed flat cyclic voltammograms in the potential window for ferrocene oxidation (Figure 3.9).

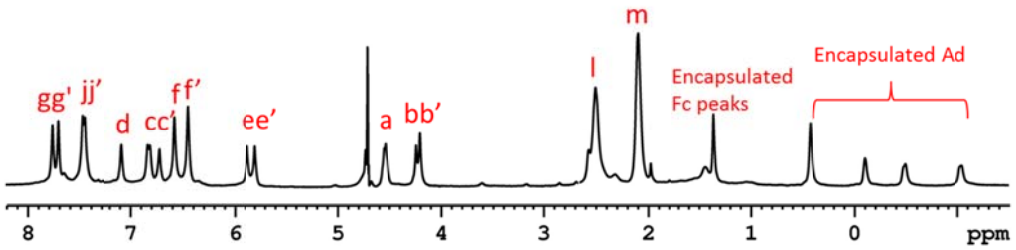

Figure 3.8 *^{1}H NMR spectrum (500 MHz, 10 mM borate buffer pH 8.9 in D_2O) of guest **13** (0.5 mM) in the presence of 2.0 equiv **11**.*

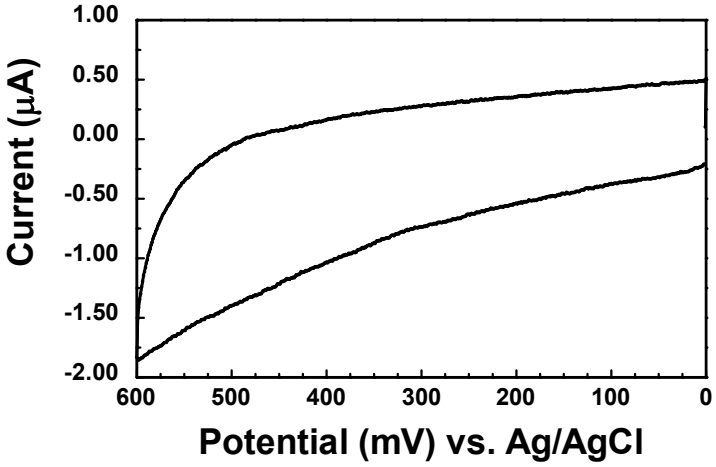

Figure 3.9 *Cyclic voltammetric response on glassy carbon (0.07 cm^2) of 0.5 mM guest **13** in 10 mM borate buffer (pH 8.9) also containing 50 mM NaCl in the presence of 2.0 equiv **11**. Scan rate: 0.1 V s^{-1}.*

Noticeably, guests **12** and **13** have similar sizes and both fill ca. 62% of the available space within the cavity of capsule $\mathbf{11}_2$, suggesting that these guests are not too far from optimal inclusion fit according to Rebek's rule,[53] which establishes 55% occupation as ideal in host-guest inclusion phenomena. However, the level of occupation of the cavity suggests a tight fit of either guest inside the dimeric molecular capsule.

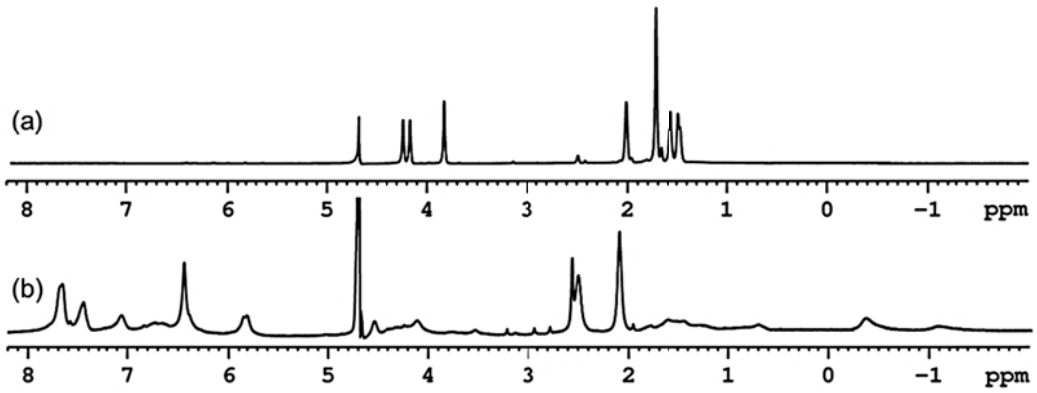

Figure 3.10 *^{1}H NMR spectra (500 MHz, 10 mM borate buffer pH 8.9 in D_2O) of guest **14** (0.5 mM) (a) in the absence and (b) in the presence of 2.0 equiv **11**.*

In contrast to guests **12** and **13**, guest **14** contains two adamantyl units connected to the central ferrocenyl unit. When 2.0 equiv of cavitand **11** was added, the inclusion of the terminal adamantyl units of guest **14** within the host was evident from the upfield shift of the adamantyl hydrogen signals (Figure 3.10). The extensive broadening of guest and host signals observed in the ^{1}H NMR experiments is probably due to the rapid exchange among bound and unbound states involving guest **14** and cavitand **11**. This is related to the flexibility of guest **14** and the relatively dynamic binding between the adamantyl groups and the cavitand hosts, which results in a more flexible and labile supramolecular assembly.

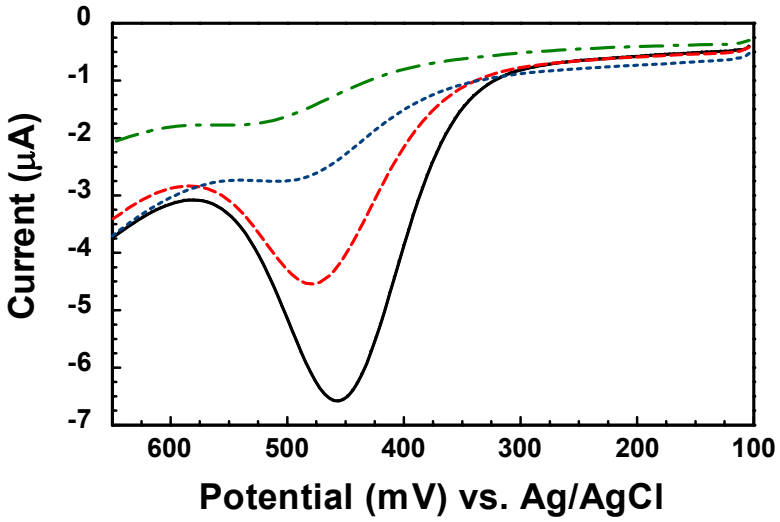

Figure 3.11 *Square wave voltammetric responses on glassy carbon (0.07 cm^2) of 0.5 mM guest **14** in 10 mM borate buffer (pH 8.9) also containing 50 mM NaCl in the absence (solid line), in the presence of 1.0 equiv (discontinuous line), 2.0 equiv (dotted line) and 3.0 equiv (dash-dote line) of host **11**. Scan rate: 0.1 V s^{-1}.*

Square wave voltammetry (SWV) was also used to investigate the interactions between guest **14** and cavitand **11**. When 2.0 equiv of **11** was added to a solution containing 0.5 mM guest **14**, the current for the oxidation of the ferrocene subunit was reduced owing to the slow diffusional motion of the complex (Figure 2.11), but not completely depressed, suggesting that the electroactive ferrocenyl unit in guest **14** was still "exposed" to the electrode. The half-wave potential ($E_{1/2}$) for the oxidation of the ferrocene subunit also shifted positively, compared to the value for the free guest, presumably indicating that the

ferrocene subunit surrounded by two bulky cavitands, though not completely sealed inside a capsule, still experiences a relatively hydrophobic microenvironment, which would stabilize the reduced form of the central ferrocenyl unit and hinder the solvation of the oxidized ferrocenium residue by water molecules. Due to the large size of guest **14**, formation of the snugly closed capsule around this guest is sterically impossible.

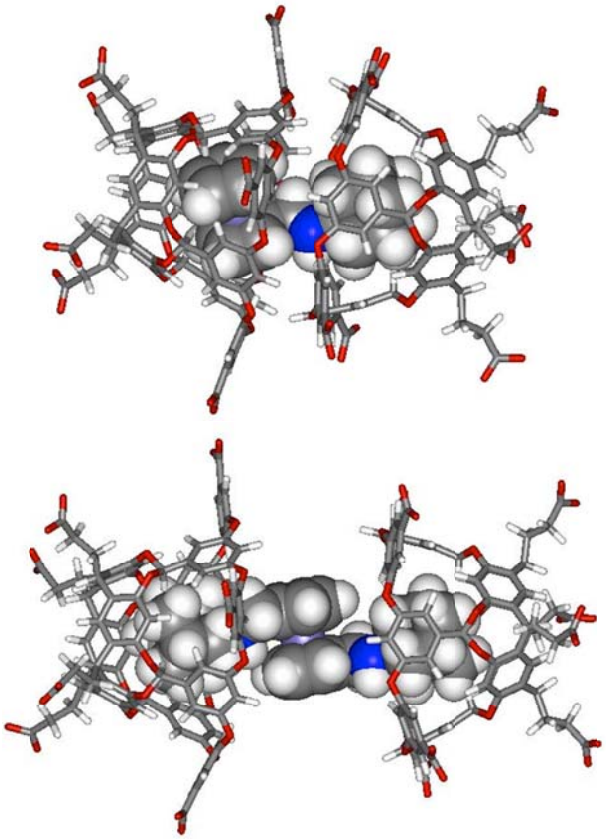

Figure 3.12 *Energy minimized structures (PM3) of the supramolecular assemblies formed by interaction of two molecules of cavitand* ***11*** *with guest* ***14*** *(top) and with guest* ***12*** *(bottom).*

From these experimental results, we postulate a pseudo-capsular structure for the complex in which each of the adamantyl units of guest **14** is included by cavitand **11**, leaving the connecting ferrocenyl unit of the guest still exposed to the solution, through the cleft formed between the two capping cavitands (Figure 3.12). Rebek and co-workers have reported a similar pseudo-capsular assembly.[54]

3.3 Summary

In conclusion, we have presented data showing very clearly that cavitand **11** forms dimeric capsules around the bulky guests **12** and **13** in aqueous solution. Notably, we have not been able to obtain experimental evidence for the simultaneous encapsulation of freely diffusing adamatane and ferrocene. Both NMR spectroscopic and voltammetric data are consistent with the complete encapsulation of **12** and **13** inside $\mathbf{11}_2$ capsules. In contrast to this, guest **14** leads to a 1:2 complex with two molecules of cavitand **11** bound to the terminal adamantyl residues. This complex is not, however, a "sealed" molecular capsule, and the middle ferrocenyl residue does not appear to be included inside the supramolecular assembly, as evidenced by the measurable

voltammetric response recorded for the electrochemical oxidation of the ferrocenyl unit.

3.4 Experimental Section

Materials. The cavitand host (compound **11**) was prepared as reported by Gibb and co-workers.[16,51] All other chemicals were of the highest purity available and purchased from commercial suppliers.

Synthesis of adamantyl(ferrocenylmethyl)amine (12): To an absolute methanol solution (50 mL) of ferrocenecarboxaldehyde (200 mg, 0.93 mmol) and 1-adamantylamine (948 mg, 6.3 mmol) also containing activated 4A type molecular sieves was added 5 M HCl in methanol to adjust the pH of the solution to ca. 7. After stirring for 1 h at r.t. under N_2, $NaBH_3CN$ (352 mg, 5.6 mmol) was added to the reaction mixture, which was then heated and stirred at 60 ^{o}C for 2 days. The resulting mixture was filtered through Celite 545 and then concentrated in vacuo to give a red solid, which was purified by column chromatography on Al_2O_3 (neutral) using chloroform and ethyl acetate (5:1) as the eluent. The yellow solid product was obtained after solvent evaporation and recrystallized from methanol (130 mg, yield: 36.1%). ESI-HRMS (m/z) calcdfor $C_{21}H_{28}NFe$:

350.1571, found: 350.1579. ^{1}H NMR (500 MHz, D_2O): 1.54 (ds, 3H), 1.62 (ds, 3H), 1.78 (s, 6H), 2.07 (s, 3H), 3.92 (s, 2H), 4.16 (s, 5H), 4.20 (s, 2H), 4.27 (s, 2H). ^{13}C NMR (125 MHz, D_2O): 28.75, 34.86, 37.94, 39.41, 57.46, 68.91, 69.55, 69.90, 76.73.

Synthesis of adamantylferrocenecarboxylamide (13): Ferrocenecarboxaldehyde (200 mg, 0.87 mmol) was mixed with 1-adamantylamine (158 mg, 1.04 mmol) in 200 mL anhydrous dichloromethane. To this solution n-HATU (397 mg, 1.04 mmol) and proton sponge (224 mg, 1.04 mmol) were added. The reaction mixture was stirred under N_2 at r.t. for 1 day and then concentrated in vacuo to give a red solid, which was purified by column chromatography (SiO_2) using hexane/chloroform/ethyl acetate (2/2/1) as the eluent. The final product was obtained (200.8 mg, yield: 63.6%) after solvent evaporation and recrystallized from $CH_3CN/CHCl_3$ (1/1). ESI-HRMS (m/z) calcd for $C_{21}H_{26}NOFe$: 364.1364, found: 364.1351. ^{1}H NMR (500 MHz, d_6-DMSO): 1.63 (s, 6H), 2.02 (s, 9H), 4.11 (s, 5H), 4.27 (t, 2H), 4.80 (t, 2H), 6.72 (s, 1H). ^{13}C NMR (125 MHz, d_6-DMSO): 29.37, 36.59, 41.71, 50.69, 68.77, 69.83, 70.21, 78.04, 168.62.

1,1'-Bis(adamantylaminomethyl)ferrocene (14): To an absolute methanol solution (60 mL) of 1,1'-

ferrocenedicarboxaldehyde (200 mg, 0.83 mmol) and 1-adamantylamine (998 mg, 6.6 mmol) also containing 4A type molecular sieves was added 5 M HCl in methanol to adjust the pH of the solution to ca.7. After stirring for 1 h at r.t. under N_2, $NaBH_3CN$ (415 mg, 6.6 mmol) was added to the reaction mixture which was then refluxed for 2 days. The resulting mixture was filtered through Celite 545 and then concentrated to give a red residue, which was purified by column chromatography on Al_2O_3 (neutral) using $CHCl_3$/EtOAc/MeOH (20/4/1) as the eluent. The yellow solid product was obtained after the solvent was evaporated and recrystallized from hot methanol (90.5 mg, yield: 21.4%). ESI-HRMS (m/z) calcd for $C_{32}H_{45}N_2Fe$: 513.2932, found: 513.2940. ^1H NMR (500 MHz, D_2O): 1.50 (ds, 6H), 1.59 (ds, 6H), 1.74 (s, 12H), 2.04 (s, 6H), 3.86 (s, 4H), 4.20 (s, 4H), 4.26 (s, 4H). ^{13}C NMR (125 MHz, D_2O): 28.91, 35.66, 38.05, 39.09, 56.98, 70.52, 71.98, 78.98.

Electrochemistry: The voltammetric experiments were recorded using a single-compartment cell fitted with a glassy carbon working electrode (0.071 cm^2), a platinum auxiliary electrode, and a Ag/AgCl reference electrode. The working electrode was polished immediately before the experiments using a water/alumina (0.05 μm) slurry on a

felt surface. The solution was thoroughly deoxygenated by purging with high purity nitrogen gas and maintained under a nitrogen atmosphere during the experiments.

Computational Studies: Energy minimization of supramolecular structures was carried out using the PM3 semi-empirical method as implemented in the Gaussian software package (03 version). Guest molecular volumes were calculated with YASARA and compared with the cavity volumes computed using the SPDB viewer (version 4.04).

CHAPTER 4

BINDING OF CUCURBIT[7]URIL WITH A TRIS(VIOLOGEN) DERIVATIVE GUEST

4.1 General Discussion

In Chapter 1 we had a brief introduction of binding cucurbit[7]uril with viologen (V^{2+}) guests. In this chapter, we will present more details based on our research work.

Viologens (V^{2+}) can undergo two consecutive one-electron reductions to firstly form a fairly hydrophobic radical cation species (V^{+}) and then a fully reduced neutral (V) species,[55] which may precipitate on the working electrode and distort the shapes of the voltammetric peaks. Both reduction processes can take place at accessible potentials in aqueous and non-aqueous solutions with electrochemical reversibility. Kaifer's group had previously pointed out that the removal of one positive charge from V^{2+} ($V^{2+} + e^{-} = V^{+}$) has a relatively minor effect on the host-guest binding affinity with CB7 compared to that of hydrophobic interactions, based on the experimental result that the $E_{1/2}$ value for the process shifts only 25 mV cathodically in the presence of one equivalent of CB7.[37]

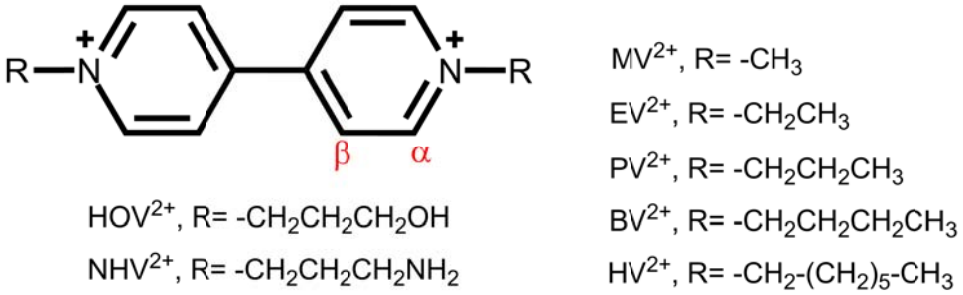

Figure 4.1 *Structures of viologen dications used as guests for CB7.*[56]

Moon and Kaifer studied a series of viologen guests (see Figure 4.1) binding with one equivalent of CB7 in aqueous solution and showed an interesting trend.[56] For the more polar HOV^{2+} and NHV^{2+} guests, CB7 will selectively reside on the viologen aromatic residue, where favorable ion-dipole interactions between both quaternized nitrogens and the carbonyl oxygens at the cavity openings (portals) of CB7 can develop. Similarly, CB7 prefers the central bipyridinium nucleus when the viologen's *N*-substituents are short aliphatic chains, such as methyl and ethyl. As the chain of the aliphatic substituent lengthens, so does the hydrophobicity, which partially switches the binding position of CB7 from the central aromatic residue to one of the terminal alkyl substituents, resulting in a mixture of complexes, for example with PV^{2+}. When the *N*-substituent becomes sufficiently hydrophobic, such as butyl and heptyl,

CB7 exclusively interacts with one of the aliphatic groups and forms the external binding complexes.

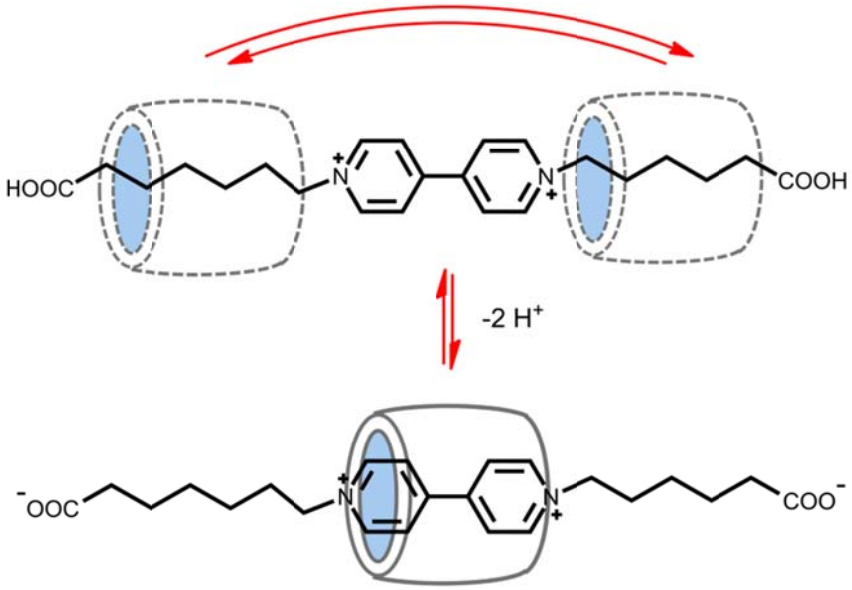

Figure 4.2 *CB7 binding of a dicarboxylate-terminated viologen guest in its protonated and deprotonated states.*[57]

Kaifer's group also designed a dicarboxylate-terminated viologen guest and demonstrated that by adjusting the pH of the aqueous solution, CB7 can be manipulated to sit on either central viologen site or one of the external two side arms.[57] As shown in Figure 4.2, when the dicarboxylate-terminated viologen guest is protonated, the CB7 host binds on one of the two equivalent binding sites of the guest and undergoes fast exchange. However, as the solution becomes more basic, strong electrostatic repulsions between the deprotonated terminal

carboxylates and the carbonyl oxygens on the CB7 host portals can push CB7 to engulf the central viologen site and lead to a less dynamic complex.

Scherman's group synthesized two tris(viologen)derivative compounds **15** and **16** in Figure 4.3, and investigated the self-assembly with three equivalents of CB8 in gas phase without solvent effects.[58] Our group is interested in the synthesis of novel cage molecules via "click" reaction (Copper (I)-Catalyzed Azide-Alkyne Cycloaddition (CuAAC)), and an intermediate compound **17** (Scheme 4.1) was synthesized for this purpose. In this chapter, we focus on the self-assembly of guest **17** with three equivalents of CB7 in aqueous solution and how the encapsulation will impact on the guest.

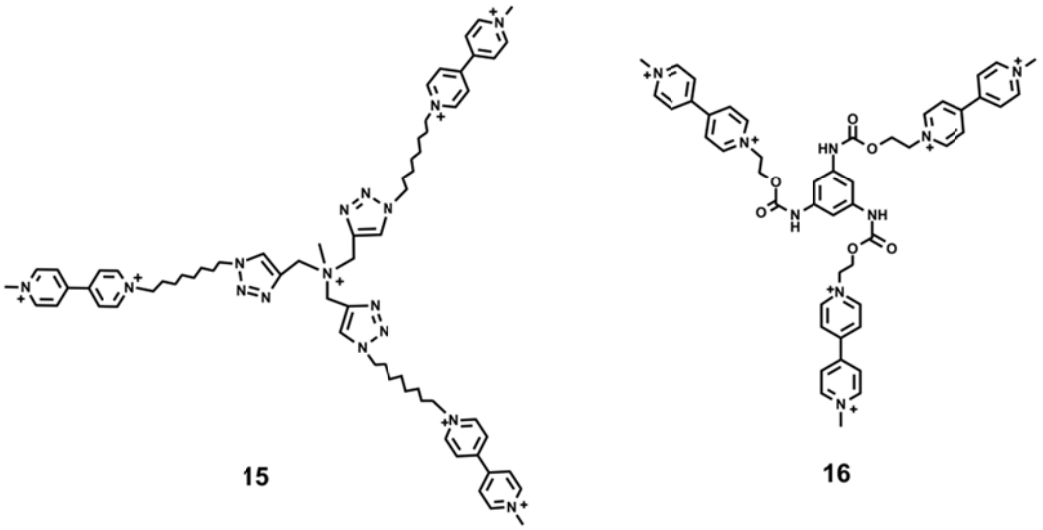

Figure 4.3 *Structures of tris(viologen) derivative guests **15** and **16**.*

4.2 Experimental Results and Discussion

The general synthesis route for tris(viologen) guest **17** is showed in Scheme 4.1. The as-synthesized **17·6PF$_6$** can be ion-exchanged to **17·6Cl** or **17·6Br**, which are extremely soluble in aqueous solution and very hygroscopic. In order to conveniently store and use the compound, we keep the as-synthesized **17·6PF$_6$**, which is slightly soluble in aqueous solution with solubility around 0.5 mM, enough to get reasonable ^{1}H NMR spectroscopic data and run electrochemistry experiments.

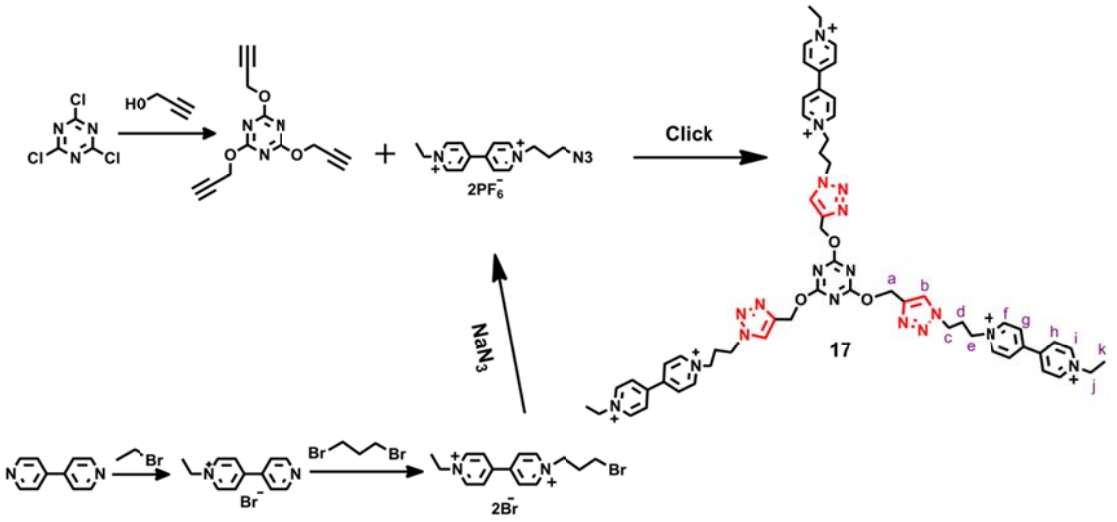

Scheme 4.1 *A general synthesis route for tris(viologen) guest* ***17****.*

We started our investigation by examining ^{1}H NMR spectroscopic data of **17** in the presence of variable amounts of host CB7. The experimental data are shown in

Figure 4.4. As CB7 is added (G:H=1:1.5), all the peaks are shifted to their final positions and broadened except terminal peaks “j” and “k”, which remain sharp. When the CB7 concentration reaches 3 equiv., in contrast, all the previously broadened peaks are sharpened and the originally sharp peaks “j” and “k” are broadened. Further additions of CB7 (G:H=1:6) no longer have any significant effect on the spectra except peaks “j” and “k”, which are further broadened. All the peaks assigned on Figure 4.4 are based on 2D NMR COSY experiments, and we are specifically interested in the situation where the concentration of guest versus host is equal to 1:3, assuming that all viologen moieties can be included inside CB7 (refer to Figure 4.5 for peak assignments). Peaks “g” and “h” corresponding to the β viologen protons show a 1.5 ppm upfield displacement from originally 8.4 ppm, in the absence of host, to 6.9 ppm when encapsulated inside CB7. The α-protons of the bipyridinium moiety are almost unchanged. These changes are consistent with the published results and are characteristic of the viologen·CB7 complex.[59] The downfield shift of peak “a” and peak “b”, instead, means the 1,2,3-triazole group of guest **17** does not undergo any encapsulation since the interactions with the electronegative oxygens on the CB7 portal cause reduced

electron density and the nuclei are therefore deshielded. The interesting part comes from peaks "c" and "d": peak "c" experiences a huge upfield shift(Δδ~+2.8 ppm), from originally 4.55 ppm to 1.75 ppm, in contrast, peak "d" significantly shifted to a lower field from 2.7 ppm to 4.7 ppm (Δδ~-2.0 ppm). It is difficult to explain here why the adjacent peak "c" and "d" suffer such huge different influences by CB7. The other peaks "e", "j" and "k", close to the quaternized nitrogens of the viologen unit undergo considerable chemical shift to higher magnetic field.

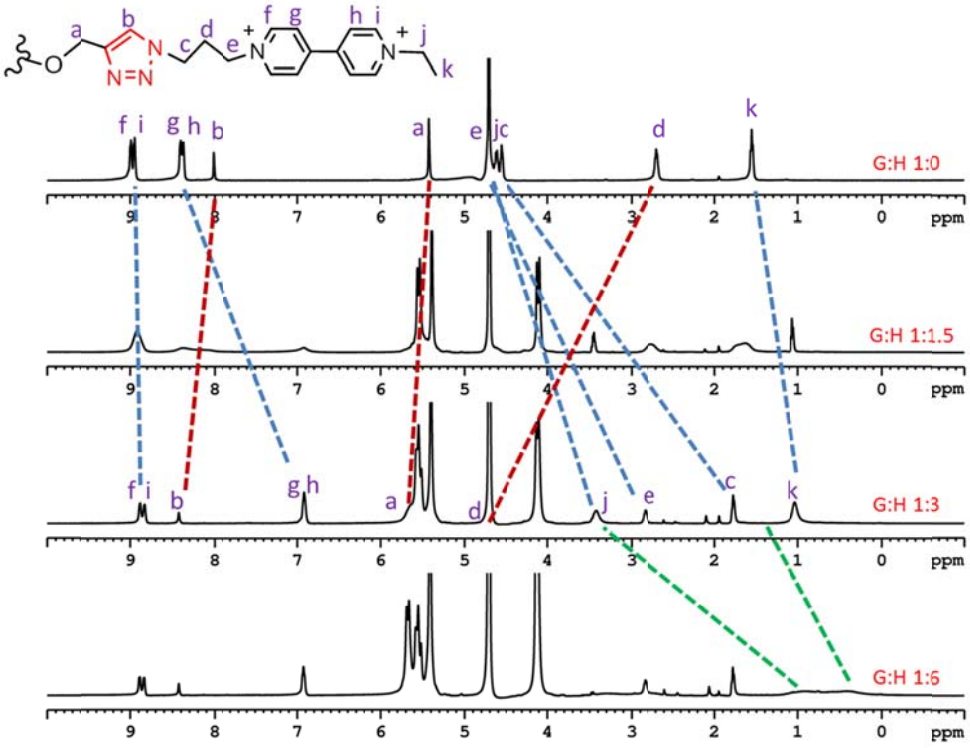

Figure 4.4 *^{1}H NMR spectra (500 MHz, in D_2O) of guest compound* ***17*** *(0.5 mM) in the presence of increasing concentrations of host CB7.*

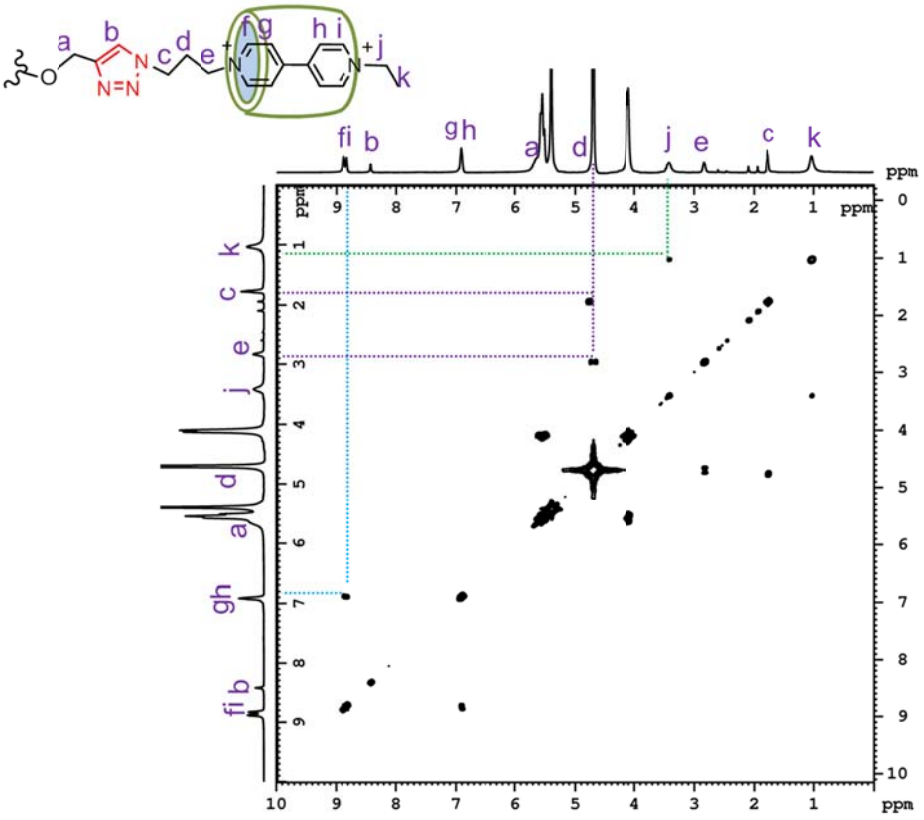

Figure 4.5 *2D NMR COSY spectrum (500 MHz, in D_2O) of guest compound* ***17*** *(0.5 mM) in the presence of 3.0 equiv of host CB7.*

We did a UV-Vis spectroscopic titration by monitoring the intensity of the electronic absorption band at a wavelength of 260 nm, which is characteristic of the viologen moiety in guest **17** (Figure 4.6 left). As the CB7 concentration increases in the solution, the detected intensity decreases. Until the n_H/n_G ratio reaches around 2.4, which is the ratio of CB7 concentration over guest **17** concentration, the intensity tends to level off. We also

use a Job-plot method to determine the stoichiometry of the binding between guest **17** and CB7 (Figure 4.6 right). In this method, the total molar concentration of guest **17** and CB7 are held constant, but their mole fractions are varied. A measurable parameter $\Delta A*X_{guest}$, which is proportional to the complex concentration, is plotted against the mole fractions of guest **17**. The maximum on the plot with mole fraction of **17** equals 0.33, corresponding to the stoichiometry of G/H as 1:2, which stands for **17**·$CB7_2$ complex. According to the graph, there are also considerable **17**·$CB7_3$ and **17**·CB7 complexes in solution. The Job-plot results are consistent with the results of UV-Vis titration, even though both of them do not show the theoretical 1:3 stoichiometry expected for the **17**·$CB7_3$ complex.

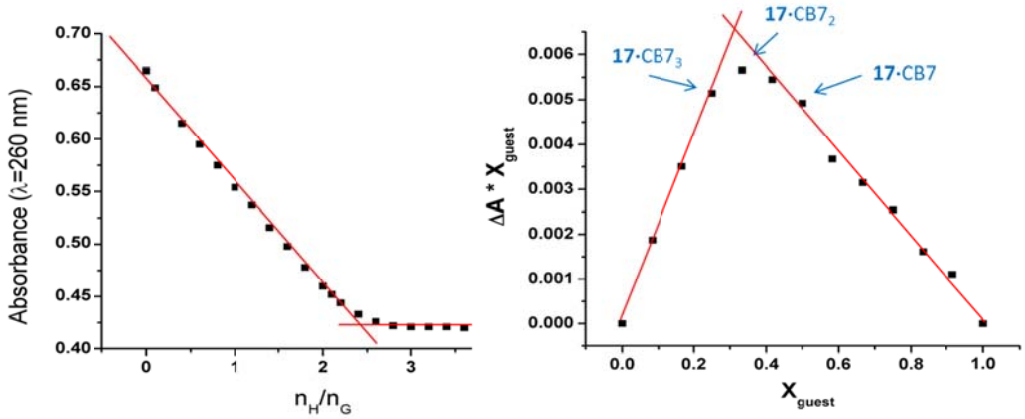

Figure 4.6 *UV-Vis spectroscopic titration results of CB7 to guest **17** (left) and Job-plot results for mole fractions of guest **17** (right).*

We submitted a sample containing one equivalent of **17** and three equivalents of CB7 for ESI-TOF mass spectrometry to investigate the presence of **17**·$CB7_3$ complex. From the spectroscopic results in Figure 4.7, we can conclude that the **17**·$CB7_3$ complex shows remarkable stability in the gas phase. The most intense signal is the parent complex without any counter ion, namely [**17**·$CB7_3$]$^{6+}$ (m/z=756.6008, z=6). As the number of attached PF_6^- counter ions to the supramolecular complex increases, the signal intensity of the complex decreases. We are still able to detect [**17·3PF$_6$**·$CB7_3$]$^{3+}$ (m/z=1658.1500, z=3) complex, even though the intensity is very low. By comparing to the theoretical data of [**17**·$CB7_3$]$^{6+}$ complex, our results convincingly prove the formation of the **17**·$CB7_3$ complex.

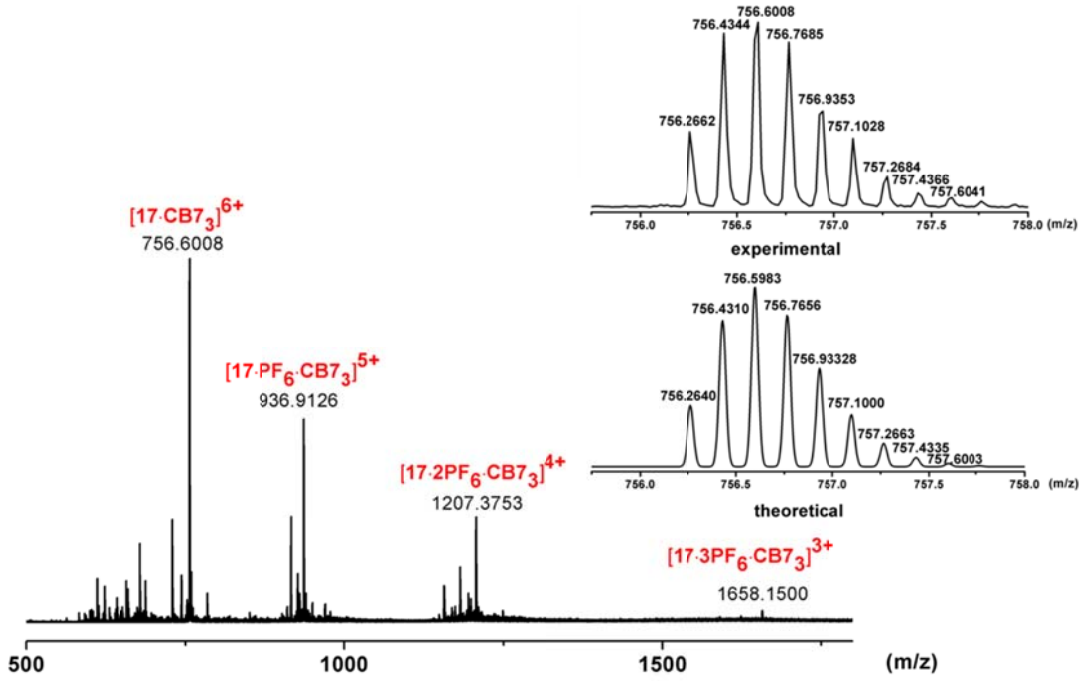

Figure 4.7 Full *ESI-TOF mass spectrum of* ***17***·$6PF_6$·$CB7_3$ *and comparison between experimental and theoretical fragment of* [***17***·$CB7_3$]$^{6+}$ *(upper right).*

We built a preliminary molecular modeling for the **17**·$CB7_3$ complex and the result is shown in Figure 4.8. From the computational result, we can see that each of the three viologen moieties in guest **17** is bound by a CB7 host to form the G:H 1:3 complex. We cannot clearly explain here why peaks "c" and "d" have abnormal chemical shifts based on this modeling result.

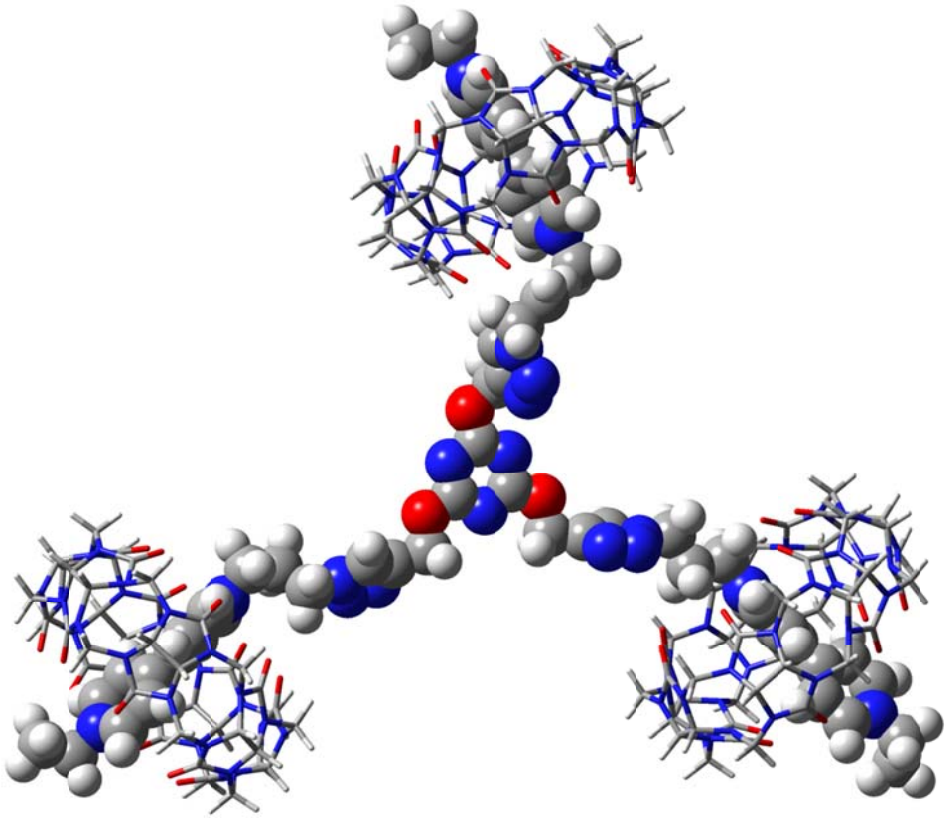

Figure 4.8 *Energy-minimized (PM3)* ***17***·$CB7_3$ *complex.*

We also carried out cyclic voltammetry (CV) experiments by adding one equiv. of CB7 each time into the 0.5 mM **17** solution (Figure 4.9). We can see that the voltammetric shape of the free guest in the CV result is distorted, with a very sharp oxidization peak around -400 mV and well separated reduction-oxidation process in potential range -630 ~ -1000 mV. As the host CB7 is added, the potential of the first reduction peak gradually moves to more negative values and the reversed sharp oxidation

peak reduces its currents and moves toward more positive potentials then back to an even more negative one. The second reduction-oxidation process gradually reduces their currents to show a slower electrochemical kinetics.

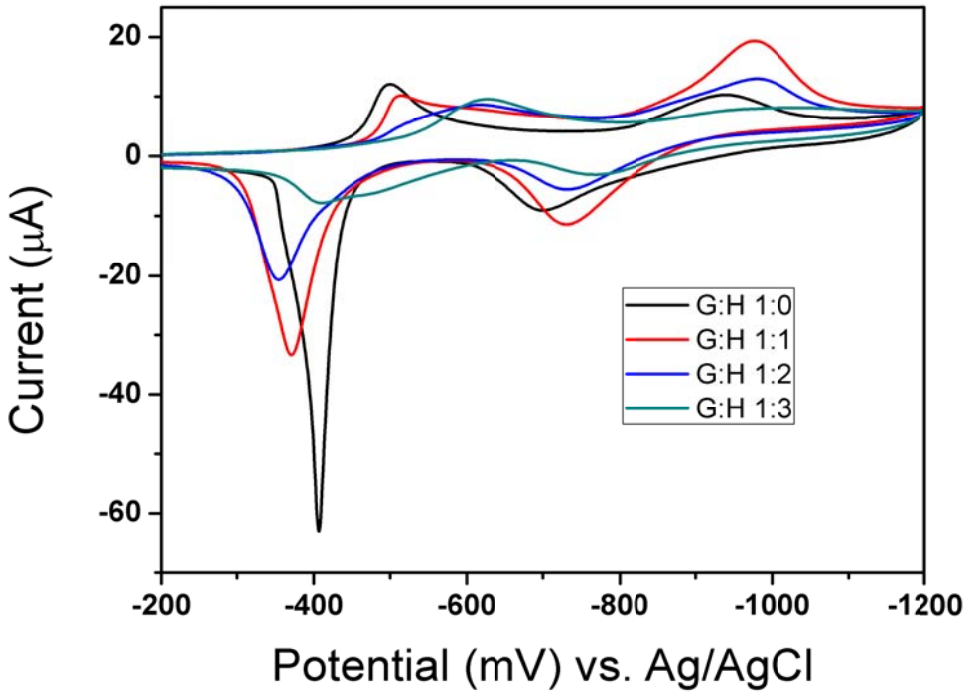

Figure 4.9 *Cyclic voltammetric responses on glassy carbon (0.07 cm^2) of 0.5 mM guest* ***17*** *containing 50 mM NaCl in the absence (black), in the presence of 1.0 equiv (red), 2.0 equiv (blue) and 3.0 equiv (green) of CB7. Scan rate: 0.1 V s^{-1}.*

We cannot totally understand the electron transfer process for this **17**·$CB7_3$ complex, but we have substantial experience in our group that the reduction of viologens (V^{2+}) to a fully neutral (V) species may precipitate the neutral (V) species on the working electrode and distort the shapes

of the voltammetric peaks. Therefore, we narrow the potential scan range of the **17**·$CB7_3$ complex by only focus on the first reduction-oxidation process, namely from $V^{2+} + e^- = V^+$ and then $V^+ - e^- = V^{2+}$. Our data in Figure 4.10 show that the guest voltammetry still has a distorted shape which tells us that the sharp oxidation peak is not distorted by fully reduced neutral species precipitated on the electrode surface, but by the fairly hydrophobic radical cation species (V^+). Upon addition of CB7, the reduction potential gradually moves from (-480 mV) to a more negative value (-620 mV), which corresponds to the reduction of the encapsulated viologen species. The oxidation peak gradually reduces its currents upon addition of CB7. Once CB7 concentration reaches three times of guest **17** concentration, the oxidation peak moves to a negative potential (-550 mV) which belongs to the oxidation of encapsulated radical cation species (V^+). From the G:H 1:3 voltammetry result (refer to the amplified insert in Figure 4.10), we can clearly see that viologen species of **17**·$CB7_3$ complex undergo reversible reduction-oxidation process with reduced currents at the potential rang -450 mV to -700 mV, which tells us that stabilized by CB7 the viologen species are more difficult to reduce and that the bulky size of

17·$CB7_3$ complex drags down the diffusion rate and, thus, decreases the current levels.

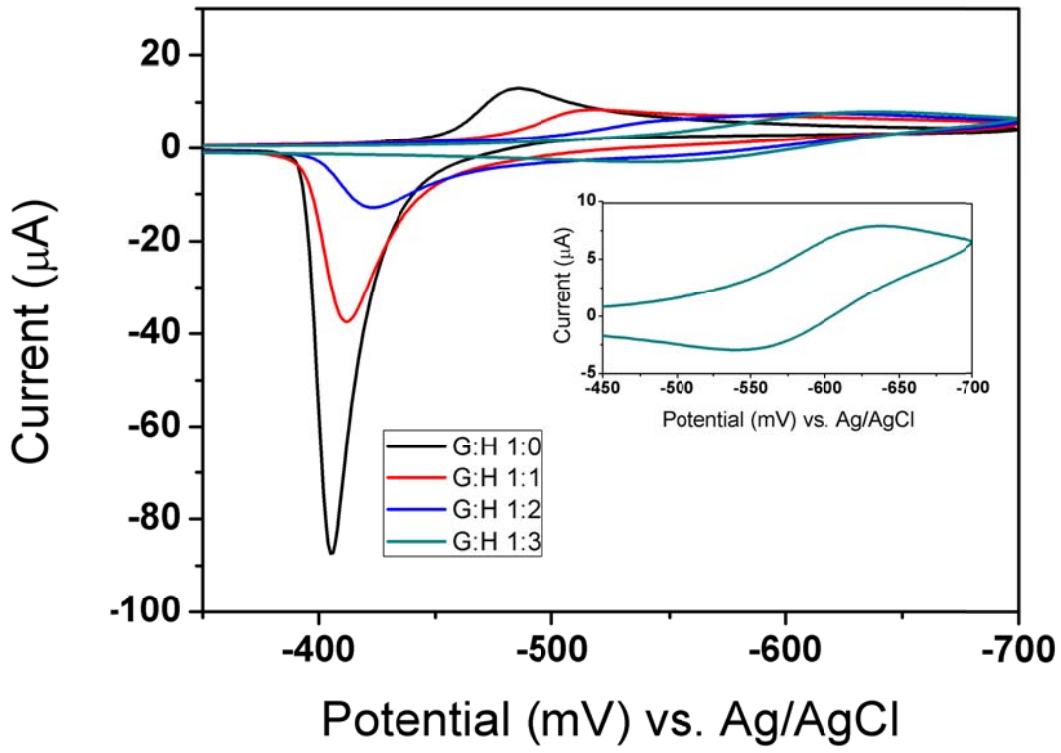

Figure 4.10 *Cyclic voltammetric responses on glassy carbon (0.07 cm^2) of 0.5 mM guest* ***17*** *containing 50 mM NaCl in the absence (black), in the presence of 1.0 equiv (red), 2.0 equiv (blue) and 3.0 equiv (green) of CB7. Scan rate: 0.1 V s^{-1}.*

Since the difficulty of clearly explaining the chemical shifts of peaks "c" and "d", we prepared a control compound **18**, composed of a single branch of the tris(viologen) guest **17** (Figure 4.11). We did similar studies by examining ^{1}H NMR spectroscopic data of **18** in the presence of variable amounts of host CB7. The results show

that guest **18**interacts with CB7 in a manner that is very similar to the previously discussed **17**·$CB7_3$ complex (Figure 4.4), with peaks "a", "b" and "d" undergoing downfield shifts and the remaining peaks experiencing upfield shifts. These results mean that each branch of the tris(viologen) guest **17** is an independent entity for the interaction with CB7, even though they are connected by a 1,3,5-triazine core.

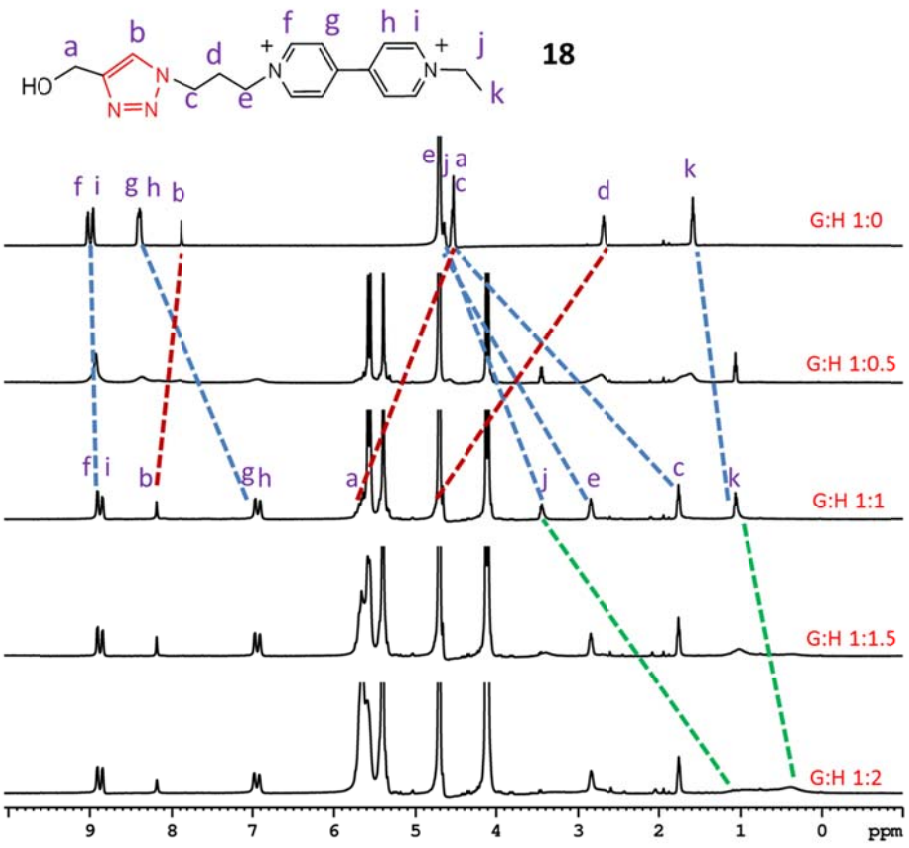

Figure 4.11 *^{1}H NMR spectra (500 MHz, in D_2O) of guest compound **18** (0.5 mM) in the presence of increasing concentrations of host CB7.*

In fact, we have done some preliminary molecular modeling computations on the molecular assemblies and the results in Figure 4.12 suggest that the flexible propyl (-$CH_2CH_2CH_2$-) connector that links bipyridinium moiety and 1,2,3-triazole moiety together is twisted around one portal of CB7, pushing proton "d" away from the portal and protons "c" and "e" comparatively closer to the portal, which may be one of the reasons that cause the abnormal chemical shifts of protons "c" and "d".

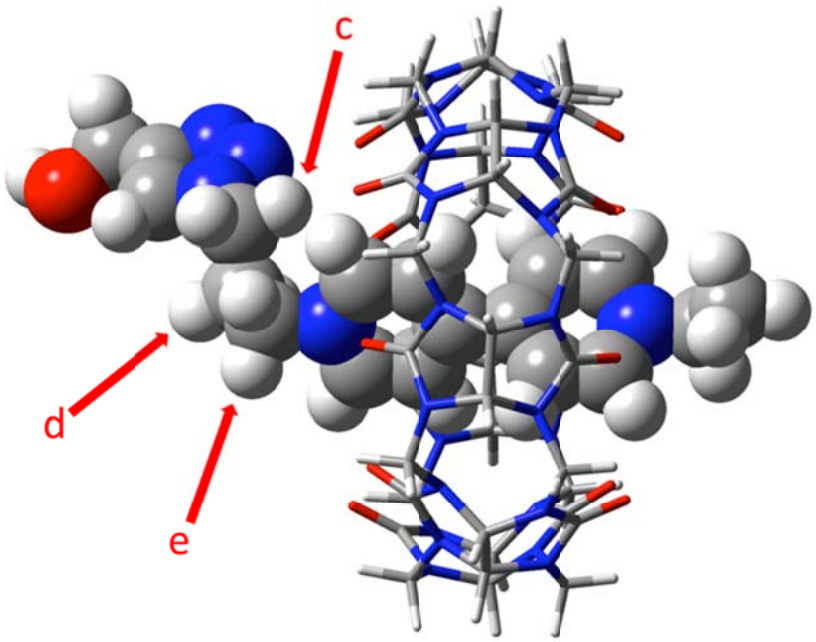

Figure 4.12 *Energy-minimized (DFT-B3LYP)* ***18***·*CB7 complex.*

The cyclic voltammetry results in Figure 4.13 show that free guest **18** has two reversible peaks exhibiting very

fast electrochemical kinetics and the observed voltammetric currents are controlled by diffusional effects. Upon addition of CB7, the half potential for the first reduction-oxidation process in the presence of one equivalent of CB7 shifts around 25 mV to more negative value. However, for the second reduction-oxidation process, the currents for the guest are reduced and the shapes of the peaks are distorted, as the precipitate of neutral species deposits on the electrode surface. Our electrochemistry result is consistent with other similar systems already reported as viologen·CB7 complexes.

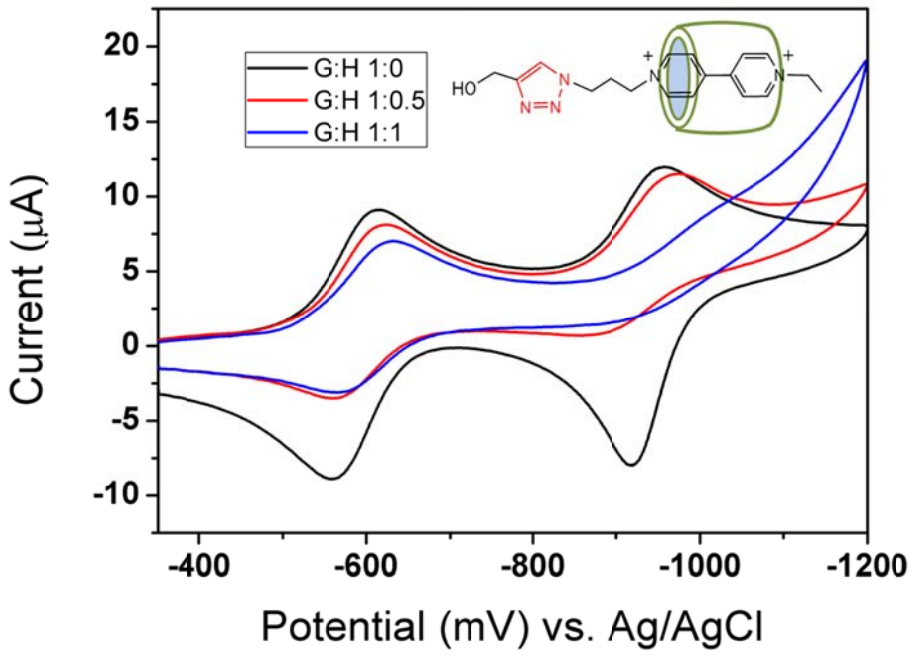

Figure 4.13 *Cyclic voltammetric responses on glassy carbon (0.07 cm^2) of 0.5 mM guest* ***18*** *containing 50 mM NaCl in the absence (black), in the presence of 0.5 equiv (red) and 1.0 equiv (blue) of CB7. Scan rate: 0.1 V s^{-1}.*

We also designed another control guest **19** for binding with CB7 (see Figure 4.14). Instead of flexible propyl connector, guest **19** has a shorter and rigidified alkyl chain, ethyl group, therefore the distance between the bipyridinium moiety and the 1,2,3-triazole moiety is shortened. We repeated the ^{1}H NMR experiments with CB7 as we did before. As shown in Figure 4.11, peaks "a", "b" and "c" undergo downfield shifts and the remaining peaks experience upfield shifts. Especially, peak "e" upfield shifts 3.5 ppm for **19**·CB7 complex.

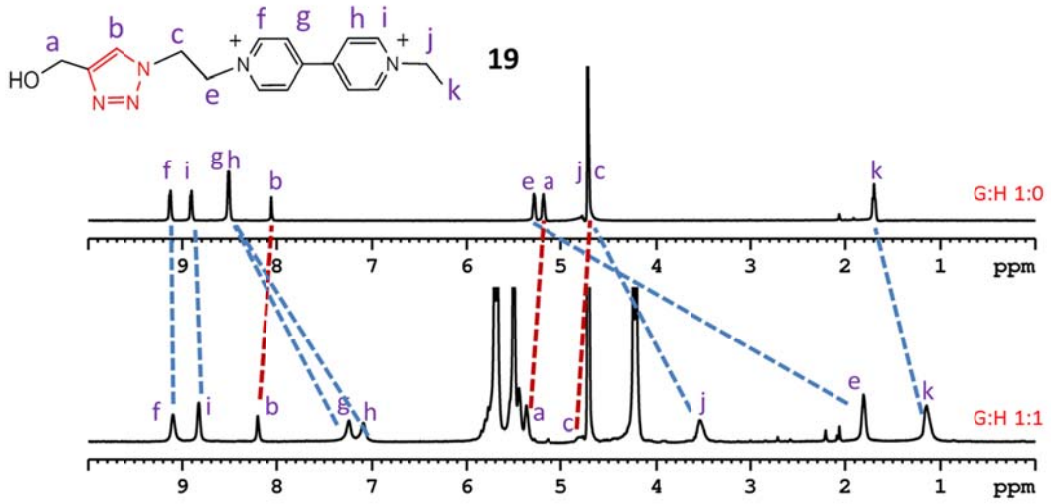

Figure 4.14 *^{1}H NMR spectra (500 MHz, in D_2O) of guest compound **19** (0.5 mM) in the absent (top) and in the presence of 1.0 equiv of host CB7 (bottom).*

When comparing ^{1}H NMR spectroscopic data with **17**·$CB7_3$ and **18**·CB7 complexes, in **19**·CB7complex, the "c" protons act

as if they were “d” protons since they move to a chemical shift that belongs to “d” protons in **17**·$CB7_3$ and **18**·CB7 complexes, and the “e” protons shift to a position that used to be “c” protons in the **17**·$CB7_3$ and **18**·CB7 complexes (refer to the proton labels in parentheses for guest **19** in Figure 4.15). These important data tell us that the abnormal behavior of peaks “c” and “d” in our previous discussion indeed come from the twisted propyl chains that the “c” protons twist closer to one portal of CB7 and their electron clouds are strongly influenced by the portal oxygens at that spatial position and give a significantly upfield shift. Contained by the twisted “c” protons, the adjacent “d” protons step back to a spatial position that is shielded from the effect of the portal oxygens, thus have a much lower chemical shift.

We have also done some preliminary molecular modeling computation on the **19**·CB7 complex and the result is shown in Figure 4.15. From the figure we can clearly see that “e” protons are very close to one of the CB7 portals, therefore their counterpart “c” protons in **17**·$CB7_3$ and **18**·CB7 complexes must be folded up to CB7 to get the same effect. This twisted structure contains the protons “d” in the same spatial positions as the “c” protons in the **19**·CB7 complex

and the increased distance from CB7 diminishes the effect of the portal oxygens.

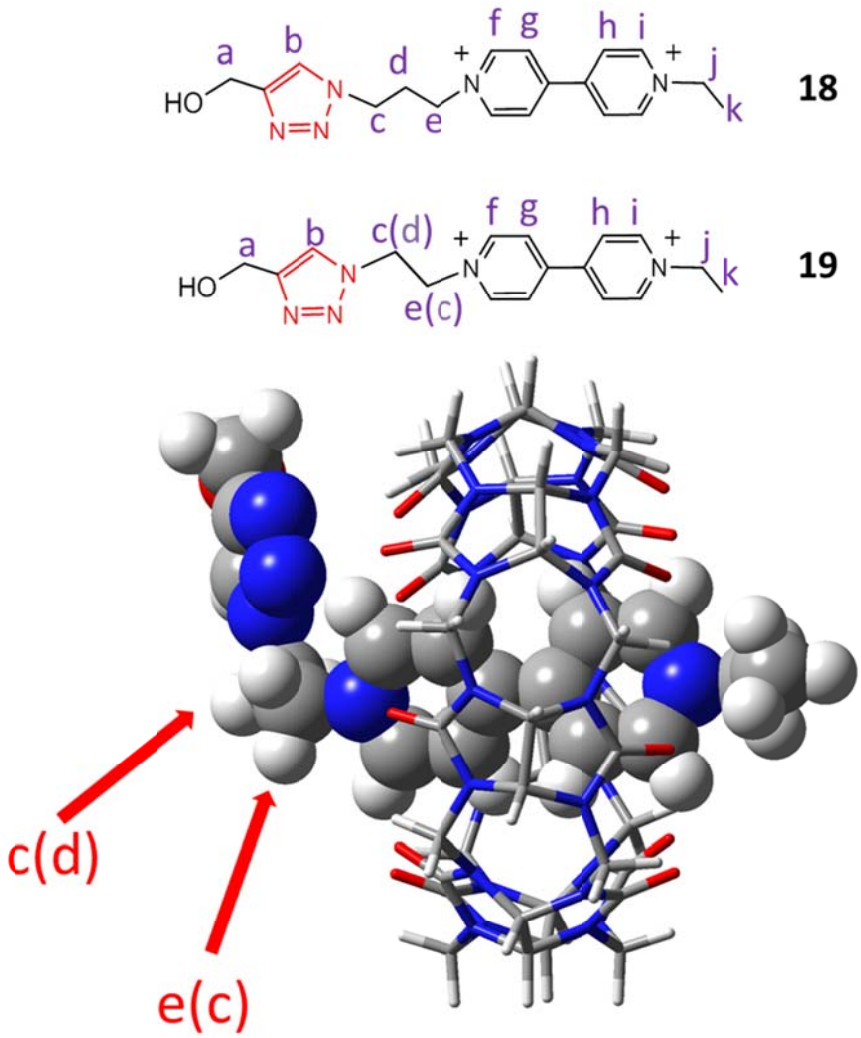

Figure 4.15 *Comparison between the protons on guests **18** and **19** and energy-minimized (DFT-B3LYP) **19**·CB7 complex.*

The electrochemistry result show in Figure 4.16 is similar to the results of **18**·CB7 complex except that there is no potential change for the first reduction-oxidation

process upon CB7 addition. This means that the encapsulation of viologen has no obvious impact on the stability of either oxidation state.

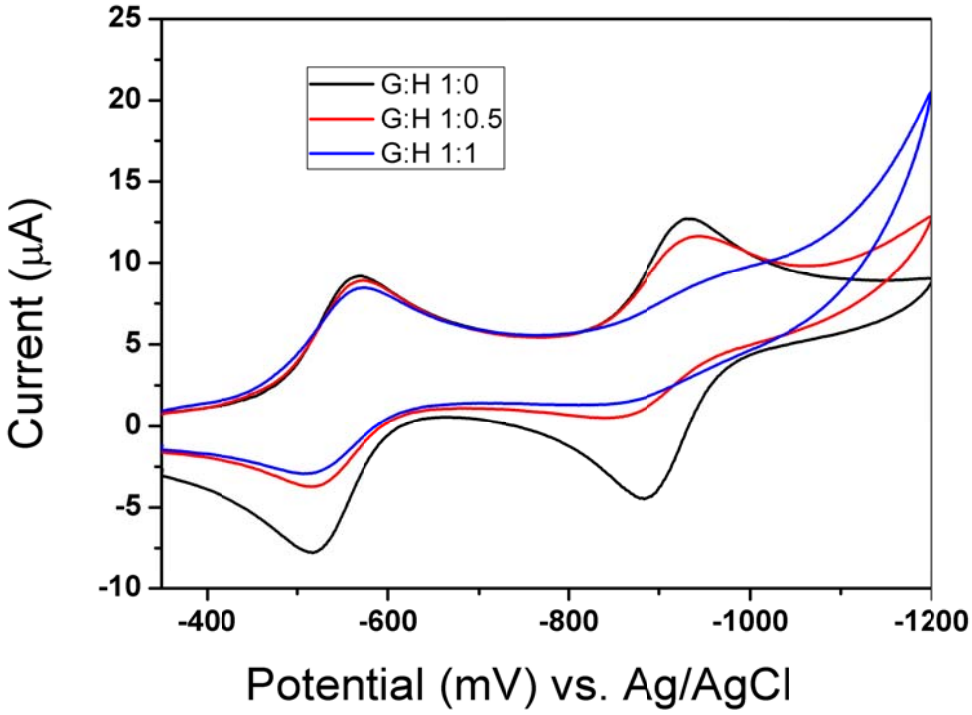

Figure 4.16 *Cyclic voltammetric response on glassy carbon (0.07 cm^2) of 0.5 mM guest **19** containing 50 mM NaCl in the absence (black), in the presence of 0.5 equiv (red) and 1.0 equiv (blue) of CB7. Scan rate: 0.1 V s^{-1}.*

Since we have formed **17**·$CB7_3$ complex, we are interested in calculating the binding constant for this system. Kaifer's group has previously reported 1:1 binding constant for viologen·CB7 complexes (K ~ 10^5-10^6 M^{-1})[37,38], and here we want to derive a model that can be applied to 1:3 G:H complex. We employ an approach that involves the formation

of a 1:1 complex (eq. 1) with complexation constant K_1, followed by association of a second host molecule with the 1:1 complex to form the 1:2 complex (eq 2) with complexation constant K_2, then a third host molecule with 1:2 complex to form the 1:3 complex (eq. 3) with complexation constant K_3.

$$G + H \rightleftharpoons GH \qquad K_1 = \frac{[GH]}{[G][H]} \qquad (1)$$

$$GH + H \rightleftharpoons GH_2 \qquad K_2 = \frac{[GH_2]}{[GH][H]} \qquad (2)$$

$$GH_2 + H \rightleftharpoons GH_3 \qquad K_3 = \frac{[GH_3]}{[GH_2][H]} \qquad (3)$$

A_{obs}, the absorption of guest **17**, was recorded by monitoring the UV-Vis spectra at 260 nm wavelength upon titration of guest **17** by addition of aqueous solution of CB7. The data points were plotted against the concentration ratio of CB7 over guest **17** as shown in Figure 4.6 left. And A_{obs} can be determined using eq 4:

$$A = \chi_0 A_0 + \chi_1 A_1 + \chi_2 A_2 + \chi_3 A_3 \qquad (4)$$

Where,

$$[G_0] = [G] + [GH] + [GH_2] + [GH_3]$$

$$= [G] + K_1[G][H] + K_1K_2[G][H]^2 + K_1K_2K_3[G][H]^3$$

$$[H_0] = [H] + [GH] + 2[GH_2] + 3[GH_3]$$

$$= [H] + K_1[G][H] + 2K_1K_2[G][H]^2 + 3K_1K_2K_3[G][H]^3$$

$$\chi_0 = \frac{[G]}{[G_0]}$$

$$\chi_1 = \frac{[GH]}{[G_0]} = \frac{K_1[G][H]}{[G_0]}$$

$$\chi_2 = \frac{[GH_2]}{[G_0]} = \frac{K_1K_2[G][H]^2}{[G_0]}$$

$$\chi_3 = \frac{[GH_3]}{[G_0]} = \frac{K_1K_2K_3[G][H]^3}{[G_0]}$$

Rewrite eq. 4 to give eq. 5 as following:

$$A = \frac{[G]}{[G_0]}(A_0 + K_1[H]A_1 + K_1K_2[H]^2A_2 + K_1K_2K_3[H]^3A_3)$$

$$= \frac{A_0 + K_1[H]A_1 + K_1K_2[H]^2A_2 + K_1K_2K_3[H]^3A_3}{1 + K_1[H] + K_1K_2[H]^2 + K_1K_2K_3[H]^3} \qquad (5)$$

Where,

$$A_3 = A_\infty$$

$$A_1 = A_0 - \frac{A_0 - A_\infty}{3} = \frac{2}{3}A_0 + \frac{1}{3}A_\infty$$

$$A_2 = A_0 - 2\frac{A_0 - A_\infty}{3} = \frac{1}{3}A_0 + \frac{2}{3}A_\infty$$

We calculate K_1 by monitoring the UV-Vis spectra at 260 nm wavelength upon titration of guest **18** by addition of

aqueous solution of CB7, and get the value 5.6×10^4 M^{-1}, which is lower than previous reported viologen·CB7 complexes in Kaifer's group.[37,38] The comparatively lower binding constant for **18**·CB7 complex reflects relatively weaker binding affinities between CB7 and our viologen moieties, and also explains why we cannot get exact 1:3 stoichiometry for **17**·$CB7_3$ complex through Job-plot. We tried to calculate K_2 and K_3 by fitting our experimental data of **17**·$CB7_3$ complex to eq. 1-5, but we could not obtain reasonable results yet.

4.3 Summary

In conclusion, we have presented data showing very clearly that CB7 forms trimeric complexes around the tris(viologen) guest **17** in aqueous solution. Both NMR spectroscopic and voltammetric data are consistent with the encapsulation of viologen residue inside host CB7 as reported in literature. From the results of ESI-TOF mass spectrum, we conclude that a supramolecular architecture, **17**·$CB7_3$ complex, is formed and very stable in gas phase. The UV-Vis and Job-plot results show a relatively weak binding effect in **17**·$CB7_3$ complex in aqueous solution. The electrochemical data give us a significant potential shift for the first reduction-oxidation process upon formation of

17·$CB7_3$ complex. We also designed and prepared two control guests **18** and **19,** trying to understand the abnormal chemical shift changes of proton "c" and "d" of guest **17** upon encapsulation by CB7. The ^1H NMR results support that each viologen branch acts as if they are independently interacting with CB7 and proton "c" is in a special position that is hugely impacted by oxygens located at the portal of CB7, yielding a remarkable 2.8 ppm upfield shift. The binding constant value for **18**·CB7 complex also proves that CB7 does not have very strong binding affinity on the viologen moiety of these compounds, leading to fast association-dissociation dynamics in aqueous solution.

4.4 Experimental Section

Materials. All starting chemicals were of the highest purity available and purchased from commercial suppliers.

Synthesis of 2,4,6-tris(prop-2-ynyloxy)-1,3,5-triazine (17a) has been previously reported.[60] Propargyl alcohol (10 ml) was added slowly to a suspension of cyanuric chloride (2.2 g, 12.1 mmol) in 15 ml THF at room temperature followed by K_2CO_3 (5.2g, 36.3 mmol). Reaction was heated to 60 ^0C overnight. The reaction mixture was filtered. After evaporation of solvent, the residue was dissolved in 80 ml

CH_2Cl_2, and washed with diluted hydrochloric acid (10%) and saturated brine. Then dried over $MgSO_4$ and evaporated the solvent, 2.6 g (90% yield) of **17a** as white solid was obtained. ESI-TOF MS (m/z) calcd for $[C_{12}H_9N_3O_3Na]^+$: 266.0542, found:266.0551. ^{1}H NMR (500 MHz, d_6-DMSO): 3.68 (s, 1H), 5.08 (s, 2H). ^{13}C NMR (125 MHz, d_6-DMSO): 56.21, 78.34, 79.11.

Synthesis of 1-ethyl-4,4′-bipyridinium bromide (17b): Bromoethane (3.16 g, 29 mmol) dissolved in 35 ml toluene was added to an intensively stirred solution of 4,4′-bipyridine (7.8g, 50 mmol) in 15 ml toluene at room temperature within 1h. The solution was stirred at room temperature for 15h and then refluxed for 2 more days. After reaction, precipitate was filtered and washed with toluene to get 4.5 g (58% yield) yellow product. ESI-TOF MS (m/z) calcd for $[C_{12}H_{13}N_2]^+$: 185.1079, found: 185.1089. ^{1}H NMR (500 MHz, d_6-DMSO): 1.59 (t, 3H), 4.70 (q, 2H), 8.06 (ds, 2H), 8.67 (ds, 2H), 8.88 (ds, 2H), 9.29 (ds, 2H). ^{13}C NMR (125 MHz, d_6-DMSO): 16.80, 56.44, 122.36, 125.81, 141.32, 145.32, 151.46, 152.63.

Synthesis of 1-(3-bromopropyl)-1′-ethyl-4,4′-bipyridiniumbromide(17c) was based on the reported procedure:[61] 528 mg (2 mmol) of 1-methyl-4,4′-bipyridinium

bromide (**17b**) was dissolved in 35 ml hot acetonitrile. When solution became clear, 6g (30 mmol) of dibromopropane was added via syringe to the solution and reacted for 40 hours at reflux. After the reaction mixture cooled down to room temperature, the crude product was filtered and washed with acetonitrile to get 750 mg (80% yield)of the pure product (**17c**) as a yellow precipitate. ESI-TOF MS (m/z) calcd for $[C_{15}H_{19}N_2Br_2]^+$: 386.9895, found: 386.9835. ^{1}H NMR (500 MHz, d_6-DMSO): 1.62 (t, 3H), 2.61 (t, 2H),3.65 (p, 2H), 4.77 (q, 2H), 4.86 (t, 2H), 8.86 (ds, 4H), 9.47 (ds, 4H). ^{13}C NMR (125 MHz, d_6-DMSO): 16.78, 30.62, 33.53, 57.00, 60.09, 126.98, 127.05, 146.17, 146.58, 148.85, 149.19.

Synthesis of 1-(3-azidopropyl)-1'-ethyl-4,4'-bipyridiniumhexafluorophosphate (17d) was based on the reported procedure:[61] A mixture of 1-(3-bromopropyl)-1'-ethyl-4,4'-bipyridinium bromide (**17c**) (0.47g, 1 mmol, 1M) and sodium azide (0.195g, 3 mmol, 3M) in 1 ml of water was heated at 80 ^{0}C overnight. The solution was evaporated to dryness to give a brown solid. The solid was dissolved in 1 ml of methanol and filtered to remove an excess of sodium azide. The filtrate was dried under vacuum to solid. The solid was then dissolved in a H_2O/MeCN (3:1) mixture and a saturated aqueous solution of NH_4PF_6 was added to this

mixture. The resulting yellow/brown precipitate was filtered, washed with H_2O and dried under reduced pressure to give 240 mg (43% yield) final product (**17d**) as purple solid. ESI-TOF MS (m/z) calcd for $[C_{15}H_{19}N_5PF_6]^+$: 414.1282, found: 414.1171. ^{1}H NMR (500 MHz, d_6-DMSO): 1.62 (t, 3H), 2.29 (p, 2H),3.54 (t, 2H), 4.72 (q, 2H), 4.77 (t, 2H), 8.80 (ds, 4H), 9.40 (ds, 4H). ^{13}C NMR (125 MHz, d_6-DMSO): 16.77, 30.15, 48.06, 57.07, 59.19, 127.00, 146.20, 146.63, 149.00, 149.24.

Synthesis of tris(viologen)guest(17): A degassed solution of $[Cu(MeCN)_4]PF_6$ (75 mg, 0.2 mmol) in MeCN (0.5 mL) was added to a degassed solution of 1-(3-azidopropyl)-1′-ethyl-4,4′-bipyridinium hexafluorophosphate (**17d**) (625 mg, 1.2 mmol) and 2,4,6-tris(prop-2-ynyloxy)-1,3,5-triazine (**17a**) (97.3 mg, 0.4 mmol) in Me_2CO (30 ml) under N_2. The solution was stirred for 2 days at 30 ^{0}C before column chromatography on silica gel (CH_2Cl_2/CH_3CN 6:4) monitored by TLC (10:1:1 MeCN: H_2O: Sat NH_4PF_6) to afford the expected product **17·PF$_6$** as 220 mg (42% yield) light yellow powder. The product can also be converted to **17·Cl$_6$** by ion exchange with tetrabutylammonium chloride. ESI-TOF MS (m/z) calcd for $[C_{57}H_{66}N_{18}O_3Cl_4]^{2+}$: 596.2145, found: 596.1857. ^{1}H NMR (500 MHz, d_6-DMSO): 1.62 (t, 3H), 2.64 (p, 2H),4.58 (t, 2H), 4.72 (q,

2H), 4.77 (t, 2H), 8.34 (s, 1H), 8.80 (m, 4H), 9.38 (m, 4H). ^{13}C NMR (125 MHz, d_6-DMSO): 16.31, 30.77, 46.50, 56.533, 58.40, 60.92, 125.34, 126.52, 141.39, 145.68, 146.05, 148.35, 148.65, 172.26.

Synthesis of control compound triazole-viologen (18): A degassed solution of $[Cu(MeCN)_4]PF_6$ (37.5 mg, 0.1 mmol) in MeCN (0.5 mL) was added to a degassed solution of 1-(3-azidopropyl)-1'-ethyl-4,4'-bipyridinium hexafluorophosphate (**17d**) (260 mg, 0.5 mmol) and propargyl alcohol(28 mg, 0.5 mmol) in Me_2CO (15 ml) under N_2. The solution was stirred for 2 days at 30 ^{0}C before column chromatography on silica gel (CH_2Cl_2/CH_3CN 1:5) monitored by TLC (10:1:1 MeCN: H_2O: Sat NH_4PF_6) to afford the expected product **18** as 230 mg (75% yield) light yellow powders. ESI-TOF MS (m/z) calcd for $[C_{18}H_{23}N_5OPF_6]^+$: 470.1544, found: 470.1556. ^{1}H NMR (500 MHz, d_6-DMSO): 1.62 (t, 3H), 2.64 (p, 2H),4.48 (ds, 2H), 4.50 (t, 2H), 4.72 (q, 2H), 4.77 (t, 2H), 5.21 (t, 1H, O**H**), 7.99 (s, 1H), 8.86 (s, 4H), 9.31 (ds, 2H), 9.38 (ds, 2H). ^{13}C NMR (125 MHz, d_6-DMSO): 16.77, 31.06, 46.80, 54.24, 57.06, 59.14, 146.12, 146.47, 148.62, 148.85, 149.12.

Synthesis of control compound triazole-viologen (19) is similar to the synthesis of control compound **18**, the only difference is using dibromoethane as starting material to

get 1-(3-bromoethyl)-1′-ethyl-4,4′-bipyridinium bromide and then 1-(3-azidoethyl)-1′-ethyl-4,4′-bipyridinium hexafluorophosphate). The expected product **19** is a brown solid with 250 mg in 83% yield. ESI-TOF MS (m/z) calcd for $[C_{17}H_{21}N_5OPF_6]^+$: 456.1388, found: 456.1393. ^{1}H NMR (500 MHz, d_6-DMSO): 1.61 (t, 3H), 4.51 (t, 2H),4.72 (q, 2H), 5.13 (s, 2H), 5.23 (t, 2H), 5.25 (s, 1H, O**H**), 8.03 (s, 1H), 8.80 (s, 4H), 9.23 (ds, 2H), 9.40 (ds, 2H). ^{13}C NMR (125 MHz, d_6-DMSO): 16.77, 49.53, 55.41, 57.16, 60.58, 124.01, 126.86, 127.10, 146.15, 146.78, 148.65, 148.93, 149.75.

Electrochemistry: The voltammetric experiments were recorded using a single-compartment cell fitted with a glassy carbon working electrode (0.071 cm^2), a platinum auxiliary electrode, and a Ag/AgCl reference electrode. The working electrode was polished immediately before the experiments using a water/alumina (0.05 µm) slurry on a felt surface. The solution was thoroughly deoxygenated by purging with high purity nitrogen gas and maintained under a nitrogen atmosphere during the experiments.

Computational Studies: Energy minimization of supramolecular structures was carried out using the DFT-B3LYP method (basis set: 3-21G) as implemented in the

Gaussian software package (09 version) without solvent effect.

CHAPTER 5

CAGE MOLECULES FORMED BY "CLICK" REACTIONS

5.1 General Discussion

"Cage" type molecules have been attracting continuous interest from supramolecular chemists all over the world because of their rigid, three-dimensional (3D) molecular frames that enclose space to encapsulate smaller guest molecules. Various shaped cage molecules, for example, sphere, cylinder, cone, and prism, have been synthesized either through covalent bond formation[62] or noncovalent interactions[63], such as hydrogen bonds and metal-ligand coordination bonds. In recent years, cage molecules based on metal-ligand directed assembly have developed rapidly and facilitated potential applications in gas storage, drug delivery, catalysis and so on. In this chapter, only cage molecules built from covalent chemical bonds possessing high stability will be covered.

Mei-Xiang Wang's group reported a molecular triangular prism **20** based on oxygen atom bridged bicyclocalix-aromatics that employs 1,3,5-tris(4-hydroxyphenyl)benzene **(20a)** as equilateral triangular bases for "top" and "bottom" and cyanuric chlorides as the three pillars.[64] The synthesis

procedures shown in Scheme 5.1 are based on error-and-trial with different bases and solvents. In many cases, only oligomeric or polymeric substances were observed. One-spot synthesis has a maximum yield around 13% and an improved stepwise synthesis can enhance the yield up to 38%. By using of cyanuric chlorides, the resulting triangular prism can be further functionalized on the edge positions around the periphery.

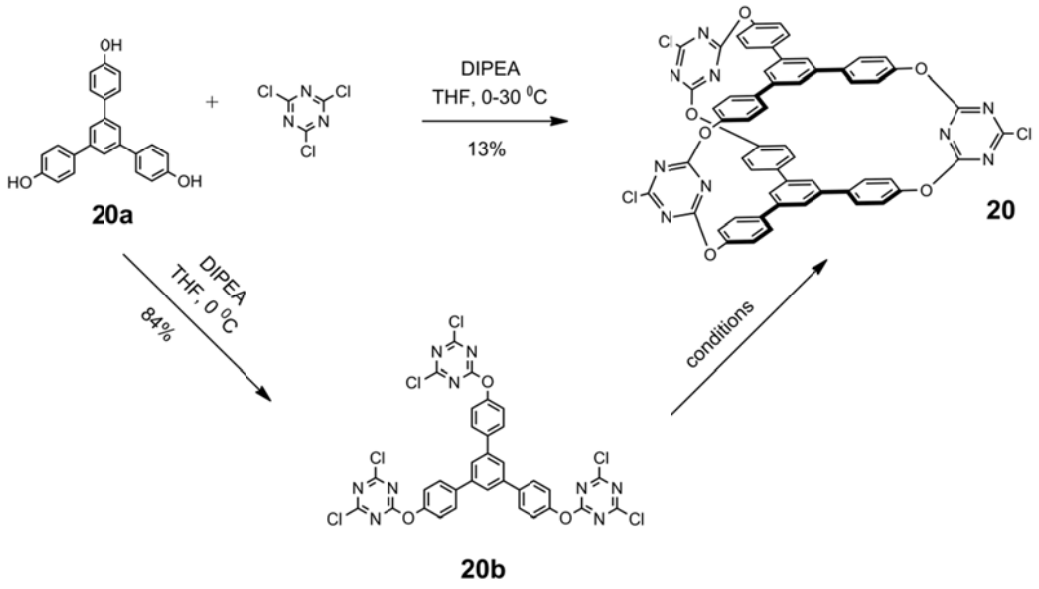

Scheme 5.1 *General procedures to synthesize the triangular prism cage* ***20****.*[64]

"Click chemistry"[65-67] is a term that was introduced by K. B. Sharpless in 2001 to describe a family of chemical transformations that comply with a set of specific criteria: high yielding, wide in scope, create only byproducts that

can be removed without chromatography, stereospecific, simple to perform, and can be conducted in easily removable or benign solvents. This concept was developed in parallel with the interest within the pharmaceutical, materials, and other industries in capabilities for generating large libraries of compounds for screening in discovery research.[68] "Click chemistry" is based on several types of reactions, but copper catalyzed azide-alkyne cycloaddition (CuAAC)[69] is the most widely employed. This reaction occurs between an organic azide and a terminal acetylene with the help of a copper catalyst at room temperature, producing a cyclic triazole as product (Scheme 5.2).

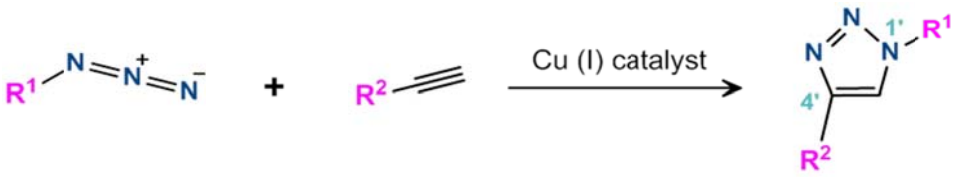

Scheme 5.2 *Copper (I)-catalyzed azide-alkyne cycloaddition (CuAAC).*

Since its introduction, CuAAC has rapidly found applications in numerous fields. The reaction is surely responsible for the tremendous popularity of the "click" concept and many simply associate "click chemistry" to mean triazole formation between an azide and an alkyne. Francisco Santoyo-Gonzalez and coworkers synthesized a type

of molecular nanocages, under the principle of "click chemistry", providing a platform to simplify and reduce laborious synthesis of three-dimensional shape-persistent molecules.[70] They used procedures (shown in Scheme 5.3) that have found application mainly in the synthesis of polymers since "click chemistry" is a highly efficient cross-linking reaction. Therefore, in order to build the higher level molecular nanocage, they need to overcome the intermolecular reactions that lead to polymers after the first click of polyalkynes and polyazides. To achieve this, they performed their experiments under highly diluted conditions in an aromatic solvent such as toluene that acts as a template by means of π-stacking interactions. Their results showed that the product cages are highly insoluble in various solvents and encapsulate toluene molecules inside the cage cavity.

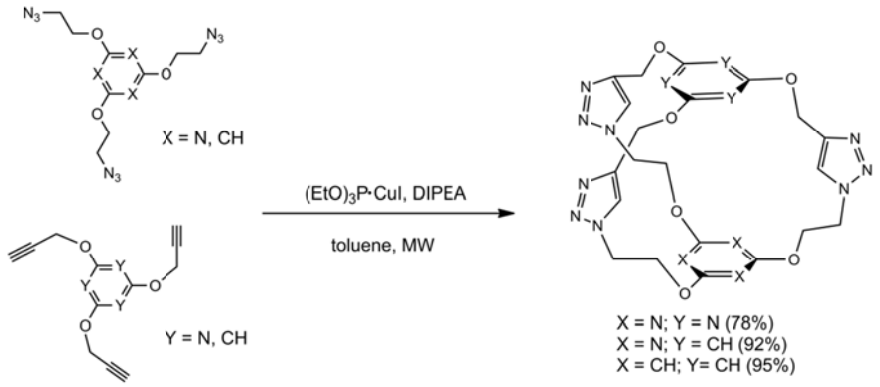

Scheme 5.3 *Procedures employed for the synthesis of a type of molecular nanocages by "click chemistry".*[70]

Up to the present, the construction of supramolecular cages with large cavities in an efficient way still remains a challenge. In designing these sophisticated molecular architectures, the geometry of the molecules is very important, even small changes in the shapes of molecules can have a profound influence on cage formation. Intramolecular interactions also play critical roles in producing three dimensional cage products and avoiding other side reactions. In this chapter, we will present our interest in designing larger cage molecules via "click" reaction and show how the design of the starting molecules affect the formation of the cage molecules.

5.2 Experimental Results and Discussion

To explore the experimental conditions for "click" reaction, we started with a simple experiment between 1,4-diethynylbenzene (**21a**) and 2-azidoethanol (**21b**), using the organic soluble copper (I) complex $(EtO)_3P{\cdot}CuI$ as catalyst (Scheme 5.4). From the ESI-TOF mass spectrum result, calcd for $[C_{14}N_6O_2H_{17}]^+$: 301.1413, found: 301.1426, we confirm that resulting compound **21** was successfully synthesized. Herein, we build our confidence to synthesize more complicated cage molecules.

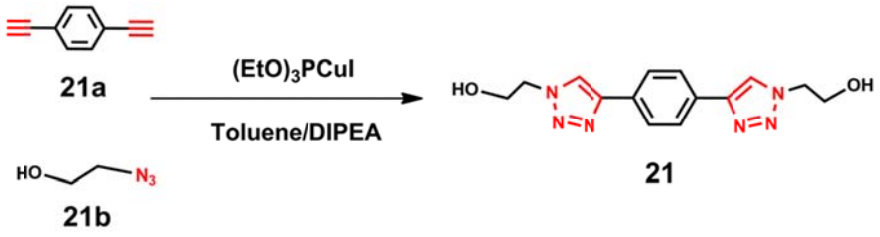

Scheme 5.4 *A general procedure to synthesize a simple product **21** via "click" reactions.*

The cage molecule obtained by Francisco Santoyo-Gonzalez and coworkers is too small to encapsulate molecules other than toluene. Therefore we proposed a scheme to enlarge the cage by inserting a ligand **21a** that connects the "top" and "bottom" **22a** together (see Scheme 5.5). Our result shows that a yellow powder is precipitated from toluene based on highly diluted solution (0.3 mM) and this precipitate cannot be dissolved in any solvent. We could not get any convincing evidence to prove that the precipitate is our targeting product **22** since all the attempts to dissolve the precipitate in various solvents at elevated temperature while stirring failed. We speculate two possible identities for the precipitate. First, the precipitate may be our targeting cage molecule **22**. By looking at the chemical configuration of cage **22**, this symmetrical triangular prism itself is likely to be highly insoluble. A more probable outcome is that the yellow

precipitate is made up of oligomers or polymers by highly efficient cross-linking "click" reactions.

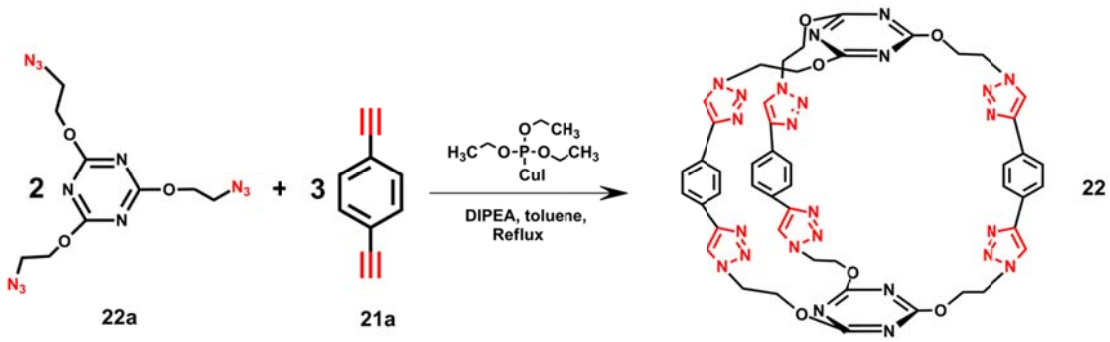

Scheme 5.5 *A general proposal to synthesizea larger molecular cage **22** via six "click" reactions.*

To form cage **22**, we must overcome two obstacles. First of all, intramolecular ligation of dialkynes (**21a**) and triazides (**22a**) after the first click must predominate over the intermolecular reactions that lead to the formation of polymers. Secondly, starting materials must be able to self-assemble to form well-organized cage architectures from highly disordered status. Since organizing starting materials is an entropically unfavorable process ($\Delta S << 0$), the reaction must be driven by enough enthalpical force to make sure $\Delta H < T\Delta S$, therefore according to $\Delta G = \Delta H - T\Delta S$, Gibbs free energy for the six-click assembly can be negative to allow the reaction to happen. When we explored experimental conditions, we used highly diluted

concentration (~0.3 mM) to help reduce the chances for starting materials to collide together and form cross-linking polymers. Meanwhile, a suitable template that can shape the cage molecule by hydrophobic forces *and* π-stacking interactions would effectively assist in forming the cage molecule and trap the template in the inner cavity. Usually, solvent itself is a good template. In our case, toluene as solvent is too small to act as a template and to stabilize the system by cofacial π-stacking interactions. Based on the above discussion, we decided to revise our proposal by reducing the quantity of "click" reactions in one cage molecule without sacrificing the cavity size of the cage.

Inspired by the molecular triangular prism **20**, we designed a new scheme for the synthesis of cage **23**. We improved **20** by introducing longer pillars that support the molecular "top" and "bottom" **20a**, which will provide a larger cavity for bigger guest molecules to reside inside (see Scheme 5.6). However, when we carried out the experiment using three "click" reactions to close up the cage, a yellow precipitate arose from toluene and the precipitate couldn't be dissolved any more in other solvents. Since **20a** is highly hydrophobic due to the four

benzene rings, two of these units brought together by "click" reaction creating a triangular prism cage may lead to decreased solubility.

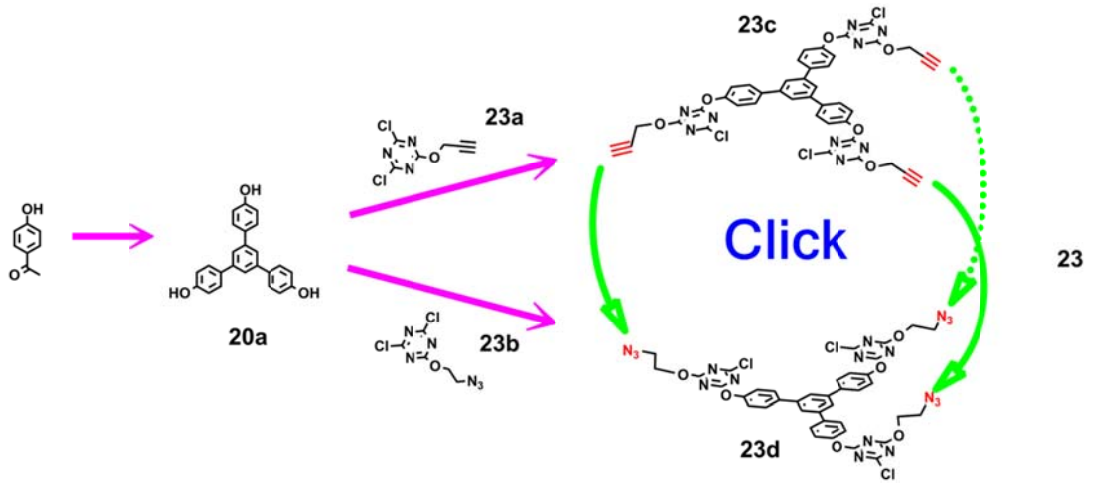

Scheme 5.6 *A general proposal to synthesize a larger molecular cage* ***23*** *via three "click" reactions.*

We introduce a viologen derivative **24a** since viologen derivatives have considerable solubility in aqueous solution, and our ultimate goal is to synthesize a cage that can be dissolved in water and has hydrophobic cavity to encapsulate nonpolar guests by non-covalent interactions. To begin with, we tried to synthesize an intermediate compound **24** that is only half of a whole cage, and then we can build the other half cage on the *N*-terminal of theviologen moiety. We designed a synthesis procedure as shown in Scheme 5.7. However, when we carried out the

experiment under the conditions previously explored for click reactions, three equivalents of **24a** with one equivalent of **22a** produced a sticky dark brown residue and showed no desired peaks in ^{1}H NMR. Since **24a** does not dissolve in toluene, we also tried in other solvents, such as THF/H_2O/EtOH 1:2:2, H_2O/t-BuOH 2:1, $CHCl_3$-MeOH co-solvent and DMF, similar sticky dark brown or black residue were produced. We do not understand why we cannot synthesize intermediate compound **24**, since click reaction should work very well between the two starting materials.

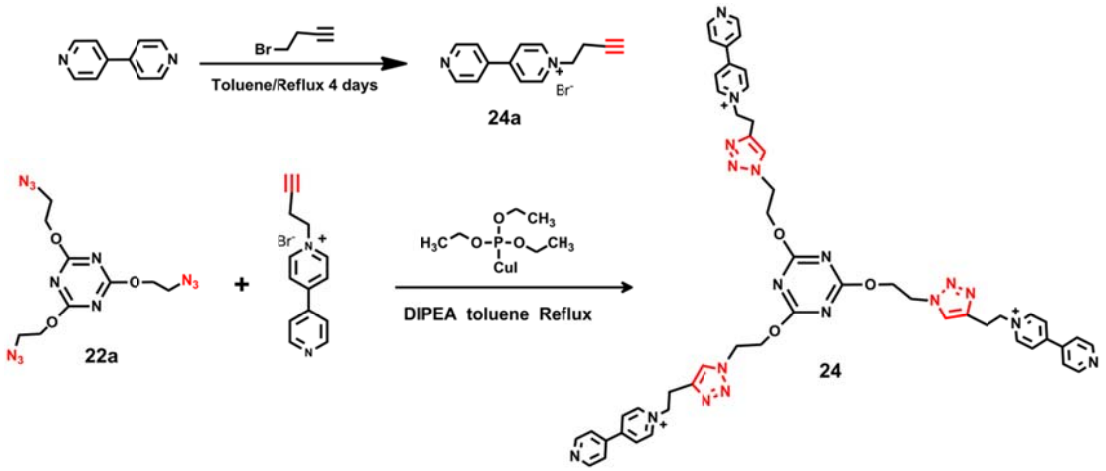

Scheme 5.7 *A general proposal to synthesize a half cage intermediate **24** via "click" reactions.*

To address this problem, we designed a pair of comparison experiments in Scheme 5.8. For the same experimental conditions, 2-azidoethanol can click with **25a** to get the targeting product **25**, but cannot click with the

counterpart **26a** to produce the reasonable product **26**. The possible explanation for these different results is that copper (I) catalyst can form coordination bond with *N*-terminal of viologen derivatives since the terminal nitrogen is a good electron donor for copper ions. This way, the copper (I) complex would not act as a "click" catalyst but coordinate with the reaction starting material and hinder the reaction from happening.

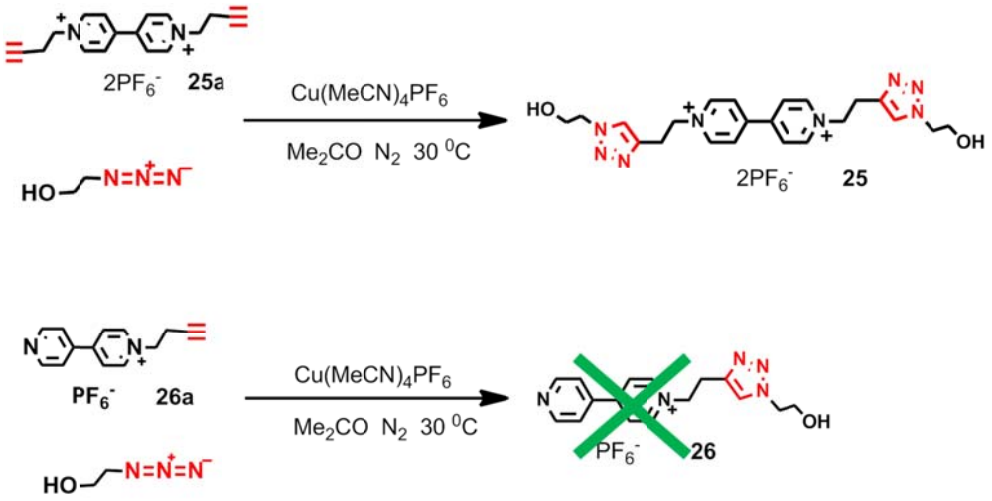

Scheme 5.8 *Comparison experiments between two viologen derivatives.*

After trial and error, we proposed another improved scheme for the "click" cage. Since **22a** as a liquid product is unstable and easy to decompose under storage, we need to prepare it fresh for each use. Comparatively, **17a** is a white solid with much better stability, meanwhile azide-

ended viologen derivatives (**17d**) were prepared by us (Chapter 4) as solids that can be stored and used very conveniently. Following Scheme 5.9, we tried a one-spot synthesis for "click" cage **27** by adding two equivalents of **17a** as "top" and "bottom" caps and three equivalents of **27a** as pillars in degassed acetone (~ 0.3 mM) with $[Cu(MeCN)_4]PF_6$ as catalyst. After two days of reaction at room temperature, we got similar results as with cages **22** and **23**, that is, only polymers were produced. We also tried to add excess of **27a** to make the caps/pillars ratio around 1:10 and hoped to get an intermediate without all the "clicks" made. To our disappointment, only polymers were obtained.

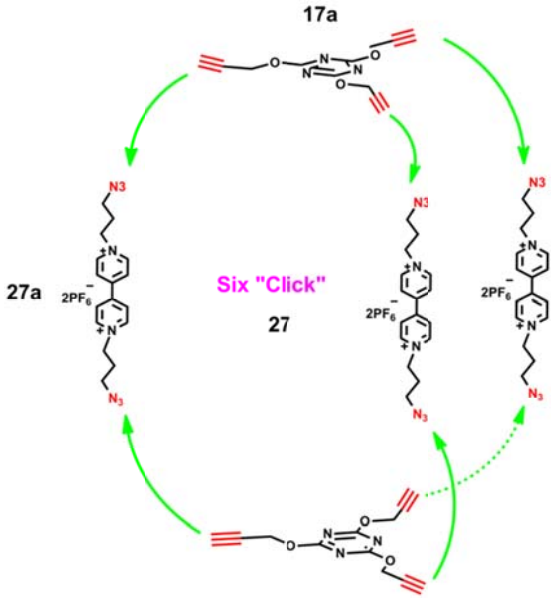

Scheme 5.9 *Proposal for one-step synthesis of "click" cage **27**.*

Since we had successfully synthesized the tris(viologen) **17**, we decided to build the cage molecule **27** by a stepwise synthesis. As shown in Scheme 5.10, the pillar compound **27b** can first "click" with the cap compound **17a** to form an intermediate **27d** (refer to Scheme 5.11) that is similar to compound **17**. However, the intermediate product **27d** has bromide ends which can be exchanged with sodium azide and converted to azide ends and ready for the second round of "click" reactions. In this way, we can reduce the number of "click" reactions and better control the reaction direction.

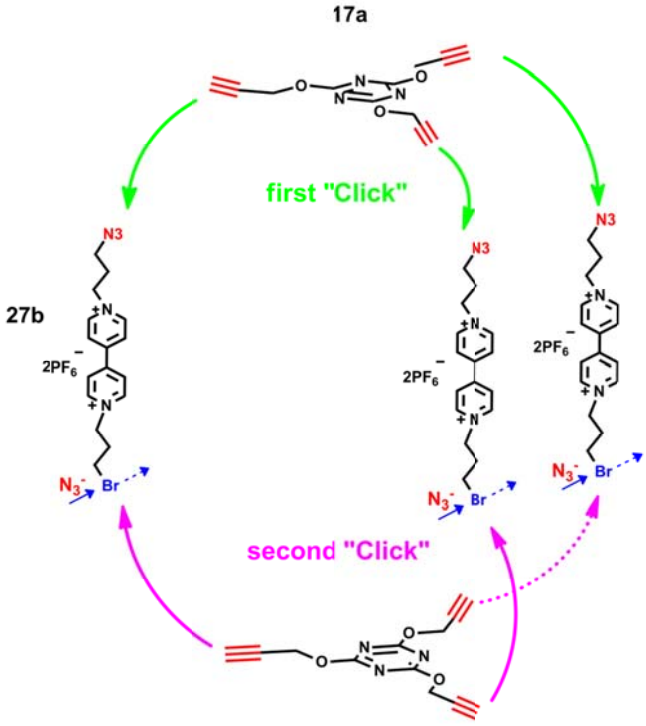

Scheme 5.10 *Proposal for a stepwise synthesis of "click" cage* ***27****.*

The proposal in Scheme 5.10 is reasonable, but when we carried out the experiments shown in Scheme 5.11 to synthesize the pillar compound **27b**, we could not get the pure product. 4,4'-Bipyridine has two active *N*-terminals for dibromopropane bromides, and dibromopropane also has two bromide ends for *N*-terminals. We tried different solvents, different temperatures and different reaction times for the reaction, but we always obtained **27c** mixed with side product polymers (up to 80% purity). We tried to remove the polymer impurities, and our results showed that the desired product and the polymers have similar chemical properties and are very difficult to separate. Therefore, we used the approximate 80% purity of **27c** to react with 0.5 equiv. of sodium azide. Beside the desired **27b**, we introduced more impurities from either the starting materials **27c** or both bromide ends converted to azides **27a** (Scheme 5.11). Azide ends and bromide ends have similar polarity and show up as one spot in TLC, therefore column chromatography is not an effective way here. We directly used the mixture (~50% purity) and converted their counter ions to PF_6^- and then tried the first "click". We obtained the intermediate product **27d** with less than 10% yield to our best result. Column chromatography helps removing most of the starting materials, but there are still around 20%

impurities with similar polarity to the product which are extremely difficult to remove.

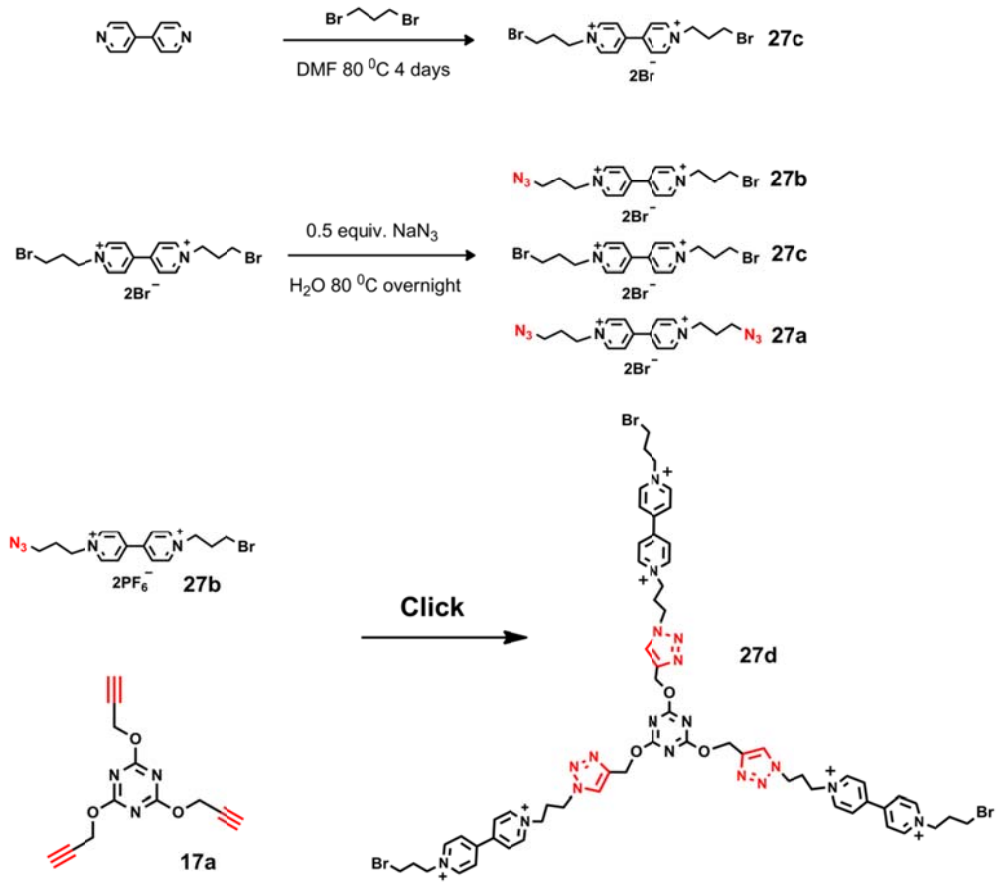

Scheme 5.11 *Procedures for the synthesis of compound* ***27c, 27b*** *and* ***27d.***

To foresee the plausibility of forming cage **27**, we have done some preliminary molecular modeling computations on the cage molecular **27**. From the results shown in Figure 5.1, it is clear to see that this cage molecule is extremely flexible and has the tendency to become a flat plane which adds more difficulties to close up the cage via

second "click" instead of producing polymers without twisting molecules around. Templates may help shape the cage molecule and reduce cross-linking polymer reactions, but we do not have a suitable template for this system yet.

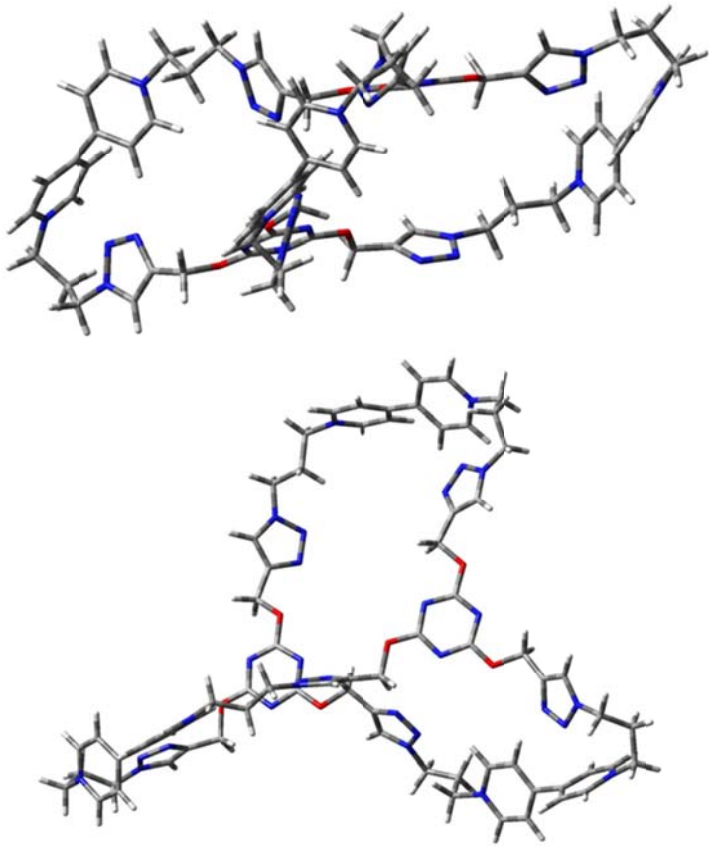

Figure 5.1 *Energy-minimized (DFT-B3LYP) for the proposed cage molecule* ***27****. Top: side view; bottom: front view.*

5.3 Summary

In conclusion, we have presented in this chapter our design and synthetic efforts to build a molecular

architecture that can hold up small guest molecules via "click" chemistry. From the experimental results of several proposed synthetic schemes, we can conclude that it is extremely easy to produce polymers instead of shaped cage molecules via "click" chemistry since "click" reactions are very efficient and non-selective. A template that can shape the cage cavity and has non-covalent effects with the forming cage can help reduce the random reactions and lead to more controlled results.

5.4 Experimental Section

Materials. All starting chemicals were of the highest purity available and purchased from commercial suppliers.

2-Azidoethanol (21b) was prepared by a modification of the method of Hooper et al.[71] To a 250 mL round bottom flask was added 2-bromoethanol (37.5 g, 0.3 mol) and sodium azide (32.5 g, 0.5 mol) in 100 mL of water. The mixture was stirred at 80 ^{0}C for 8 h and then cooled to room temperature. The solution was extracted with ether (3×100 ml), dried with sodium sulfate overnight, and filtered. After the removal of the solvent under vacuum, 2-azidoethanol wasobtained as a colorless liquid (90% yield).

Synthesis of compound 21: A mixture of 1,4-diethynylbenzene (**21a**) (3.47g, 0.0275 mol), 2-azidoethanol (**21b**) (4.3g, 0.05 mol), DIPEA (9.69g, 0.075 mol) and the copper catalyst [$(EtO)_3P{\cdot}CuI$] (0.89g, 0.0025 mol) was added to 75 mL toluene. The solution was refluxed for 1 h before precipitate was filtered and washed with toluene. ESI-TOF mass spectrum result, calcd for $[C_{14}N_6O_2H_{17}]^+$: 301.1413, found:301.1426. ^1H NMR (500 MHz, d_6-DMSO): 3.82 (q, 2H), 4.45 (t, 2H), 5.12 (t, 1H), 7.93 (ds, 2H), 8.54 (s, 1H).

2,4,6-Tris(2-azidoethoxy)-1,3,5-triazine (22a) was synthesized based on a reported procedure.[72] To a cold solution of cyanuric chloride (1.87 g, 10 mmol) and 2-azido ethanol (**21b**) (5.2 g, 60 mmol) in dry acetonitrile (25 ml) was added dropwise a solution of DIPEA (7 ml) in acetonitrile (10 ml). The reaction mixture was kept at room temperature for 2 days. After evaporation the crude product was dissolved in chloroform (150 ml) and washed with water (50 ml). The organic phase was dried (Na_2SO_4), filtered and evaporated. Column chromatography (CH_2Cl_2-ether 20:1) gave the product **22a** as a liquid. ^1H NMR ($CDCl_3$, 300 MHz): 4.59 (t, 1H), 3.68 (t, 6H); ^{13}C NMR ($CDCl_3$, 75 MHz): 49.4, 67.3, 171.8.

Synthesis of cage molecule 22: A mixture of 1,4-diethynylbenzene (**21a**) (27.9 mg, 0.15 mmol), 2,4,6-tris(2-azidoethoxy)-1,3,5-triazine (**22a**) (33.6 mg, 0.10 mmol), DIPEA (0.15 ml) and the copper catalyst [$(EtO)_3P{\cdot}CuI$] (20 mg, 0.05 mmol) in 500 ml toluene under reflux for 1 h. The precipitate was filtered and washed with toluene for further characterization. The residue was concentrated and dried for further product analysis.

1,3,5-Tris(4-hydroxyphenyl)benzene (20a) was synthesized based on a reported procedure.[64] $SiCl_4$ (50.97 g, 300 mmol) was added slowly by syringe to a stirred solution of *p*-methoxyacetophenone (15 g, 100 mmol) in dry ethanol (100 mL) at 0 ^{0}C. The mixture was stirred for 6 hours and then further refluxed for 2 hours. The reaction mixture was then cooled to room temperature and poured into 200 mL water, extracted with CH_2Cl_2 (150 ml × 3), Dried ($MgSO_4$), filtered and concentrated on a rotary evaporator. Crystallization from ethanol gave 1,3,5-tris(4-methoxyphenyl)benzene (11 g, 83%) as light yellow solid. ^{1}H NMR(300 MHz, $CDCl_3$): 3.87 (s, 9H), 7.01 (d, 6H), 7.62 (d, 6H), 7.65 (s, 3H); ^{13}C NMR (75 MHz, $CDCl_3$): 55.3, 114.2, 123.8, 128.3, 159.3, 133.8, 141.8.

1,3,5-Tris(4-methoxyphenyl)benzene (9.9 g, 25 mmol) was taken in flask and added to it 100 ml of acetic acid as

solvent and stirred it till reflux. Then added to it dropwise 48% aqueous HBr (37.93 g, 25.45 mL, 225 mmol) and refluxed the solution for another 30 h. The reaction mixture was concentrated on rotary evaporator to a small volume and then added to it 100 mL of water. Precipitates thus formed were filtered and washed thoroughly with water. The residue was then chromatographed on a silica gel column (100-200) with a mixture of petroleum ether and acetone (3:1) as the mobile phase to give 8.15 g **20a** (92%) as white solid. ^{1}H NMR (300 MHz, Acetone): 6.97 (d, 6H), 7.66 (d, 6H), 7.69 (s, 3H), 8.46 (s, 3H); ^{13}C NMR (75 MHz, Acetone): 116.5, 123.7, 129.1, 133.5, 142.9, 158.1.

Synthesis of 2-propargyloxy-1,3,5 triazine (23a): Cyanuric chloride (0.57 g, 3.12 mmol) was dissolved in 25 ml THF and cooled to 0 ^{0}C in an ice/water bath, followed by dropwise addition of a mixture of propargyl alcohol (0.175 g, 3.12 mmol) and DIPEA (0.4 g, 3.12 mmol) in 15 ml THF. The reaction mixture was stirred for 4 hours at 0 ^{0}C then warmed up to room temperature overnight. DIPEA salt was filtered out and the filtrate was concentrated. Filtrate was dissolved in CH_2Cl_2 then washed with water three times before dried with anhydrous Na_2SO_4. The residue was then chromatographed on a silica gel column (100-200) with a

mixture of hexane and EtOAc (6:1) as the mobile phase to give 381 mg (60%) pure product **23a** as white solid. ^{1}H NMR (500 MHz, $CDCl_3$): 2.62 (s, 1H), 5.12 (s, 1H); ^{13}C NMR (125 MHz, $CDCl_3$): 57.32, 75.65, 77.00, 170.4, 172.77.

Synthesis of 2-azidoethoxy-1,3,5 triazine(23b): Cyanuric chloride (0.57 g, 3.12 mmol) was dissolved in 25 ml THF and cooled to 0 ^{0}C in an ice/water bath, followed by drop wise addition of a mixture of 2-azidoethanol (**21b**) (0.27 g, 3.12 mmol) and DIPEA (0.4 g, 3.12 mmol) in 15 ml THF. The reaction mixture was stirred for 4 hours at 0 ^{0}C then warmed up to room temperature overnight. DIPEA salt was filtered out and the filtrate was concentrated. Filtrate was dissolved in CH_2Cl_2 wan washed with water three times before dried with anhydrous Na_2SO_4. The residue was then chromatographed on a silica gel column (100-200) with a mixture of hexane and EtOAc (6:1) as the mobile phase to give 292 mg (40%) pure product **23b** as liquid. ^{1}H NMR (500 MHz, $CDCl_3$): 3.73 (d, 2H), 4.66 (d, 2H); ^{13}C NMR (125 MHz, $CDCl_3$): 49.27, 68.17, 170.77, 172,76.

Synthesis of 23c: To a solution of 2-propargyloxy-1,3,5 triazine (**23a**) (813 mg, 4 mmol) in acetone (20 ml) was added dropwise a mixture of 1,3,5-tris(4-hydroxyphenyl)benzene (**20a**) (354 mg, 1 mmol) and K_2CO_3

(0.539 g, 3.6 mmol) in acetone during 3 hours at room temperature. The reaction then was stirred for another 2 days. After reaction, solid was filtered off and filtrated was then concentrated before running on a silica gel column (100-200) with a mixture of $CHCl_3$ and ethyl acetate (15:1) as the mobile phase to give 200 mg (20%) pure product **23c** as light yellow solid. ^{1}H NMR (500 MHz, $CDCl_3$): 2.60 (s, 1H), 5.07 (s, 2H), 7.36 (ds, 2H), 7.79 (ds, 2H), 7.83 (s, 1H); ^{13}C NMR (125 MHz, $CDCl_3$): 56.63, 121.76, 125.38, 128.65, 139.26, 141.50, 151.01, 171.69, 172.19, 173.54.

Synthesis of 23d: To a solution of 2-azidoethoxy-1,3,5 triazine (**23b**) (932 mg, 4 mmol) in acetone (20 ml) was added dropwise a mixture of 1,3,5-tris(4-hydroxyphenyl)benzene (**20a**) (354 mg, 1 mmol) and K_2CO_3 (0.539 g, 3.6 mmol) in acetone during 3 hours at room temperature. The reaction then was stirred for another 2 days. After reaction, solid was filtered off and filtrated was then concentrated before running on a silica gel column (100-200) with a mixture of $CHCl_3$ and ethyl acetate (15:1) as the mobile phase to give 270 mg (40%) pure product **23d** as white solid. ^{1}H NMR (500 MHz, $CDCl_3$): 3.70 (t, 2H), 4.59 (t, 2H), 7.34 (ds, 2H), 7.79 (ds, 2H), 7.83 (s, 1H); ^{13}C NMR

(125 MHz, $CDCl_3$): 49.35, 67.38, 121.74, 125.37, 128.68, 139.25, 141.47, 151.02, 172.09, 172.22, 173.51.

Synthesis of 23: A solution of **23c** (86 mg, 0.1 mmol), **23d** (95 mg, 0.1 mmol), DIPEA (159 µl, 0.014 mmol) in toluene (300 ml) refluxing for 5h. The precipitate was filtered and washed with toluene for further characterization. The residue was concentrated and dried under vacuum for further product analysis.

Synthesis of 4,4'-bipyridine-4-but-1-yne bromide salt (24a): 4,4'-Bipyridine (1.17 g, 7.5 mmol) reacted with 4-bromo-1-butyne (1.0 g, 7.5 mmol) in toluene (30 ml) under reflux for 4 days. After reaction, precipitate was filtered and washed with toluene to get 1.9 g (87%) yellow powder as product **24a**. ^1H NMR (500 MHz, d_6-DMSO): 3.04 (t, 2H), 3.13 (s, 1H), 4.81 (t, 2H), 8.08 (ds, 2H), 8.71 (ds, 2H), 8.90 (ds, 2H), 9.24 (ds, 2H). To exchange into hexafluorophosphate salt (**26a**): the yellowish solid (**24a**) was dissolved in a H_2O/MeCN (3:1) mixture and a saturated aqueous solution of NH_4PF_6 was added to this mixture. The resulting white precipitate was filtered, washed with H_2O, and dried under reduced pressure to give final product **26a.**

Synthesis of 24: A mixture of 2,4,6-tris(2-azidoethoxy)-1,3,5-triazine (**22a**) (840 mg, 2.5 mmol) and 4,4'bipyridine-

4-but-1-yne (**24a**) (2.16g, 7.5 mmol), DIPEA (1.3 ml, 7.5 mmol) and the copper catalyst [$(EtO)_3P{\cdot}CuI$] (89 mg, 0.25 mmol) in 50 ml toluene under reflux for 1 h. The resulting residue was concentrated and dried for further product analysis. Different solvents (THF/H_2O/EtOH 1:2:2, H_2O/t-BuOH 2:1, $CHCl_3$-MeOH cosolvent, DMF), catalyst ($CuSO_4{\cdot}5H_2O$/sodium ascorbate), base (DBU), temperature (RT, 60 ^{0}C) and reaction time (24 hours, 8h) were tried for this reaction.

Synthesis of 1,1'-di(but-3-ynyl)-4,4'-bipyridine-1,1'-diium bis(hexafluorophosphate) salt (25a) was synthesizedbased on a reported procedure.[73] A mixture of 4,4'-bipyridine (260 mg, 1.67 mmol) and p-toluenesulfonic acid but-3-ynyl ester (1.5 g, 6.69 mmol) in MeCN (10 ml) was heated to 80 ^{0}C in a sealed tube for 4 days. The solution was then cooled to room temperature and the resulting precipitate was filtered and washed with MeCN. The yellowish solid was then dissolved in a H_2O/MeCN (3:1) mixture and a saturated aqueous solution of NH_4PF_6 was added to this mixture. The resulting white precipitate was filtered, washed with H_2O, and dried under reduced pressure. The product (**25a**) was isolated as a white powder. ^{1}H NMR (500 MHz, CD_3CN): 2.44 (s, 1H), 2.98 (t, 2H), 4.78 (t, 2H), 8.42 (ds, 2H), 8.97 (ds, 2H).

Synthesis of 25: A degassed solution of $[Cu(MeCN)_4]PF_6$ (25 mg, 0.067 mmol) in MeCN (0.5 ml) was added to a degassed solution of 1,1'-di(but-3-ynyl)-4,4'-bipyridine-1,1'-diium bis(hexafluorophosphate) salt (**25a**) (107.7 mg, 0.195 mmol) and 2-azidoethanol (**21b**) (329 mg, 3.78 mmol) in Me_2CO (15 ml) under N_2. The solution was stirred for 2 days at 30 ^{0}C then filtered. Solid was washed with hexanes and dried under vacuum. ^{1}H NMR (500 MHz, d_6-DMSO): 3,46 (t, 2H), 3.75 (t, 3H), 4.38 (t, 2H), 5.02 (t, 2H), 5.03 (s, 1H), 7.94 (s, 1H), 8.78 (ds, 2H), 9.37 (ds, 2H).

Synthesis of 26 was under the same experimental conditions as synthesis of **25** by using 4,4'-bipyridine-4-but-1-yne hexafluorophosphate salt (**26a**) and 2-azidoethanol (**21b**) as starting materials.

Synthesis of 1,1'-di(3-bromopropyl)-4,4'-bipyridine (27c): 4,4'-bipyridine (260 mg, 1.67 mmol) and dibromopropane (4.65 g, 30 mmol) was added in 10 ml ACN. The mixture was heated to 80 ^{0}C for 4 days. After reaction, yellow precipitate was filtered and washed with ACN to get 400 mg 1,1'-di(3-bromopropyl)-4,4'-bipyridine with 80% purity. ^{1}H NMR (500 MHz, D_2O): 2.56 (p, 4H), 3.44 (t, 4H), 4.82 (t, 4H), 8.48 (ds, 4H), 9.08 (ds, 4H).

Synthesis of 1,1′-di(3-azidopropyl)-4,4′-bipyridine (27a): A mixture of 1,1′-di(3-bromopropyl)-4,4′-bipyridine (**27c**) (560 mg, 1 mmol, 1 M) and sodium azide (0.39 g, 6 mmol, 6 M) in 1 ml of water was heated at 80 ^{0}C for overnight. The solution was evaporated to dryness to give a brown solid. The solid was dissolved in 1 ml of methanol and filtered to remove an excess of sodium azide. The filtrate was dried under vacuum to solid. The brown solid was then dissolved in a H_2O/MeCN (3:1) mixture and a saturated aqueous solution of NH_4PF_6 was added to this mixture. The resulting precipitate was filtered, washed with H_2O, and dried under reduced pressure. ^{1}H NMR (500 MHz, d_6-DMSO): 2.293 (p, 4H), 3.35 (t, 4H), 4.77 (t, 4H), 8.82 (ds, 4H), 9.40 (ds, 4H).

Synthesis of cage molecule 27: Amixture of 1,1′-di(3-azidopropyl)-4,4′-bipyridine (**27a**) (92.1 mg, 0.15 mmol), 2,4,6-tris(prop-2-ynyloxy)-1,3,5-triazine (**17a**) (24.3 mg, 0.10 mmol), $[Cu(MeCN)_4]PF_6$ (25 mg, 0.067 mmol) was added into the degassed Me_2CO (300 ml). The solution was stirred for 2 days at 30 ^{0}C then filtered. Solid was washed with hexanes and dried under vacuum for further analysis.

Synthesis of 1-(3-azidopropyl)-1′-(3-bromopropyl)-4,4′-bipyridine (27b): The synthesis procedure is the same as the synthesis of 1,1′-di(3-azidopropyl)-4,4′-bipyridine

(**27a**) with the only difference in the amount of sodium azide which is (65 mg, 1 mmol, 1 M).

Synthesis of 27d: A degassed solution of $[Cu(MeCN)_4]PF_6$ (75 mg, 0.2 mmol) in MeCN (0.5 mL) was added to a degassed solution of 1-(3-azidopropyl)-1'-(3-bromopropyl)-4,4'-bipyridine (**27b**) (740 mg, 1.2 mmol) and 2,4,6-tris(prop-2-ynyloxy)-1,3,5-triazine (**17a**) (97.3 mg, 0.4 mmol) in Me_2CO (30 ml) under N_2. The solution was stirred for 2 days at 30 ^{0}C before column chromatography on silica gel (CH_2Cl_2/CH_3CN 6:4) monitored by TLC (10:1:1 MeCN: H_2O: Sat NH_4PF_6) to afford less than 10% yield of **27d** as light yellow powder (80% purity).

Computational Studies: Energy minimization of supramolecular structures was carried out using the DFT-B3LYP method (basis set: 3-21G) as implemented in the Gaussian software package (09 version) without solvent effect.

REFERENCE

1. (a) Steed, J. W.; Atwood, J. L., *Supramolecular Chemistry*, Second ed. Wiley, West Sussex, **2009**. (b) Prins, L. J.; Reinhoudt, D. N.; Timmerman, P., *Angew. Chem. Int. Ed.* **2001**, *40*, 2382.

2. (a) Hof, F.; Craig, S. L.; Nuckolls, C.; Rebek, J. Jr., *Angew. Chem. Int. Ed.* **2002**, *41*, 1488. (b) Lehn, J. M., *Science* **1985**, *227*, 849. (c) Lehn, J. M., *Supramolecular Chemistry: Concepts and Perspectives*, Wiley-VCH, Weinheim, Germany, **1995**.

3. (a) Cram, D. J.; Cram, J. M., *Acc. Chem. Res.* **1978**, *11*, 8. (b) Cram, D. J., *Science* **1983**, *219*, 1177. (c) Diederich, F.; Dick, K., *J. Am. Chem. Soc.* **1984**, *106*, 8024. (d) Diederich, F.; Griebel, D., *J. Am. Chem. Soc.* **1984**, *106*, 8037.

4. Cram, D. J., *Science* **1983**, *219*, 1177.

5. Cram, D. J., *Nature* **1992**, *356*, 29.

6. Cram, D. J.; Cram, J. M., *Container Molecules and Their Guests in Monographs in Supramolecular Chemistry* Vol. 4; Stoddart, J. F., Ed., Royal Society of Chemistry, Cambridge, **1994**.

7. Cram, D. J.; Tanner, M. E.; Thomas, R., *Angew. Chem. Int. Ed. Engl*. **1991**, *30*, 1024.

8. Warmuth, R.; Yoon, J., *Acc. Chem. Res.* **2001**, *34*(2), 95.

9. Cram, D. J.; Tanner, M. E.; Knobler, C. B., *J. Am. Chem. Soc.* **1991**, *113*, 7717.

10. Cram, D. J., *Angew. Chem. Int. Ed. Engl.* **1988**, *27*, 1009.

11. MacGillivray, L. R.; Atwood, J. L., *Nature* **1997**, *389*, 469.

12. Hivanyuk, A.; Rebek, J. Jr., *Proc. Natl. Acad. Sci.* (*USA*) **2001**, *98*, 7662.

13. Avram, L.; Cohen, Y., *Org. Lett.* **2003**, *5*, 2329.

14. Avram, L.; Cohen, Y., *J. Am. Chem. Soc*. **2003**, *125*, 1618.

15. Salem. T. E.; Baruch, I.; Avram, L.; Cohen, Y.; Palmert, L. C.; Rebek, J. Jr., *PNAS* **2006**,*103*(33), 12297.

16. Gibb, C. L. D.; Gibb, B. C, *J. Am. Chem. Soc.* **2004**, *126*, 11408.

17. Liu, S; Gibb, B. C., *Chem. Commun.* **2008**, *32*, 3709.

18. Baldridge, A.; Samanta, S. R.; Jayaraj, N.; Ramamurthy, V.; Tolbert, L. M., *J. Am. Chem. Soc.* **2010**, *132*, 1498.

19. Porel, M.; Jayaraj, N.; Kaanumalle, L. S.; Maddipatla, M. V. S. N.; Parthasarathy, A; Ramamurthy, V., *Langmuir* **2009**, *25*, 3473.

20. Sundaresan, A. K.; Gibb, C. L. D.; Gibb, B. C.; Ramamurthy, V., *Tetrahedron* **2009**, *65*, 7277.

21. Jayaraj, N.; Maddipatla, M. V. S. N.; Prabhakar, R.; Jockusch, S.; Turro, N. J.; Ramamurthy, V., *J. Phys. Chem. B* **2010**, *114*, 14320.

22. Parthasarathy, A.; Kaanumalle, L. S.; Ramamurthy, V., *Org. Lett.* **2007**, *9*, 5059.

23. Porel, M.; Chuang, C.; Burda, C.; Ramamurthy, V., *J. Am. Chem. Soc.* **2012**, *134*, 14718.

24. Podkoscielny, D.; Philip, I.; Gibb, C. L. D.; Gibb, B. C.; Kaifer, A. E., *Chem. Eur. J.* **2008**, *14*, 4704.

25. Podkoscielny, D.; Gadde, S.; Kaifer, A. E., *J. Am. Chem. Soc.* **2009**, *131*, 12876.

26. Qiu, Y.; Yi, S.; Kaifer, A. E., *Org. Lett.* **2011**, *13*, 1770.

27. Qiu, Y.; Yi, S.; Kaifer, A. E., *J. Org. Chem.* **2012**, 77(10), 4622.

28. Lee, J. W.; Samal, S.; Selvapalam, N.; Kim, H. J.; Kim, K., *Acc. Chem. Res.* **2003**, *36*, 621.

29. Lagona, J.; Mukhopadhyay P.; Chakrabarti S.; Isaacs L.; *Angew. Chem. Int. Ed.* **2005**, *44*, 4844.

30. Rekharsky, M. V.; Mori, T.; Yang, C.; Ko, Y. H.; Selvapalam, N.; Kim, H.; Sobransingh, D.; Kaifer, A. E.; Liu, S.; Isaacs, L.; Chen, W.; Moghaddam, S.; Gilson, M. K.; Kim, K.; Inoue, Y., *Proc. Nat. Acad. Sci.* (*USA*) **2007**, *104*, 20737.

31. Kim, J.; Jung, I. S.; Kim, S. Y.; Lee, E.; Kang, J. K.; Sakamoto, S.; Yamaguchi, K.; Kim, K., *J. Am. Chem. Soc.* **2000**, *122*, 540.

32. Amijs, C. H. M.; van Klink, G. P. M.; van Koten, G., *Dalton Trans.* **2006**, 308.

33. Fiedler, D.; Leung, D. H.; Bergman, R. G.; Raymond, K. N., *Acc. Chem. Res.* **2005**, *38*, 351.

34. Fujita, M.; Tominaga, M.; Hori, A.; Therrien, B., *Acc. Chem. Res.* **2005**, *38*, 371.

35. Fujita, M.; Umemoto, K.; Yoshizawa, M.; Fujita, N.; Kusukawa, T.; Biradha, K., *Chem. Commun.* **2001**, 509.

36. Nahir, T. M.; Bowden, E. F., *Langmuir* **2002**, *18*, 5283.

37. Ong, W.; Gómez-Kaifer, M.; Kaifer, A. E., *Org. Lett.* **2002**, *4*, 1791.

38. Ling, Y.; Mague, J. T.; Kaifer, A. E., *Chem. Eur. J.* **2007**, *13*, 7818.

39. Cui, L.; Gadde, S.; Li, W.; Kaifer, A. E., *Langmuir* **2009**, *25*, 13673.

40. Bryce, M. R., *J. Mater. Chem.* **2000**, *10*, 589-598.

41. Martín, N.; Segura, J. L., *Angew. Chem. Int. Ed.* **2001**, *40*, 1372-1409.

42. Yamada, J.; Sugimoto, T., *TTF Chemistry: Fundamentals and Applications of Tetrathiafulvalene*, Kodansha (Tokyo) and Springer (New York), **2004**.

43. Batail, P., *Chem. Rev.* **2004**, *104*, 4887.

44. Canevet, D.; Sallé, M.; Zhang, G.; Zhang, D.; Zhu, D., *Chem. Commun*. **2009**, 2245.

45. Jayaraj, N.; Zhao, Y.; Parthasarathy, A.; Porel, M.; Liu, R. S. H.; Ramamurthy, V., *Langmuir* **2009**, *25*, 10575.

46. Gadde, S.; Batchelor, E. K.; Kaifer, A. E., *Aus. J. Chem*. **2010**, *63*, 184.

47. Leheny, A. R.; Rossetti, R.; Brus, L. E., *J. Phys. Chem.* **1985**, *89*, 211.

48. Cohen, Y.; Avram, L.; Frish, L., *Angew. Chem. Int. Ed.* **2005**, *44*, 520.

49. Eddowes, M. J.; Grätzel, M., *J. Electroanal. Chem*. **1983**, *152*, 143.

50. Yoshizawa, M.; Kumazawa, K.; Fujita, M., *J. Am. Chem. Soc*. **2005**, *127*, 13456.

51. Liu, S.; Whisenhunt-Ioup, S. E.; Gibb, C. L. D.; Gibb, B. C., *Supramol Chem*. **2011**, *23*(6), 480.

52. Gupta, S.; Choudhury, R.; Krois, D.; Wagner, G.; Brinker, U. H.; Ramamurthy, V., *Org. Lett.* **2011**, *13*, 6074.

53. Rebek, J., *Angew. Chem. Int. Ed.* **2005**, *44*, 2068.

54. Lledo, A.; Restorp, P.; Rebek, J., *J. Am. Chem. Soc.* **2009**, *131*, 2440.

55. Monk, P., *The Viologens: Physicochemical Properties, Synthesis and Applications of the Salts of 4,4'-Bipyridine*, Wiley, New York, **1998**.

56. Moon, K.; Kaifer, A. E., *Org. Lett.* **2004**, *6*, 185.

57. Sindelar, V.; Silvi, S.; Kaifer, A. E., *Chem. Commun.* **2007**, 2185.

58. Cziferszky, M; Biedermann, F.; Kalbererb, M.; Scherman O. A., *Org. Biomol. Chem.* **2012**, *10*, 2447.

59. Ong, W.; Kaifer, A. E., *Angew. Chem. Int. Ed.* **2003**, *42*, 2164.

60. Wu, P.; Feldman, A. K.; Nugent, A. K.; Hawker, C. J.; Scheel, A.; Voit, B.; Pyun, J.; Frechet, J. M. J.; Sharpless, K. B.; Fokin, V. V., *Angew. Chem. Int. Ed.* **2004**, *43*, 3928.

61. Iida, S.; Asakura, N.; Tabata, K.; Okura I.; Kamachi, T., *Chembiochem.* **2006**, 7(12), 1853.

62. For representative examples of covalent chemical bondedmolecularcages, see: (a) See1, C.; Vögtle, F., *Angew. Chem. Int. Ed.* **1992**, *31*, 528. (b) Idi, B.; Christinat, N.; Tonnmann, J.; Schuttler, C.; Scopelliti, R.; Severin, K., *J. Am. Chem. Soc.* **2009**, *131*, 3154. (c) Julia, M. S.; Mariano, O. M.; Javier, L. J.; Fernando, H. M.; Francisco, S. G.,*J. Org. Chem.* **2008**, *73*, 7772. (d) Zhang, C.; Chen, C.F., *J. Org. Chem.* **2007**, *72*, 9339. (e) Kim, J.; Kim, Y. K.; Park, N.; Hahn, J. H.; Ahn, K. H.,*J. Org. Chem.* **2005**, *70*, 7087. (f) Takemura, H.; Nakshima, S.; Kon, N.; Yasutake, M.; Shinmyozu, T.; Inazu, T., *J. Am. Chem. Soc.* **2001**, *123*, 9293. (g) Kurata, H.; Nakaminami, H.; Matsumoto, K.; Kawase, T.; Oda, M., *Chem. Commun.* **2001**, 529. (h) Colquhoun, H. M.; Arico, F.; Williams, D. J., *Chem. Commun.* **2001**, 2574. (i) Kunze, A.; Bethke, S.; Gleiter, R.; Rominger, F., *Org. Lett.* **2000**, *2*, 609. (j) Araki, K.; Hayashida, H.,*Tetrahedron Lett.* **2000**, *41*, 1807. (k) Vögtle, F.; Ibach, S.; Nieger, M.; Chartroux, C.; Kruger,T.; Stephan, H.; Gloe, K., *Chem. Commun.* **1997**, 1809. (l) Davis, A. P.; Wareham, R. S., *Angew. Chem. Int. Ed.* **1998**, *16*, 2270. (m) Mascal, M.; Kerdelhue, J. L.; Blake, A. J.; Cooke, P. A., *Angew. Chem. Int. Ed.* **1999**, *38*, 1968.

63. For some examples of molecular cages formed by noncovalent interactions, see: (a) Conn, M. M.; Rebek, J. Jr., *Chem. Rev.* **1997**, *97*, 1647. (b) Mateos-Timoneda, M. A.; Crego-Calama, M.; Reinhoudt, D. N., *Chem. Soc. Rev.* **2004**, *33*, 363. (c) Shivanyuk, A.; Friese, J. C.; Doring, S.; Rebek, J. Jr., *J. Org. Chem.* **2003**, *68*, 6489. (d) Vysotsky, M. O.; Mogck, O.; Rudzevich, Y.; Shivanyuk, A.; Böhmer, V.; Brody, M. S.; Cho, Y. L.; Rudkevich, D. M.; Rebek, J. Jr.,*J. Org. Chem.* **2004**, *69*, 6115. (e) Northrop, B.; Zheng, Y. R.; Chi, K. W.; Stang, P., *J. Acc. Chem. Res.* **2009**, *42*, 1554. (f) Li, S. S.; Northrop, B.; Yuan, Q. H.; Wan, L. J.; Stang, P.,*J. Acc. Chem. Res.* **2009**, *42*, 249.(g) Stang, P. J.; Olenyuk, B., *Acc. Chem. Res.* **1997**, *30*, 502.

64. Naseer, M. M.; Wang, D.; Zhao, L.; Huang, Z.; Wang, M., *J. Org. Chem.* **2011**, *76*, 1804.

65. Kolb, H. C.; Finn, M. G.; Sharpless, K. B., *Angew. Chem. Int. Ed.* **2001**, *40*, 2004.

66. Rostovtsev, V. V.; Green, L. G.; Fokin, V. V.; Sharpless, K. B., Angew. *Chem. Int. Ed.* **2002**, *41*, 2596.

67. Tornøe, C. W.; Christensen, C.; Melda, M., *J. Org. Chem.* **2002**, *67*, 3057.

68. Hein, C. D.; Liu, X.M.; Wang, D., *Pharm. Res.* **2008**, *25*, 2216.

69. Meldal, M.; Tornøe, C. W., *Chem. Rev.* **2008**, *108*, 2952.

70. Morales-Sanfrutos, J.; Ortega-Munoz, M.; Lopez-Jaramillo, J.; Hernandez-Mateo, F.; Santoyo-Gonzalez, F., *J. Org. Chem.* **2008**, *73*, 7772.

71. Hooper, N.; Beeching, L. J.; Dyke, J. M.; Morris, A.; Ogden, J. S.; Dias, A. A.; Costa, M. L.; Barros, M. T.; Cabral, M. H.; Moutinho, A. M. C.,*J. Phys. Chem. A* **2002**, *106*, 9968.

72. Perez-Balderas, F.; Ortega-Munoz, M.; Morales-Sanfrutos, J.; Hernandez-Mateo, F.;Calvo-Flores, F. G.; Calvo-Asin, J. A.; Isac-Garcia, J.; Santoyo-Gonzalez, F., *Org. Lett.* **2003**, *5*, 1951.

73. Coskun, A.; Saha, S.; Aprahamian, I.; Stoddart, J. F., *Org. Lett.* **2008**, *10*(15), 3187.